# Regulation of photosynthesis by a potassium transporter in the diatom Phaeodactylum tricornutum

Claire Seydoux

# THÈSE

Pour obtenir le grade de

## DOCTEUR DE L'UNIVERSITÉ GRENOBLE ALPES

Spécialité : Biologie Végétale

Arrêté ministériel : 25 mai 2016

Présentée par


## Claire SEYDOUX

Thèse dirigée par **Florence COURTOIS**, Maitre de conferences, Université Grenoble Alpes
et codirigée par **Giovanni FINAZZI**, Université Grenoble Alpes

préparée au sein du **Laboratoire Laboratoire de Physiologie Cellulaire Végétale**
dans **l'École Doctorale Chimie et Sciences du Vivant**


# Régulation de la photosynthèse par un transporteur de potassium chez la diatomée Phaeodactylum tricornutum

# Regulation of photosynthesis by a potassium transporter in the diatom Phaeodactylum tricornutum

Thèse soutenue publiquement le **30 novembre 2020**,
devant le jury composé de :

**Madame FLORENCE COURTOIS**
MAITRE DE CONFERENCES HDR, UNIVERSITE GRENOBLE ALPES, Directrice de thèse
**Madame ANGELA FALCIATORE**
DIRECTRICE DE RECHERCHE, CNRS DELEGATION PARIS-CENTRE, Rapporteure
**Madame ANJA KRIEGER-LISZKAY**
DIRECTRICE DE RECHERCHE, CNRS ILE-DE-FRANCE GIF-SUR-YVETTE, Rapporteure
**Monsieur JEAN-GABRIEL VALAY**
PROFESSEUR DES UNIVERSITES, UNIVERSITE GRENOBLE ALPES, Président
**Monsieur GIOVANNI FINAZZI**
DIRECTEUR DE RECHERCHE, CNRS DELEGATION ALPES, Co-directeur de thèse
**Monsieur BENJAMIN BAILLEUL**
CHARGE DE RECHERCHE, CNRS DELEGATION PARIS-CENTRE, Examinateur

# RESUME (FRANÇAIS)

La lumière du soleil est la source d'énergie primaire sur dont dépendent directement ou indirectement tous les organismes pour leurs besoins métaboliques. Malgré les nombreux avantages de l'utilisation d'une source d'énergie abondante et inépuisable, la lumière est néanmoins intrinsèquement variable et intermittente. Afin de survivre, les organismes photosynthétiques doivent constamment adapter leur machinerie moléculaire de capture de la lumière, en particulier par l'induction de mécanismes de quenching non-photochimiques (NPQ). Le contrôle de l'équilibre entre photosynthèse et photoprotection s'effectue chez les plantes supérieures et les algues vertes par une régulation fine des composantes électrique et osmotique de la force proton motrice à travers la membrane des thylacoïdes. L'homéostasie ionique joue donc un rôle majeur dans la régulation de la photosynthèse. La modulation de la composition de la force proton motrice par des échangeurs ioniques est un moyen pour les organismes photosynthétiques de réguler efficacement l'induction du NPQ, c.à.d. en minimisant les pertes d'énergie tout en préservant la synthèse d'ATP.

Les diatomées ont un rôle écologique primordial dans les océans, notamment par leur contribution à la mitigation du réchauffement climatique par leur rôle dans la pompe biogéochimique du carbone ou par leur rôle de source de nourriture pour l'ensemble de la vie marine. Nous avons montré chez la diatomée modèle *Phaeodactylum tricornutum* que le pH des thylacoïdes régule directement l'induction et la relaxation du NPQ. Nous avons ainsi affiné le modèle de la dynamique du NPQ chez *P. tricornutum*, où le contrôle cinétique du cycle des xanthophylles par le pH joue un rôle prépondérant.

Nous avons identifié l'antiport proton/potassium KEA3 et déterminé qu'il est un régulateur important de la force proton motrice chez les diatomées. Par l'étude de mutants CRISPR-Cas9, nous avons observé que ce transporteur module le pH du lumen et ainsi permet d'adapter la réponse NPQ selon les conditions environnementales. KEA3 convertit la composante ΔpH de la force proton motrice en ΔΨ, et de ce fait n'induit aucune perte d'énergie et maintient donc la synthèse d'ATP.

# ABSTRACT (ENGLISH)

Sunlight is the inextinguishable primary energy source on which all living beings eventually rely on for their metabolic needs. In spite of the many advantages of light utilization, it conveys heavy, inherent burdens: intermittency and variability. In order to survive, photosynthetic organisms must constantly reshape their light harvesting machinery, in particular by inducing non-photochemical quenching (NPQ) mechanisms. Controlling the balance between photosynthesis and photoprotection is achieved in higher plants and green algae by a fine interplay between the electrical and the osmotic components of the thylakoid proton motive force. Ion homeostasis has therefore a key role in photosynthesis. Fine-tuning the composition of the proton motive force by specific ion exchange is a means for photosynthetic organisms to regulate NPQ induction efficiently, i.e. minimizing energy leaks and preserving ATP synthesis.

Diatoms have a foremost ecological role in the global oceans, both as key contributors of the biogeochemical carbon pump and as feedstock for marine life. In diatoms, the molecular of NPQ are just starting to be identified. We have demonstrated, using the model organism *Phaeodactylum tricornutum*, that NPQ is univocally controlled by the pH component of the proton motive force. We were thus able to refine the current model for NPQ dynamics in *P. tricornutum*, with a preponderant role of the kinetic control of the xanthophyll cycle by pH.

We have identified the K+/H+ antiporter KEA3 as a major regulator of the proton motive force in diatoms. Using a set of CRISPR-Cas9 constructed mutants, we have determined that this transporter is able to modulate the lumen pH and hence to adapt the NPQ response according to environmental conditions. KEA3 converts the ΔpH component of the proton motive force into ΔΨ, thereby not leading to any energy loss, i.e. maintaining the ATP output.

# TABLE OF CONTENTS

# 1 GENERAL INTRODUCTION

## 1.1 LIGHT AS THE FUEL OF LIFE

In order to meet their basic requirements for growth, maintenance and reproduction, all living organisms need to produce and spend energy. Since life appeared some billion years ago, only two ways of generating biological energy have emerged, each using different chemical reactions to extract electrons from pre-existing compounds.

The first one consists in oxidizing organic molecules, by means of fermentation or respiration. These reactions are spontaneous and favored by thermodynamics but limited by the availability of organic material.

The second way of producing energy consists in oxidizing mostly inorganic molecules using an endothermic reaction, which seems at quite puzzling for a system involved in energy supply. The organisms using this strategy have bypassed the underlying thermodynamic constraints by powering them with external energy input: light. Using light as a source of energy is a major biophysical and biochemical challenge since the electromagnetic energy carried by photons must eventually be converted into chemical energy usable by cellular machineries. This hindrance is counterbalanced by the inestimable advantages conveyed in light energy as it is easily available and inexhaustible.

Oxygenic photosynthesis in particular has shaped the world as we know it, by producing large amounts of organic matter out of inorganic matter and by shifting the conditions on Earth from a reducing atmosphere to the current oxidative atmosphere due to constant oxygen production. Today, all living organisms except for a few chemolithotrophic bacteria eventually rely on photosynthetic organisms to sustain their fundamental needs.

## 1.2 BIODIVERSITY OF PHOTOSYNTHETIC EUKARYOTES

### 1.2.1 Acquisition of photosynthesis by multiple endosymbiosis events

In prokaryotes, photosynthesis takes place in the cytoplasm and especially in dedicated membranes called thylakoids. In photosynthetic eukaryotes photosynthesis occurs inside a specialized organelle called plastids. All plastids have evolved from an original symbiosis between a heterotrophic progenitor and a cyanobacteria (primary endosymbiosis) or a eukaryotic phototroph (secondary endosymbiosis). The symbiont was then progressively reduced to an organelle after multiple generations of horizontal gene transfer to the host

nucleus (Bowler, Vardi and Allen, 2010; Brembu *et al.*, 2014). Notably, three lineages of photosynthetic eukaryotes appeared: the 'green' lineage or viridiplantae, to which belong land plants and green algae, the 'red' lineage or rhodophytes and the 'blue' lineage or glaucophytes.

On some occasions, these primary endosymbionts were engulfed by heterotrophic organisms and reduced to a plastid. Secondary endosymbiosis is a large source of diversity for photosynthetic eukaryotes (Falconet, 2011) as shown in Figure 1.1.

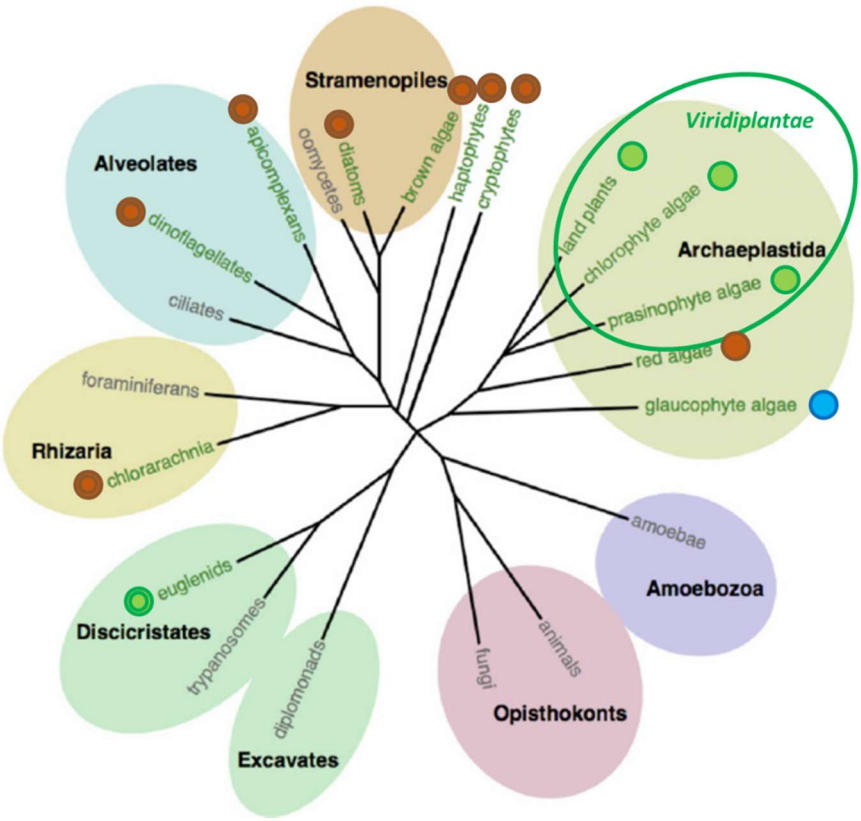


***FIGURE 1.1. DISTRIBUTION OF PLASTID ENDOSYMBIOSIS IN EUKARYOTES.***

*The Viridiplantae group comprises land plants, chlorophyte and prasinophyte algae. Archeaplastida is the only group containing primary endosymbionts. Groups of photosynthetic organisms are indicated in green. The lineage they belong to (blue, red or green) is indicated by a circle. Complex endosymbiosis are indicated by two circles intertwined. Modified from* (Cock and Coelho, 2011).

On land, the most successful family of photosynthetic organisms is the Viridiplantae one, with multicellular plants dominating the forests (Figure 1.1). In the ocean however, photosynthetic organisms are mostly unicellular and belong to Cyanobacteria for Prokaryotes and Alveolates or Stramenopiles for Eukaryotes (Carradec *et al.*, 2018). These are secondary of even tertiary endosymbionts, derived from sequential endosymbiosis events (Bhattacharya, Yoon and Hackett, 2004; Kleine, Maier and Leister, 2009). They are extremely varied in shapes and sizes (Chakraborty *et al.*, 2014; Colin *et al.*, 2017), ranging

from 2 to 200 micrometers. Their very wide biodiversity is just started to being explored thanks to a large effort from the scientific community, such as the TARA Oceans project (Carradec *et al.*, 2018; Pierella Karlusich, Ibarbalz and Bowler, 2020; Sunagawa *et al.*, 2020).

The phytoplankton plays a major ecological role: not only is it the basis of all marine food webs, but phytoplankton communities are also a major component of the biogeochemical carbon pump (Morán *et al.*, 2010; Thomas *et al.*, 2012; Legendre *et al.*, 2015). Marine phototrophs absorb dissolved carbon dioxide and transform it into organic matter that is eventually consumed by other organisms. When they sink to the ocean floor and sediment, marine living beings contribute to permanent carbon storage (Figure 1.2). Since dissolved carbon dioxide and atmospheric carbon dioxide are in a chemical equilibrium, carbon consumption by the phytoplankton contributes at alleviating global warming.

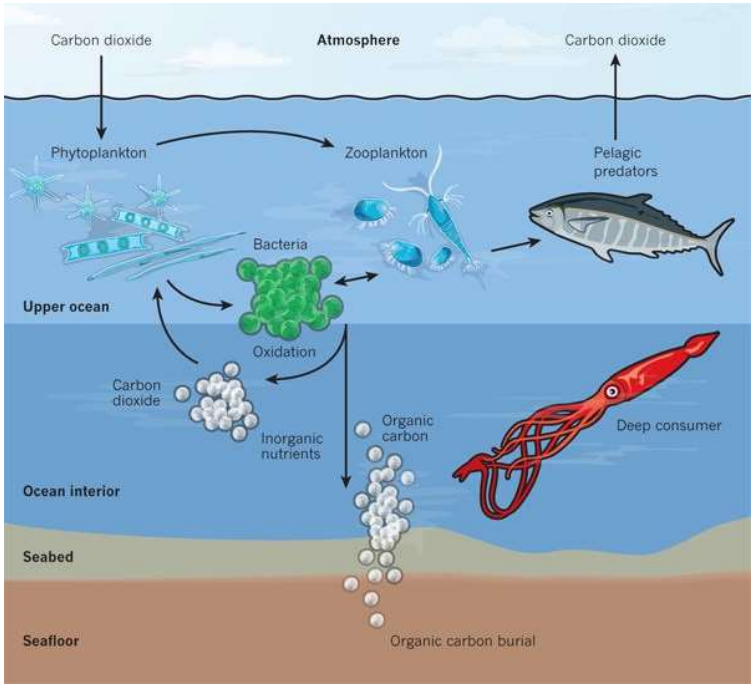


***FIGURE 1.2. THE BIOLOGICAL PUMP OF CARBON DIOXIDE IN MODERN OCEANS.***

*The phytoplankton is the first link in the biological carbon pump. Adapted from* (Falkowski, 2012).

### 1.2.2 Diatoms are key players in modern oceans

The composition of the phytoplankton in term of species is very variable depending on the time of the year and the sampling location. Diatoms are members of the stramenopiles group and dominate among the phytoplankton in coastal areas but also at high latitudes during boreal and austral summers (Tréguer *et al.*, 2018) when ocean productivity is the highest.

A few diatom genomes have recently been sequenced, among them the pennate diatom *Phaeodactylum tricornutum* and the centric diatom *Thalassiosira pseudonana* (Armbrust *et*

*al.*, 2004; Bowler *et al.*, 2008). Diatoms have many genes of unknown function (Bowler, Vardi and Allen, 2010) and the relationship between their genes are physiology remains largely unexplored.

One of the best-known diatoms is *P. tricornutum*. It exists in several morphotypes, the three major ones being pennate, triradiate or oval (Figure 1.3). Morphotype switch depends on genetic background and environmental conditions (Tesson, Gaillard and Martin-Jézéquel, 2009; Abida *et al.*, 2015). Various ecotypes have been found in coastal waters around the world, making it an ecologically relevant organism to study (Bailleul *et al.*, 2010; Abida *et al.*, 2015).

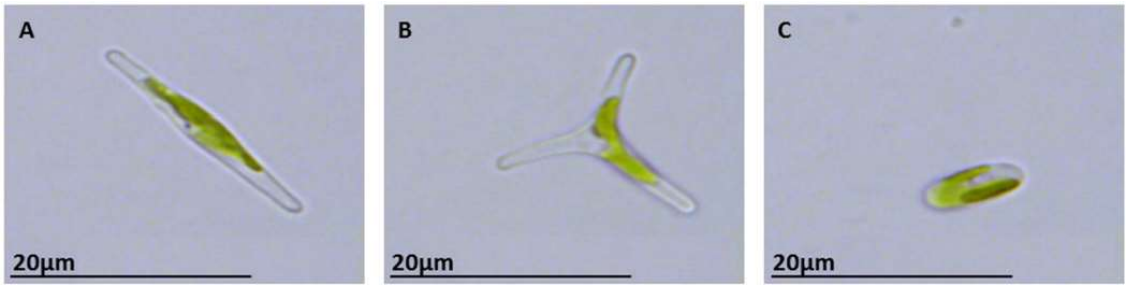


***FIGURE 1.3. LIGHT MICROSCOPY IMAGES OF THREE* P. TRICORNUTUM *MORPHOTYPES.***

*(A) Pennate morphotype. (B) Triradiate morphotype. (C) Oval morphotype. Modified from* (Ovide *et al.*, 2018)*. The chloroplast appears greenish on these micrographs.*

The diatom *P. tricornutum* has become in the recent years a model laboratory organism. It is easy to culture in laboratory conditions in artificial seawater (see Section 8.3.1). Genetic engineering tools are available for this organism, including CRISPR-Cas9 (Allorent *et al.*, 2018; Kroth *et al.*, 2018; Serif *et al.*, 2018). Additionally, diatoms and especially *P. tricornutum* have particular spectroscopic properties that are very useful to study photosynthetic features *in vivo* (Bailleul *et al.*, 2015) (see Section 8.8.2). All the work presented above has been performed on *P. tricornutum.*

## 1.3 PHOTOSYNTHESIS AND CHLOROPLAST

### 1.3.1 Chloroplast architecture in diatoms and plants

Just like other diatoms, *P. tricornutum* has a single chloroplast that takes up a large space inside the cell of around 30% (Uwizeye *et al.*, 2020) Because they derive from different endosymbiosis events, diatom and land plant chloroplast architecture are quite different (Figure 1.4). While plant chloroplasts are surrounded by two membranes that are the remains of the host endomembrane and the bacterial membrane, diatom chloroplasts have

four, originating from the bacterial membrane, the symbiont endomembrane, the symbiont plastic membrane and the host endomembrane (Flori *et al.*, 2016).

Inside the inner membrane of the chloroplast is an amorphous phase called stroma, which hosts a complex membrane system called thylakoids. Inside these membranes, photosynthetic machineries harvest light and use the energy captured to produce ATP and NADPH. In land plants and green algae, the thylakoid membranes are highly organized in stacks of membranes forming grana and lamella membranes floating in the stroma (Figure 1.4). Diatoms on the opposite display a very different thylakoid structure: the membranes are instead grouped by layers of three thylakoid interspaces, i.e. six bilayers of lipid membranes. Diatoms owe their brown color to their high concentration in fucoxanthin, their main light harvesting pigment besides chlorophyll a and c (Guglielmi *et al.*, 2005).

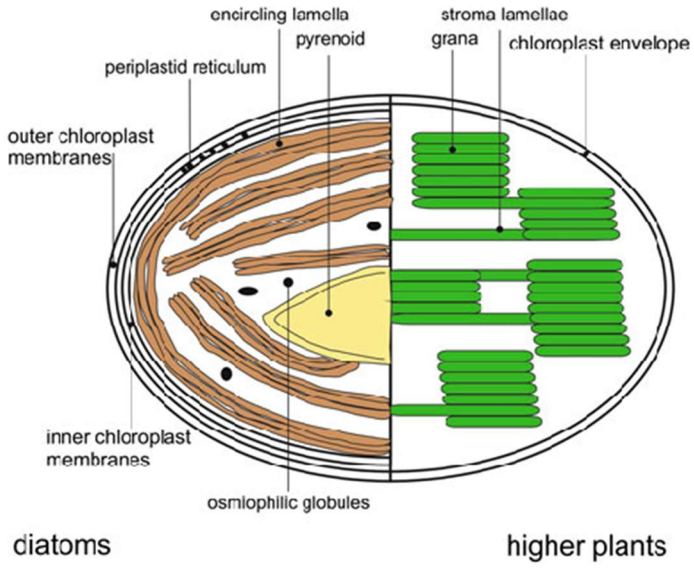


***FIGURE 1.4. SCHEMATIC COMPARISON OF THE CHLOROPLAST MEMBRANE ORGANIZATION OF DIATOMS AND HIGHER PLANTS.***

*The stromal space is here white, while the thylakoid systems are brown in diatoms and green in higher plants. Adapted from* (Grouneva *et al.*, 2013).

The carbon fixation steps preferentially takes place in the stroma of the chloroplast and, in the case of diatoms, in the pyrenoid, a RuBisCo-enriched carbon fixing compartment (Figure 1.4), which is found in several eukaryotic phototrophs (Meyer, Whittaker and Griffiths, 2017).

### 1.3.2 Photosynthetic reactions

In all photosynthetic organisms, photosynthetic reactions occur in two main steps: the light-dependent reactions, that harvest light and form energetic molecules (NADPH and ATP), and the light-independent or dark reactions that turn $CO_2$ into organic molecules

(mainly trioses phosphate). Four major protein complexes are involved in light reactions: photosystem II (PSII), cytochrome b6f, photosystem I (PSI) and ATP synthase/ATP-ase (Figure 1.6). They all are embedded into the thylakoid membrane.

Both photosystems are supercomplexes made of the association of antennas and one reaction center. The antennas are formed of protein complexes associated with pigments, in the case of diatom mostly chlorophyll a, chlorophyll c and the xanthophylls fucoxanthin, diatoxanthin and diadinoxanthin. Their combined absorption spectra covers most of the visible spectrum (Figure 1.5). Pigments are mostly involved in light collection but also take part in photosynthesis regulatory systems (Lavaud, Rousseau and Etienne, 2004).

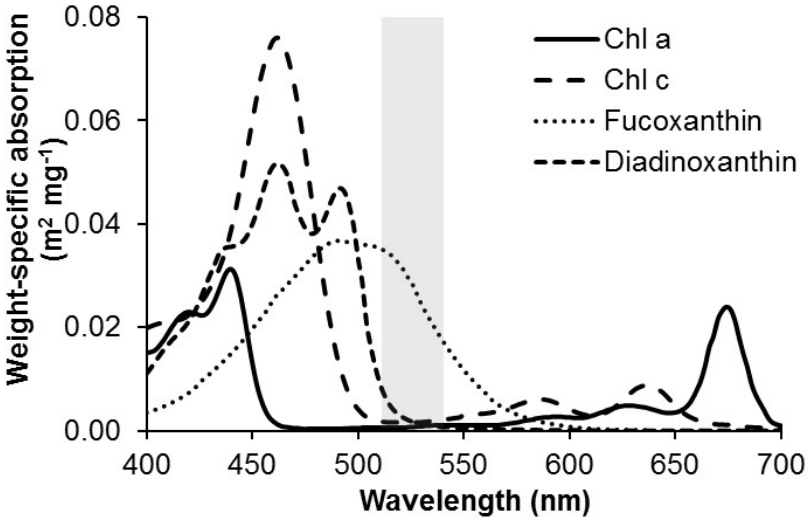


***FIGURE 1.5. ABSORPTION SPECTRA OF THE MAIN PRIMARY PIGMENTS OF DIATOMS.***

*The spectrum of diatoxanthin (not shown) is very similar to diatoxanthin. Adapted from* (Mulders, 2014).

When a photon is captured by a pigment, its energy is delocalized to the neighboring pigment and eventually excites a pair of chlorophyll in the reaction center. The energy of the excited chlorophyll is used to perform charge separation. Photosystem II (PSII) uses light energy to split water via its oxygen evolving complex (OEC). The electrons extracted from $H_20$ go down the redox potentials of the electron transport chain (Figure 1.6).

These electrons reduce plastoquinone (PQ) to form plastoquinol ($PQH_2$), the two protons being acquired from the stroma. Plastoquinol diffuses across the membrane, binds cytochrome $b_6f$ and reduces its redox cofactors, while the two protons are released into the thylakoid lumen. Electrons are transferred from $PQH_2$ to plastocyanin in the green lineage or cytochrome $c_6$ in diatoms and other organisms (Howe *et al.*, 2006). Both plastocyanin and cytochrome $c_6$ are soluble carriers bearing Cu or Fe in their redox center. They are located in the thylakoid lumen. $PQH_2$ – plastocyanin/cytochrome $c_6$ electron transfer occurs

via a bifurcated process in the $b_6f$ (the Q cycle) owing to the different stoichiometry: two electrons are stored in $PQH_2$ while plastocyanin/cytochrome $c_6$ can only accept one electron (Mitchell, 1975). Plastocyanin or cytochrome $c_6$ then transfers its electron to photosystem I (PSI). When excited by light, PSI is able to reduce ferredoxin, another soluble carrier containing a Fe-S cluster as a redox center, located in the stroma. Electrons are then transferred to ferredoxin $NADP^+$ reductase and eventually to NADPH on the stromal side of the membrane (Figure 1.6).

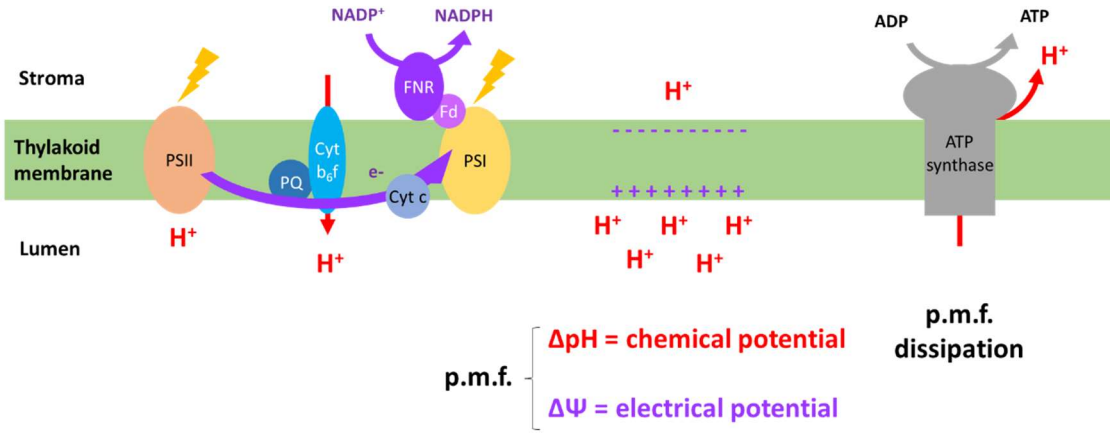


***FIGURE 1.6 ELECTRON TRANSPORT CHAIN IN THE THYLAKOID MEMBRANE.***

*PSII: photosystem II. PSI: photosystem I. PQ: plastoquinone. Fd: ferredoxin. FNR: ferredoxin $NADP^+$ reductase. Cyt $b_6f$: cytochrome $b_6f$. Cyt c: cytochrome $c_6$.*

Just like in the mitochondrion, electron transfer in the thylakoid membrane is coupled with protons pumping across the membrane. The proton resulting proton gradient across the membrane is eventually used for photophosphorylation of ADP into ATP by the ATP-synthase.

### 1.3.3 The proton motive force as transient energy storage

The photosynthetic chain performs the task of converting electromagnetic energy into chemical energy. To do so, several processes of different natures are involved, each described by various scientific disciplines. The capture of a photon by an antenna pigment, energy transfer to the reaction center and excitation of chlorophyll are best explained by particle physics. The many redox reactions of photosynthesis require electrochemistry and biochemistry, while the transport processes of plastoquinone and cytochrome $c_6$ are described using fluid mechanics (Kirchhoff *et al.*, 2008). Additionally, some steps involve changes in protein structure, e.g. a rotation of the ATP-synthase catalytic head (Boyer, 1999) or a conformational switch of the Rieske Iron-Sulfur Protein (ISP) (Berry, Guergova-Kuras and Crofts, 2000) and are understood thanks to structural biology.

Because all of these processes are extremely diverse, their timescales are also very varied (Chow, 2003). The fastest reactions are the one relative to radiation physics: photon capture occurs within fs timeframe; excitation energy transfer and primary photochemistry within around 100 ps while the slowest step of electron flow takes place in the microsecond-millisecond range. The slowest step is believed to be the oxidation of PQ that takes about 10 ms (De Vitry *et al.*, 2004). ATP synthesis has a time constant of about 10 ms too (Joliot and Joliot, 2008). The ATP-synthase has thus a quite similar turnover capacity as the electron flow chain. In *A. thaliana*, this complex can also be activated or inactivated depending on the redox state of the thylakoid lumen (Kohzuma *et al.*, 2013).

To cope with the diversity of reaction rates involved in photosynthesis, energy is transiently stored in the form of a proton gradient before it fuels ATP synthesis (Figure 1.6). The resulting proton motive force (p.m.f.) is of a dual nature: it is both osmotic (ΔpH) and electric (ΔΨ) as it can be described as the sum of its components:

$$p.m.f. = \Delta\Psi - \frac{2.3R.T}{F}\Delta pH$$

***EQUATION 1.1***

*R is the molar gas constant, F the Faraday constant and T the temperature.*

Protons or charges are thermodynamically equivalent for the ATP-synthase, i.e. a proton can be translocated across a membrane through the ATP synthase driven independently by the osmotic or electric component of the p.m.f.

# 1.4 LIGHT PROTECTION

## 1.4.1 Need for light protection

### *1.4.1.1 Light and oxidative stress*

Photons require no prior energy input to be captured and utilized, however this great advantage is balanced by the fact that sunlight is, by definition, variable in intensity and intermittent.

When the light energy available is too low, the cellular energy requirements must be tuned down accordingly in order for the organism to survive. High light on the opposite entails an even more stringent threat as it can cause oxidative stress. Indeed, absorption of a photon results in the excitation of a chlorophyll. An excited chlorophyll may relax to its ground state using four pathways: (1) photochemistry, (2) fluorescence, (3) heat dissipation or (4)

recombination to a triplet state, eventually leading to the formation of reactive oxygen species, especially singlet oxygen $^1O_2$ (Krieger-Liszkay, 2005).

Even though ROS contribute to the signaling system of chloroplasts and promote acclimation to stress (Foyer and Shigeoka, 2011), singlet oxygen in particular may irreversibly oxidize photosynthetic proteins. The D1 subunit in the PSII reaction center is for instance extremely sensitive to ROS-driven damage. This particular subunit has a very high turnover, being replaced about once every 30 minutes. Photosynthetic organisms must circumvent the inevitable damage caused by ROS even at low irradiances, hence a need for photoprotection.

#### *1.4.1.2 Timescales of photoprotection*

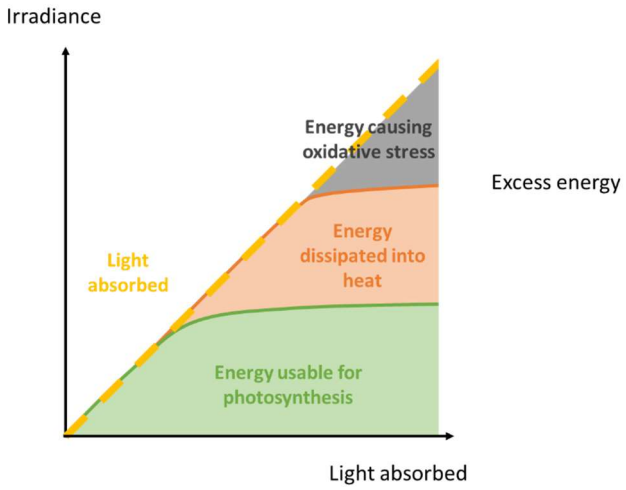


***FIGURE 1.7 USE OF LIGHT ENERGY BY A PHOTOSYNTHETIC CELL DEPENDING ON THE LIGHT IRRADIANCE.***

*The amount of light energy absorbed by a photosynthetic organism depends solely on the photosystem antennae architecture. Light capture is therefore a linear function of light irradiance. Biological phenomena such as photosynthesis (green) or heat dissipation (red) of energy are on the other hand limited by the amount of biochemical effectors (respectively the photosynthetic chain and effectors of photoprotection), hence the saturation at high irradiance. Photoinhibition (grey) occurs when both photosynthesis and photoprotection are saturated and ROS production cannot be avoided.*

To protect themselves from excessive light, photosynthetic organisms activate photoprotective mechanisms. It may involve anatomic, physiological and molecular responses. For instance, a plant moved from shade to light would react by quenching its PSII antennae to dissipate excess energy into heat first, and then by adapting its morphology in the long term (Bascuñán-Godoy *et al.*, 2010). Longer term changes may involve producing smaller leaves and modifying its PSI to PSII ratio (Falkowski *et al.*, 1981).

These phenomena occur at different time and scales, but they all participate in photoprotection.

However efficient they are, morphological changes or protein neo-synthesis are not suitable responses to a sudden shift to high light, since these mechanisms are too slow to avoid excessive ROS formation in the short-term. As a consequence, cells have developed fast photoprotective mechanisms.

Decreasing the relative contribution of ROS formation in chlorophyll relaxation implies increasing the contribution of the other pathways (photochemistry, fluorescence or heat). Photosynthetic energy quenching is saturated in high light due to the rate of the biochemical reactions in the cells, especially carbon assimilation. A maximum 2% of the energy absorbed by chlorophyll can be re-emitted as fluorescence (Maxwell and Johnson, 2000). It ensues that the thermal dissipation of excess energy is the only pathway that can be enhanced when photosynthesis is saturated (Figure 1.7).

These short-term photoprotective mechanisms promote heat dissipation of chlorophyll excitation and rely on pre-existing biochemical effectors. They take place in seconds to minutes and are appropriate responses to sudden light shifts.

### 1.4.2 Principle of non-photochemical quenching measurements

Photosynthetic parameters can be measured *in vivo* by taking advantage of the spectral characteristics of the sample. While a chlorophyll in a solution has a constant fluorescence yield, its yield *in vivo* depends on the efficiency of the other light quenching pathways (photochemistry and heat dissipation) and of the extent of photoinhibition (Maxwell and Johnson, 2000).

When dark-adapted, unquenched cells are exposed to a light only intense enough to trigger photosynthesis (not inducing neither heat dissipation of excess energy nor ROS formation), most of the energy absorbed is used for photosynthesis and only a small part is reemitted as fluorescence. This minimum level of fluorescence is called $F_0$.

When dark-adapted, unquenched cells are exposed to a short (less than 1s) saturating light intensity, photochemistry is saturated and a higher part of the photon flux is reemitted as fluorescence. The fluorescence yield is then maximum and called $F_m$. The parameter $\frac{F_v}{F_m} = \frac{F_m - F_0}{F_m}$ can thus be used as an indication of the efficiency of PSII in the dark (Butler, 1978).

When a cell culture is exposed to light for a longer time (e.g. a few minutes), Non-Photochemical Quenching (NPQ) occurs and some of the light energy collected is turned into heat. Because of this, the fluorescence maximum yield is not $F_m$ anymore but $F_m'$, with

$F_m' < F_m$. The parameter $NPQ = \frac{F_m - F_m'}{F_m'}$ can be used to estimate the amplitude of NPQ in a cell (Maxwell and Johnson, 2000). It is worth noting that defined as such NPQ corresponds to the fraction of PSII fluorescence quenching that is not due to reaction center photochemistry. Photoinhibition is thus comprised in NPQ.

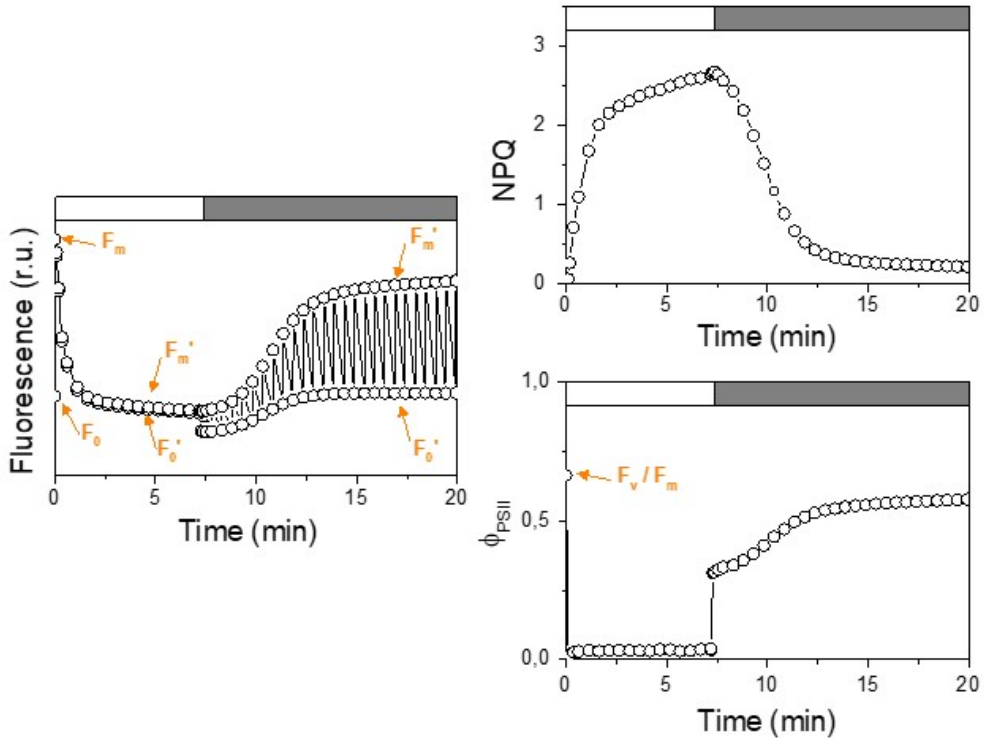


***FIGURE 1.8. FLUORESCENCE TRACE OF A SAMPLE ILLUMINATED AND RESULTING CALCULATIONS OF NPQ AND $\Phi_{PSII}$.***

P. tricornutum *cells were exposed to high light (white box, 1200 µmol photons.m$^{-2}$) followed by low light (dark grey box, 30 µmol.photons.m$^{-2}$). NPQ and $\Phi_{PSII}$ were calculated according to the formulas from Table 1.1.*

When a culture is exposed to light i.e. when photochemistry occurs, the yield of fluorescence diminishes accordingly as compared to the dark-adapted state. This level of fluorescence is called $F_s$, with $F_s > F_0$. The parameter $\Phi_{PSII} = \frac{F_m' - F_s}{F_m'}$ can be used as an indication of the efficiency of PSII in the light. In the dark $\Phi_{PSII} = F_v/F_m$ (Maxwell and Johnson, 2000).

These parameters are summarized in Table 1.1. A typical fluorescence trace is shown in Figure 1.8. All technical details on fluorescence measurements are available in Section 8.8.1.

| Name | Expression |
|---|---|
| Photosynthetic efficiency in the dark | $\frac{F_v}{F_m} = \frac{F_m - F_0}{F_m}$ |
| Photosynthetic efficiency at a light intensity I | $\Phi_{PSII}(I) = \frac{F'_m(I) - F_s(I)}{F'_m(I)}$ |
| Non-photochemical quenching NPQ at a light intensity *I* | $\frac{F_m - F'_m(I)}{F'_m(I)}$ |
| Electron transfer rate (ETR) | $ETR(I) = I.\Phi_{PSII}(I).\frac{A_{PSII}}{A_{PSI} + A_{PSII}}$ |
| Relative electron transfer rate (rETR) | $rETR(I) = I.\Phi_{PSII}(I)$ |

***TABLE 1.1. MAIN PARAMETERS USED TO DESCRIBE THE STATE OF A PHOTOSYNTHETIC SAMPLE.***

*The term $\frac{A_{PSII}}{A_{PSI}+A_{PSII}}$ corresponds to the fraction of light energy captured by PSII. This parameter can be easily measured by absorbance spectroscopy (see Section 8.8.2) but this is not compatible with the high throughput fluorescence measurements used for most of the experiments described in this manuscript (see Section 8.8.1). Consequently, rETR will be presented instead of ETR.*

## 1.4.3 Effectors of energy quenching (qE)

### *1.4.3.1 Components of NPQ*

Although the calculation of NPQ is easily achieved by monitoring PSII fluorescence, the underlying molecular mechanisms are complex, numerous and not yet fully elucidated. The fastest of all is the energy-dependent quenching or qE (Krause, 1991). This mechanism will be the most extensively discussed in the following of this manuscript. A second important NPQ mechanism is state transitions, or qT. State transitions consist in the migration of phosphorylated PSII antenna to PSI, thereby decreasing PSII absorption cross-section (Bellaflore *et al.*, 2005). Eventually, NPQ may also take the form of photoinhibition or qI, i.e. the irremediable damage of PSII reaction center due to ROS production (Krieger-Liszkay, Fufezan and Trebst, 2008).

State transitions have never been observed in diatoms (Owens, 1986). NPQ in diatoms can thus be restricted to the two components qI and qE. qE mechanisms in the red and green lineage involve the interconversion of xanthophyll pigments as well as specialized effector proteins.

### *1.4.3.2 Xanthophyll cycle*

Xanthophylls are carotenoids pigments found in photosystem antennae and are major actors of photoprotection. While the biochemical conversion of xanthophylls in plant chloroplasts following high light exposure was discovered a long time ago (Yamamoto, Nakayama and Chichester, 1962), its involvement in NPQ was only established about 30

years after (Demmig-Adams and Adams, 1996) and the precise mechanism of this quenching is still a matter of debate today.

In the green lineage as well as in some stramenopiles (Goss and Lepetit, 2015), this cycle consists in the two-step conversion of zeaxanthin into violaxanthin, through the intermediate molecule antheraxanthin. The reaction is reversed in the dark or under limiting light. The enzymes responsible for this conversion are respectively violaxanthin de-epoxidase (VDE) and zeaxanthin epoxidase (ZEP) (Hieber, Bugos and Yamamoto, 2000). In plants, the enzyme VDE is localized inside the thylakoid lumen (Schubert *et al.*, 2002) while ZEP is associated to the thylakoid membrane on the stromal side. These xanthophylls are bound to antennae of the photosystems and promote heat dissipation of absorbed light energy.

In diatoms, another xanthophyll cycle is dominating in term of pool size. This cycle involves the one-step conversion of diadinoxanthin (Dd) into diatoxanthin (Dt) (Lohr and Wilhelm, 1999) (Figure 1.9). Notably, NPQ is proportional to the amount of diatoxanthin formed (Lavaud *et al.*, 2002), often presented as the De-Epoxidation State (D.E.S) corresponding to the fraction of Dt among the Dd + Dt pool. This relationship may be modified using different species of diatoms, ecotypes or culture conditions (Lavaud *et al.*, 2002; Lavaud, Rousseau and Etienne, 2004).

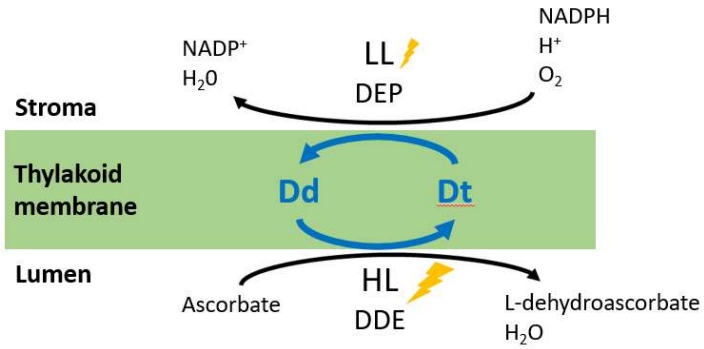


***FIGURE 1.9 SCHEME OF THE XANTHOPHYLL CYCLE IN DIATOMS.***

*Diadinoxanthin (Dd) and diatoxanthin (Dt) are bound to antennae. The location of the enzymes is inferred from that determined in higher plants. The substrates of each enzyme are shown. LL: low light. HL: high light. DDE: diadinoxanthin de-epoxidase. DEP: diatoxanthin epoxidase.*

The enzymes involved in the xanthophyll cycle of diatoms are commonly named diadinoxanthin de-epoxidase (DDE) and diatoxanthin epoxidase (DEP) (Figure 1.9), yet the proteins have not yet been formally identified. The *P. tricornutum* genome encodes for 4 homologues of VDE and 3 homologues of ZEP, and the process of assigning each of them with a specific substrate is only being started (Eilers *et al.*, 2016).

#### *1.4.3.3 Specialized proteins*

In some mutants of *A. thaliana*, in spite of a perfectly functional xanthophyll cycle in high light, NPQ was however absent. This lead to the identification of the first of the protein NPQ effector, namely PSBS (Li *et al.*, 2000), a PSII subunit. Later on, the Light Harvesting Complex Stress-Related proteins (LHCSR) and their homologues LHCX were identified as NPQ effectors in the green alga *C. reinhardtii* and in the diatom *P. tricornutum* (Peers *et al.*, 2009; Bailleul *et al.*, 2010), respectively. PSBS has appeared in the green lineage and is thus absent from the red lineage, including diatoms (Niyogi and Truong, 2013; Giovagnetti and Ruban, 2018).

Just like the LHCSR family in *C. reinhardtii*, the LHCX family in diatoms is multigenic. Notably, there are four different isoforms in *P. tricornutum* and up to eleven in the diatom *Fragiliaropsis cylindrus*. Light changes trigger changes in LHCX expression and eventually protein accumulation (Chauton *et al.*, 2013; Nymark *et al.*, 2013; Taddei *et al.*, 2016). The extent of NPQ depends directly on LHCX accumulation (Bailleul *et al.*, 2010; Buck *et al.*, 2019). Out of the four isoforms, LHCX1 is constitutive under standard low light growth conditions while the others are inducible under a variety of environmental conditions such as high light (LHCX2 and LHCX3), prolonged darkness (LHCX4) or nutrient limitation (Taddei *et al.*, 2016). All of the isoforms except LHCX4 contribute to the extent of NPQ (Bailleul *et al.*, 2010; Taddei *et al.*, 2016; Hao *et al.*, 2018; Buck *et al.*, 2019).

### 1.4.4 Regulation of NPQ effectors by the proton motive force

In the green and red lineage, strong evidence exists for the proton motive force, and especially the ΔpH component, being involved in NPQ induction and relaxation. *In vitro* studies have revealed that both VDE and DDE are activated by low pH (Bratt *et al.*, 1995; Jakob, Goss and Wilhelm, 2001; Grouneva *et al.*, 2006). In addition, the effector proteins PSBS and LHCSR are protonable (Li *et al.*, 2004; Ballottari *et al.*, 2016).

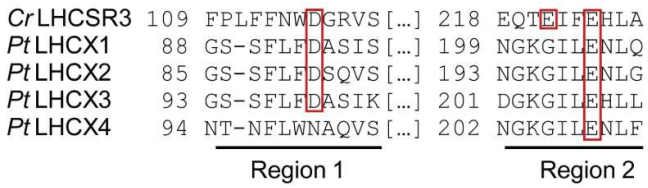


***FIGURE 1.10. PROTEIN ALIGNMENT OF* C. REINHARDTII *LHCSR3 AND* P. TRICORNUTUM *LHCX FAMILY.***

*The protonable residues important for LHCSR3 activation are highlighted by a red box. Adapted from* (Taddei *et al.*, 2016).

In the green alga *C. reinhardtii*, the pH-dependency of the LHCSR proteins is well established and the acid sensitive residues necessary for the quenching function of the protein have been identified (Ballottari *et al.*, 2016). Out of the three protonable residues found in LHCSR1 and LHCSR3 in *C. reinhardtii*, only two are conserved in LHCX1, LHCX2 and LHCX3 and one in LHCX4 in *P. tricornutum* (Taddei *et al.*, 2016), raising the questions of whether the quenching function of these proteins can be activated by protonation (Figure 1.10).

The increase of electron flow following high light exposure induces a decrease in lumen pH, thereby triggering NPQ responses that decrease the yield of photochemistry. The action of the proton motive force on NPQ can therefore be understood as a self-control loop mechanism.

## 1.5 ION CHANNELS AND TRANSPORTERS IN PHOTOSYNTHESIS REGULATION

The proton motive force is an ionic force as it relies on the existence of a proton gradient. As a consequence, the dynamics of the p.m.f. affect ion homeostasis across the thylakoid membrane. Ion channels and transporters that could counter-balance the p.m.f. are therefore good candidates to regulate the p.m.f. and eventually photosynthesis.

### 1.5.1 Chloroplastic ion channels and transporters

Chloroplasts are highly compartmentalized organelles. This is all the more true in diatoms (see Section 1.3) where the chloroplast is surrounded by a higher number of membranes than in the green lineage. This requests a complex and extensive import machinery for proteins, metabolites but also ions (Marchand *et al.*, 2018).

Recently, many ion channels and transporters involved in chloroplast and thylakoid ion homeostasis have been described in *A. thaliana*. Among them, we can cite the thylakoid localized chloride channels VCCN and ClCe (Duan *et al.*, 2016; Herdean, Teardo, *et al.*, 2016), the thylakoid manganese transporter PAM71 (Schneider *et al.*, 2016), the chloroplast envelope manganese transporter CMT1 (Eisenhut *et al.*, 2018), the chloroplast calcium transporter CCHA1 (Wang *et al.*, 2016). The chloroplast envelope potassium transporters KEA1 and KEA2 (Aranda-Sicilia *et al.*, 2012) and the thylakoid potassium transporter KEA3 (Armbruster *et al.*, 2014) have been identified as key players of photosynthesis regulation. These transporters will be of particular interest in the following of this manuscript.

### 1.5.2 The KEA and Kef families

In *A. thaliana*, the KEA family ($K^+$ exchanger antiporter) is composed of 6 members, numbered from 1 to 6. This family is divided in two distinct clades (Chanroj *et al.*, 2012). The first clade, comprising KEA1, KEA2 and KEA3, has a large transmembrane cation/$H^+$ antiporter domain and a Regulator of $K^+$ Conductance domain (RCK), also named $K^+$ Transport Nucleotide domain (KTN). The second clade, comprising KEA4, KEA5 and KEA6, only has a cation/$H^+$ antiporter domain (Figure 1.11).

This family is homologue to KefC in *E. coli* which bears one cation/$H^+$ antiporter domain and a RCK domain (Figure 1.11). Although irrelevant for photosynthesis study, this protein has been extensively studied from a functional point of view and could therefore provide interesting insight as far as the regulation and function of the KEA family is concerned.

The six KEA proteins have varied localizations and functions in *A. thaliana*.

KEA4 to 6 have different expression patterns in plant organs but are redundant in function: the *kea4kea5kea6* triple KO-mutant is sensitive to salt stress, low potassium and to N-deprivation at low pH. These proteins are not present in the chloroplast but in the Golgi apparatus, the endosome and the vacuole (Zhu *et al.*, 2018; Wang *et al.*, 2019).

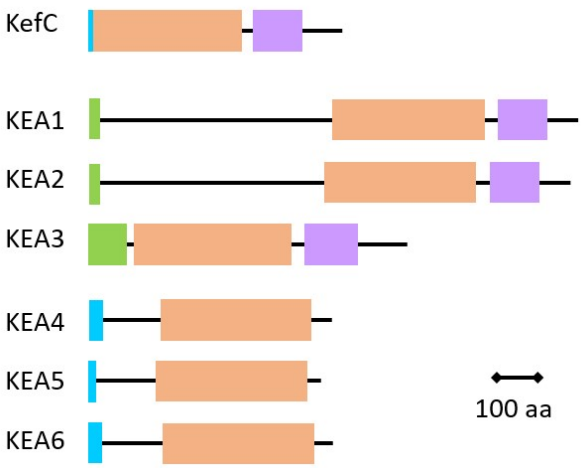


***FIGURE 1.11 DOMAIN ARCHITECTURE OF THE PRIMARY SEQUENCES OF THE KEA FAMILY IN* A. THALIANA *AND KEFC IN* E. COLI.**

*Blue: signal peptide. Orange: cation/$H^+$ antiporter domain. Purple: regulator of $K^+$ conductance. Green: chloroplast transit peptide.*

The three other members of the KEA family in *A. thaliana* are localized in the chloroplast. KEA1 and KEA2 both localize in the chloroplast envelope and have a redundant function: only the *kea1kea2* double KO-mutant is affected in growth, plastid development and photosynthesis efficiency (Aranda-Sicilia *et al.*, 2012, 2016; Kunz *et al.*, 2014). This mutant

is also affected in plastid development, with lower levels of essential photosynthetic proteins in developing leaves. KEA1 and KEA2 also contribute to cellular responses to hyperosmotic stress (Stephan *et al.*, 2016).

KEA3 is embedded in the thylakoid membrane and enriched in the stroma lamellae (Armbruster *et al.*, 2014; Kunz *et al.*, 2014). Besides, KEA3 accelerates acclimation from dark to low light and from high light to low light by promoting NPQ relaxation (Armbruster *et al.*, 2014, 2016; Wang *et al.*, 2017; Correa-Galvis *et al.*, 2020). The RCK domain of the protein is localized on the stromal side (Wang *et al.*, 2017), and this domain is involved in modulating KEA3 activity (Armbruster *et al.*, 2016; Tsujii *et al.*, 2019).

All members of the KEA family were shown to confer $K^+$ transport activity (Aranda-Sicilia *et al.*, 2012; Tsujii *et al.*, 2019). $H^+$ transport was not detected in KEA3 by Tsuji et al. A rationale for this could be that the pH tested in this study ranged from 6 to 8 while previous reports have shown that the phenotype of KO-mutants lacking one of the KEA is more pronounced at more acidic pH (Wang *et al.*, 2019).

While it is accepted that the KEA proteins function as $K^+/H^+$ antiporters, the underlying molecular mechanism of this transport remains unclear. KEA1, KEA2 and KEA3 could be regulated by their RCK domain and other self-regulation motifs (Armbruster *et al.*, 2016; Bölter *et al.*, 2019), however the role of these motifs cannot be properly studied unless the protein is studied *in vitro* by electrophysiological studies or crystallization.

## 1.6 AIM OF THE THESIS: ION TRANSPORTERS AS A TOOL TO INVESTIGATE PHOTOPROTECTION MECHANISMS IN DIATOMS

Diatoms have a major ecological role in the global oceans, both as key contributors of the biological carbon pump and as feedstock for marine life. Their success relies on their high capacity to adapt to variations in their environment by activating fast and efficient photoprotection mechanisms. Controlling the balance between photosynthesis and photoprotection is achieved in plants through a fine interplay between the electrical and the osmotic components of the p.m.f. In diatoms, the molecular actors of this control are just starting to be identified.

Ion homeostasis has a dual role in photosynthesis regulation. First, ions are mandatory cofactors for many proteins of the photosynthetic chain, e.g. manganese and calcium in the oxygen evolving complex or iron for the hemes of cytochrome $b_6f$ and cytochrome $c_6$. Second, photophosphorylation of ADP relies on the buildup of an ionic gradient. ATP synthesis is fueled by the sum of the osmotic ($\Delta pH$) and electric ($\Delta\Psi$) components of the

proton motive force, while NPQ relies mostly on ΔpH. Therefore, fine-tuning the composition of the proton motive force by specific ion exchange is a means for photosynthetic organisms to regulate NPQ induction efficiently, i.e. minimizing energy leaks and preserving ATP synthesis.

Various ion channels and transporters are embedded in the chloroplast and especially the thylakoid membrane. These proteins are regulators of the p.m.f. since they affect ΔpH and ΔΨ. The transporter KEA3 appears of particular interest for this purpose as it catalyzes electroneutral $K^+/H^+$ exchange across the thylakoid membrane. It could thus be involved in modulating NPQ responses in diatoms while studying this transporter could help to clarifying the regulation of NPQ by the p.m.f.

So far, even though predicted homologues of some chloroplast ion channels and transporters from *A. thaliana* can be found in diatoms genomes (Pfeil, Schoefs and Spetea, 2014; Marchand *et al.*, 2018), none of them has been formally identified and characterized. The aim of my thesis will thus be to study the role of $K^+/H^+$ exchanger KEA3 in the regulation of photosynthesis in the diatom *Phaeodactylum tricornutum* (Figure 1.12).

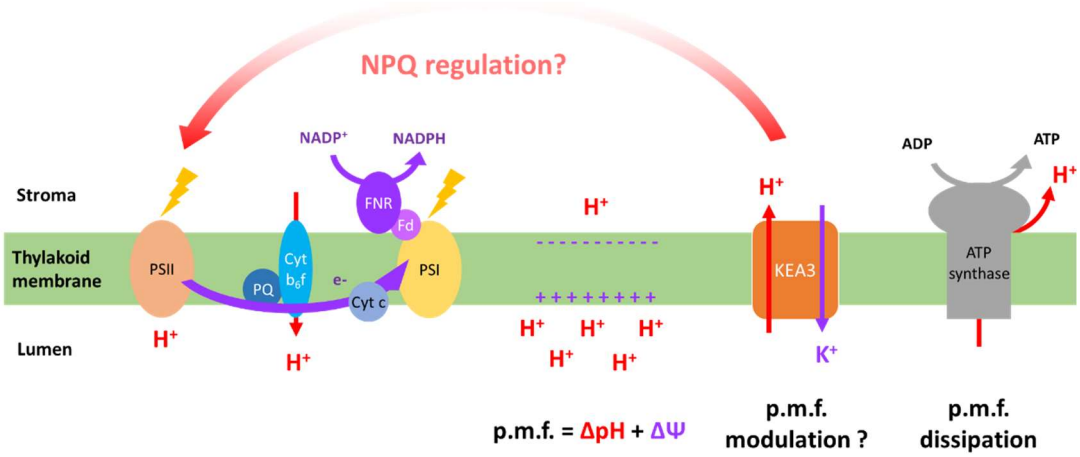


***FIGURE 1.12. WORKING HYPOTHESIS OF THIS MANUSCRIPT.***

*The photosynthetic chain builds up a proton motive force that powers ATP synthesis. KEA3 would be involved in modulating the p.m.f. composition and therefore contribute to NPQ regulation.*

For this purpose, we have first shown that the lumen pH strictly controls NPQ induction in diatoms. We have then identified the K+/H+ antiporter KEA3 in the diatom *Phaeodactylum tricornutum* and constructed a set of KO-mutants and complemented mutants. The physiology of these newly created strains was investigated under different light transitions. Eventually, we attempted to build a model of photoprotection in diatoms in order to recapitulate our findings.

# 2 NPQ IS STRICTLY CONTROLLED BY LUMEN PH IN DIATOMS

The dependency of NPQ to thylakoid lumen acidification is well established in the green lineage, as the proteins PSBS, LHCSR and the enzyme VDE are all activated by low pH. In diatoms, there are indications that NPQ also depends on lumen pH acidification.

These studies have all been performed either as enzymatic assays on partially purified thylakoids (Jakob, Goss and Wilhelm, 2001; Grouneva *et al.*, 2006) or *in vivo* using ammonium chloride ($NH_4Cl$) as an uncoupler of the proton gradient (Mewes and Richter, 2002; Ruban *et al.*, 2004; Goss *et al.*, 2006). Existing protocols for diatom chloroplast identification do not leave the organelles as functionally preserved as for plants (Schober *et al.*, 2018).

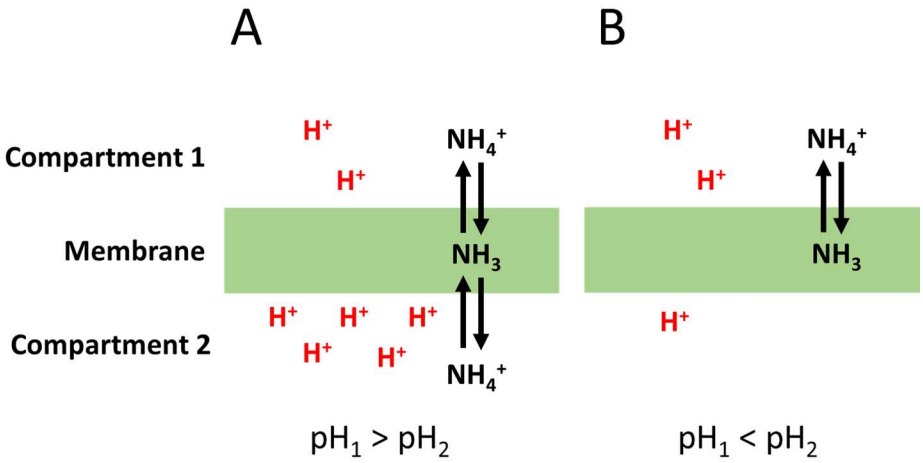


***FIGURE 2.1. MECHANISM OF PENETRATION OF AMMONIUM CHLORIDE INSIDE BIOLOGICAL MEMBRANES.***

*Ammonium ions freely diffuse inside compartments. Upon reaching a membrane, they may lose a proton and form ammoniac gas that freely diffuses across the membrane. If the other side of the membrane (compartment 2) is acidic, ammoniac is protonated into ammonium and diffuses into the next compartment. If the second compartment is less acidic than the second, no proton equilibration takes place.*

Besides, the use of ammonium chloride to study photosynthesis may be criticized. Ammonium chloride allows for protons to cross a membrane only if the pH on the other side of the membrane would be low enough (Crofts, 1967). Since in diatoms chloroplasts are surrounded by four different membranes, $NH_4Cl$ would penetrate from the external

medium to the thylakoid lumen only if all the compartments were crossed in descending pH (Figure 2.1). Penetration could also be forced by adding $NH_4Cl$ in excess to the external medium. Ammonium is also the nitrogen source in some diatom culture media (Ryther and Guillard, 1962), i.e. ammonium can be transported and metabolized by a diatom. For these reasons, ammonium chloride deeply perturbs algal physiology. It may therefore not be the most suitable option to study photosynthesis.

High doses of ammonium chloride abolished NPQ if added before or during illumination (Ruban *et al.*, 2004). It was also suggested (Goss *et al.*, 2006) that the proton gradient was only required for diatoxanthin synthesis and was no longer required once NPQ was activated. In order to solve this apparent contradiction, we induced NPQ in the diatom *P. tricornutum* solely by modifying the pH in all cellular compartments.

## 2.1 NPQ INDUCTION IN THE DARK

### 2.1.1 Induction of NPQ in the dark by an acid shift

We monitored the external pH of *P. tricornutum* cells and measured the fluorescence parameters using a Pulse Amplitude Modulation (PAM) Fluorometer. All experimental details of these experiments are described in the Methods Section (see Section 8.8.1).

Nigericin is an ionophore catalyzing $K^+/H^+$ exchange across biological membranes (Figure 2.2). This chemical occurs naturally as a bacterial toxin (Graven, Estrada-O and Lardy, 1966). At low concentrations, nigericin decreases ΔpH and compensates part of the proton motive force with ΔΨ (Ahmed and Booth, 1983; Pu, Wang and Chen, 1995). It has been widely used to investigate functional response to pH *in vivo* (Ahmed and Booth, 1983; Johnson and Ruban, 2014; Armbruster *et al.*, 2016) in several photosynthetic and non-photosynthetic organisms.

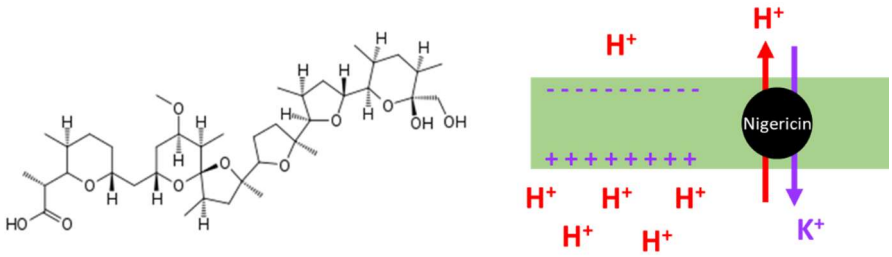


***FIGURE 2.2. CARTOON SHOWING THE CHEMICAL STRUCTURE OF NIGERICIN AND THE MECHANISM OF NIGERICIN-DRIVEN $K^+/H^+$ EXCHANGE ACROSS A BIOLOGICAL MEMBRANE IN RESPONSE TO A PROTON GRADIENT.***

In the experiment presented below, WT *P. tricornutum* cells were first exposed to high light to reach their maximum NPQ level ($NPQ_{max}$). NPQ was then relaxed in low light (Figure 2.3). The light was switched off and nigericin was added (black arrow). At this stage, the value of the external pH was 7.8

The nigericin concentration used (20 µM) was sufficient to drive diffusion of protons added from the external medium to the inner compartments of the cell. Indeed, addition of acetic acid (red arrow) to the cell suspension successfully decreased the external pH to 4.5, while promoting a sharp decrease in PSII maximum fluorescence $F_{max}$. Adding potassium hydroxide (blue arrow, Figure 2.3) increased the medium pH to its original value and unquenched PSII. This indicates that acid-induced quenching of PSII is reversible.

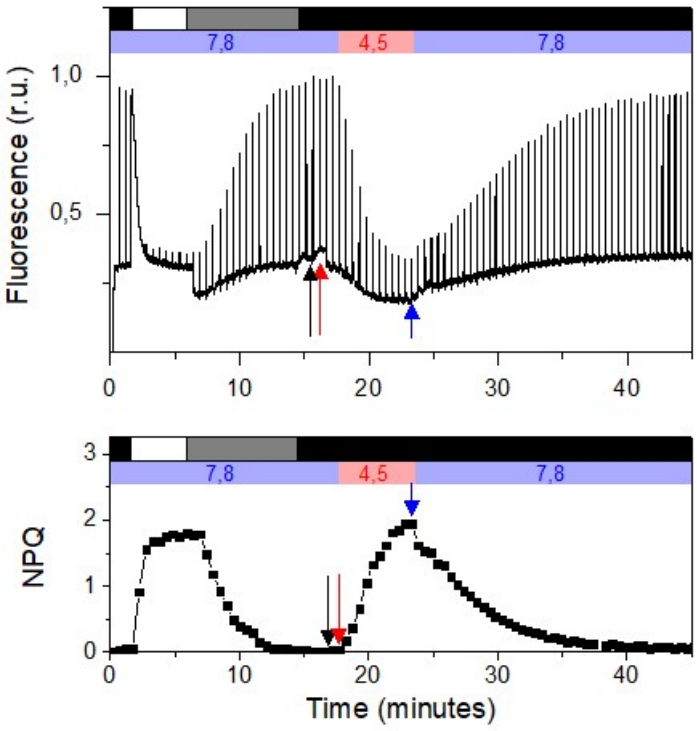


***FIGURE 2.3 NPQ INDUCTION IN THE DARK IN* P. TRICORNUTUM.**

P. tricornutum *cells ($15.10^6$ cells/ml) were exposed to high light (1200 µmol.photons.$m^{-2}$, white box) followed by low light (30 µmol.photons.$m^{-2}$, grey box) and dark (black box). Arrows indicate the successive addition of 20 µM nigericin (black arrow), 4 µM acetic acid (red arrow) and 2 µM potassium hydroxide (blue arrow). Addition of acetic acid caused a shift in the external pH from7.8 (blue box) to 4.5 (red box), while potassium hydroxide addition restored the pH to its original value. The raw fluorescence trace and NPQ calculation are shown for the same experiment.*

Adding acetic acid without nigericin did not trigger any detectable change in fluorescence (not shown). Therefore, in the experiment reported here (Figure 2.3), nigericin acted as a proton shuttle across the membranes of *P. tricornutum*. We can thus assume that without

nigericin, penetration of acidic acid is too slow or not sufficient to acidify the various cell compartments, especially since they are buffered to maintain cytoplasmic homeostasis.

Both the high light induced quenching and acid-induced quenching were reversible and did not affect PSII stability: indeed $F_v/F_m$ (see Section 1.4.2) reaches the same value as the initial one at the end of the neutral shift (Figure 2.3). The acid-induced quenching also reached the same level as the high light induced quenching (~1.8 in our conditions).

The maximum quenching in high light is characteristic of a specific cell culture at a given time (Bailleul *et al.*, 2010) and will be called $NPQ_{max}$ in the rest of this manuscript. We exposed cells to acid quenching in the same conditions as previously described and the pigment content of these cells was analyzed by HPLC (see Section 8.7 for experimental procedures). Addition of acetic acid in the dark in the presence of 20 µM nigericin did trigger the conversion of diadinoxanthin into diatoxanthin since a de-epoxidation state of ~0.4 was reached for ~0.7 $NPQ/NPQ_{max}$ (2 technical replicates, data not shown).

Both the acid-induced quenching and the high light induced quenching are able to induce pigment de-epoxidation and therefore proceed from the same mechanism. NPQ induction and relaxation in P. tricornutum are therefore dependent on pH-related changes.

## 2.1.2 NPQ depends on the external pH in permeabilized cells

### *2.1.2.1 Calibration of NPQ as a function of the external pH*

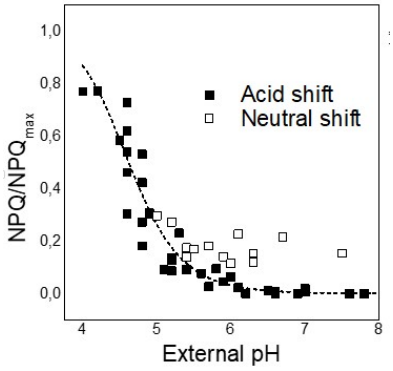


***FIGURE 2.4 CALIBRATION OF NPQ AS A FUNCTION OF THE EXTERNAL PH.***

*pH changes were performed using various doses of acetic acid (acid shift, full squares) or potassium hydroxide (neutral shift, empty squares) in the presence of 20 µM of nigericin, in the same conditions as Figure 2.3. NPQ was normalized to the maximum NPQ value reached in high light ($NPQ_{max}$). Data was fitted using a Hill function ($R^2$ = 0.90).*

We performed the same experiment as described in the previous paragraph using various doses of acid acetic. Different NPQ levels were reached in the dark (Figure 2.4). NPQ

induction was always reversible when neutralizing the external pH using potassium hydroxide.

Interestingly, the level of NPQ reached quantitatively depends on external pH (Figure 2.4). In a pH range between ~4 to 5.5, the extent of quenching is linearly correlated to the external pH. Overall, the shape of this dependency is sigmoidal, which is a characteristic shape for phenomena involving pH shifts around a $pK_a$ value.

#### *2.1.2.2 NPQ dependency to pH in a natural LHCX1 knock-down*

The LHCX proteins, homologs of the LHCSR family in *C. reinhardtii*, are involved in controlling the extent of NPQ response (Bailleul *et al.*, 2010; Taddei *et al.*, 2016; Buck *et al.*, 2019) in *P. tricornutum*. We have investigated whether the isoform LHCX1 might also be involved in controlling the pH-related dynamics of NPQ using the two ecotypes Pt1 and Pt4. Pt1 is the strain used in all other experiments but this one described in this manuscript.

The strain Pt4 constitutively expresses lower amounts of LHCX1 isoform (Bailleul *et al.*, 2010) and displays hence a lower NPQmax than for Pt1 (1.4 vs. 1.9 here, Figure 2.5.A). These two ecotypes thus good tools to study a possible pH-dependency of LHCX1 activation.

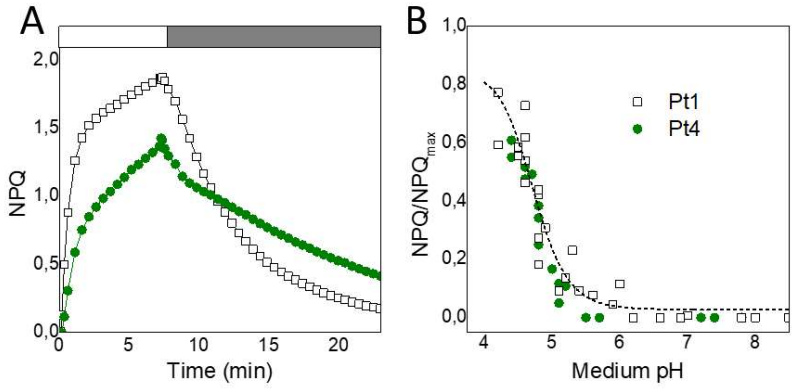


***FIGURE 2.5. COMPARISON OF NPQ INDUCTION IN PT1 AND PT4.***

*(A) NPQ was induced in high light (1200 µmol.photons.m$^{-2}$, white box) and relaxed in low light (30 µmol.photons.m$^{-2}$, dark grey box) in Pt1 and Pt4. (B) pH-dependency of acid-induced NPQ in Pt1 and Pt4. Dependency of NPQ/NPQ$_{max}$ as a function of the medium pH (preliminary results).*

We placed Pt1 and Pt4 cells were placed in the dark and added acetic acid in the presence of 20 µM nigericin using the same method as previously(Figure 2.5.B). Once NPQ is normalized to $NPQ_{max}$, the quenching profile of Pt4 is quite similar to Pt1. The sigmoidicity of the curve could possibly be different between the two ecotypes, however the $pK_a$ is very similar. This preliminary result suggests that the different amount of LHCX1 protein between Pt1 and Pt4 only controls the maximum extent of NPQ ($NPQ_{max}$) (Bailleul *et al.*, 2010; Buck *et al.*, 2019) and is not or little involved in the pH-related dynamics of NPQ.

#### 2.1.2.3 pH equilibration in the acid-quenching setup

In our setup, the external pH corresponding to a high NPQ value (close to $NPQ_{max}$) was below 5 and even reaching 4 (Figure 2.4 and Figure 2.5). When exposed to acidic pH (below 5.5 - 5.8), PSII is irreversibly damaged due to the loss of a calcium ion in the oxygen evolving complex (Spetea, Hideg and Vass, 1997; Kramer, Cruz and Kanazawa, 2003). In our experiment, PSII quenching was reversible when the external pH was neutralized with the addition of potassium hydroxide (Figure 2.3 and Figure 2.4), hinting that PSII was still perfectly functional. Consequently, the thylakoid lumen pH had never reached these very acidic values that would have otherwise irreversibly impaired PSII.

To explain this seemingly odd result, we make the hypothesis that the pH measured from the medium and the actual thylakoid lumen pH were different. This could be because pH equilibration by nigericin was incomplete in our treatment. We inferred a possible value of the thylakoid lumen pH by performing a pH calibration of the thylakoid lumen pH using the kinetics of cytochrome $b_6f$.

## 2.2 CALIBRATION OF THE PH-DEPENDENCY OF NPQ IN *P. TRICORNUTUM*

### 2.2.1 Principle

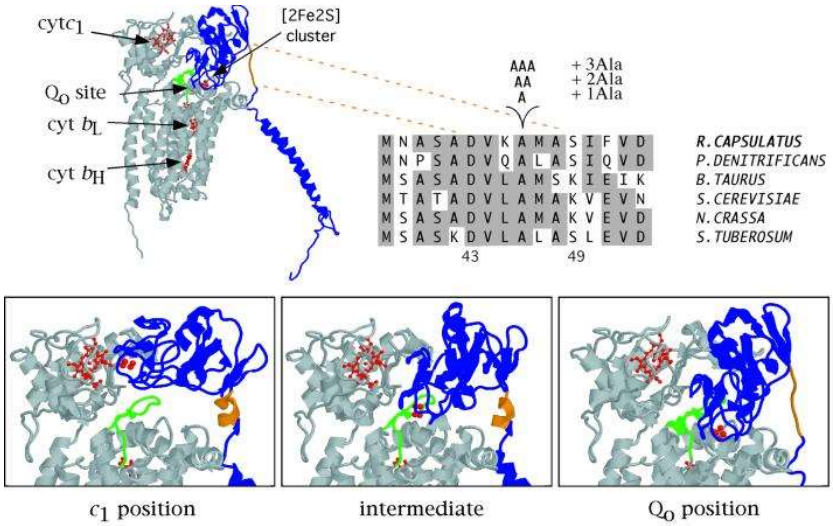


***FIGURE 2.6. THE MECHANISM FOR THE MOVEMENT OF THE RIEKSE ISP PROTEIN IS HIGHLY CONSERVED.***

*Cartoon of the Rieske ISP (highlighted in blue) in the cytochrome $bc_1$ complex from bovine heart ($c_1$ and intermediate position) and chicken heart ($Q_0$ position). Adapted from* (Darrouzet *et al.*, 2000)

Oxidation of plastoquinone by cytochrome $b_6f$ becomes the kinetically limiting step in electron transfer when light is intense (Eberhard, Finazzi and Wollman, 2008; Cardol, Forti and Finazzi, 2011; Tikhonov, 2014). During this step, two electrons are withdrawn from reduced plastoquinone along with two protons, which are sent to the thylakoid lumen. This transfer is mediated by the Rieske iron-sulphur protein (ISP). The mechanism is identical across eukaryotes and prokaryotes, both in the photosynthetic $b_6f$ complex and the related respiratory $bc_1$ complex where it was first elucidated.

This histidine residue is conserved in all chloroplastic, mitochondrial and bacterial homologues of the Rieske ISP of various species as distantly related as mammals and bacteria, including *P. tricornutum* (Figure 2.6.A). The value of the apparent $pK_a$ of this conserved residue also has very similar values across all reigns of life: it was measured at ~6 in the green alga *Chlorella sorokiniana* (Finazzi and Rappaport, 1998) (Figure 2.6.B) and at ~6.3 to 6.5 in the bacterium *Rhodobacter sphaeroides* (Berry, Guergova-Kuras and Crofts, 2000). Being conserved in such evolutionary distant organisms, one can assume with reasonable certainty that the turnover rate of cytochrome $b_6f$ is the same in *P. tricornutum.*

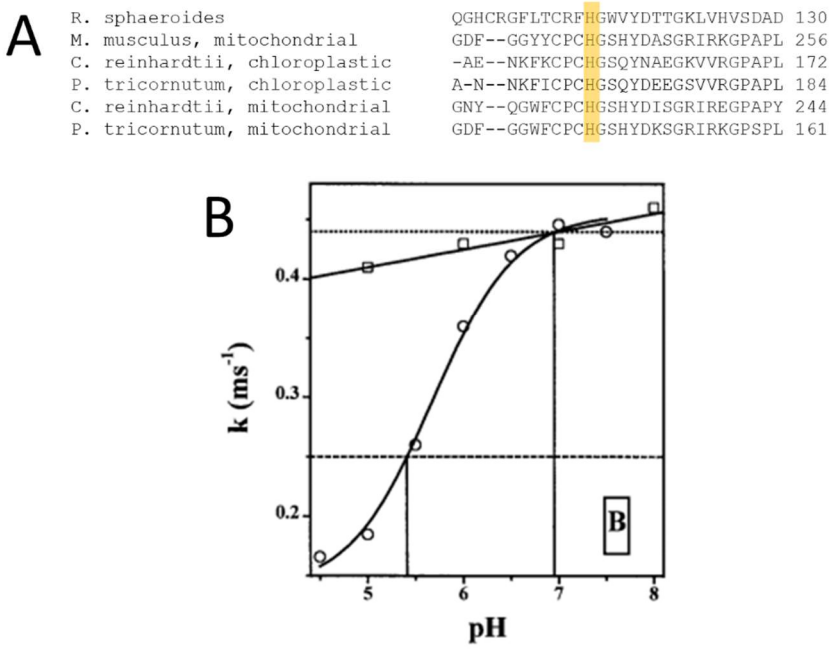


***FIGURE 2.7. THE $pK_A$ OF CYTOCHROME $B_6F$ KINETICS DEPEND ON A CONSERVED HISTIDINE RESIDUE.***

*(A) Protein alignment of sequences from the Rieske protein of various organisms (*Rhodobacter sphaeroides*, bacterium,* Mus musculus*, mammal,* Chlamydomonas reinhardtii *and* Phaeodactylum tricornutum*). The conserved histidine residue is highlighted. (B) Kinetics of the electrochromic signal corresponding to cytochrome b6f from the green alga* Chlorella sorokiniana *(adapted* from (Finazzi and Rappaport, 1998)) in the presence (circles) or the absence (squares) of nigeri*cin.*

In chloroplasts, the Rieske ISP is localized in the lumen of the thylakoids. Hence, the rate of cytochrome $b_6f$ is controlled by the value of the lumen pH. In high light conditions, the proton fluxes into the thylakoid lumen due to the water splitting reaction and to the oxidation of plastoquinone exceeds the proton fluxes from the lumen to the stroma due to ATP synthase and ion channels and transporters. The resulting drop in the lumen pH slows down cytochrome $b_6f$. This phenomenon is called photosynthetic control of cytochrome $b_6f$ (Tikhonov, 2014).

### 2.2.2 Calibration of the pH-dependency of NPQ using the $b_6f$ turnover

The dependency of the rate of cytochrome $b_6f$ to the lumen pH is extremely well conserved since it stems from an extremely highly conserved residue in the Rieske ISP. Therefore, the kinetics of this complex can be used a probe to infer the lumen pH. The rate of cytochrome $b_6f$ can be monitored *in vivo* in a non-destructive manner using spectroscopic techniques (Witt, 1979; Finazzi and Rappaport, 1998; Finazzi, 2002; Bailleul *et al.*, 2015).

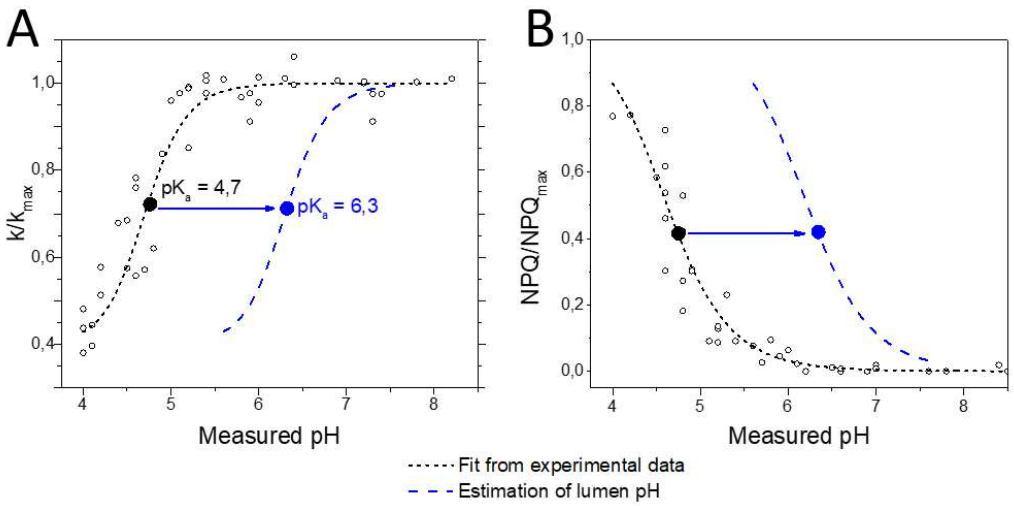


***FIGURE 2.8 ESTIMATION OF THE LUMEN PH USING THE TURNOVER OF CYTOCHROME $B_6F$.***

*(A) Dependency of the turnover of cytochrome $b_6f$ (k, normalized to its maximum values) to the external pH. Data were fitted using a Hill function ($R^2$=0.90). The lumen pH (blue line) was estimated based on $pK_a$ values found in the literature. (B) Estimated dependency of NPQ to lumen pH (data from Figure 2.4).*

We applied this method to determine the range of the lumen pH in our conditions. Acid induction of NPQ in the dark was therefore performed in partially permeabilized. *P. tricornutum* cells (20 µM nigericin) while the external medium was acidified with acetic acid. Instead of measuring PSII fluorescence, we exposed cells to a laser flash and measured the absorbance of the $b_6f$ turnover following a single charge separation (see Section 8.8.2).

The rate of $b_6f$ turnover was estimated by fitting the deconvoluted $b_6f$ redox signals with a monoexponential function (Finazzi and Rappaport, 1998) (Figure 2.8).

The curve obtained (Figure 2.8.A) was fitted using a sigmoidal function and the $pK_a$ value was estimated around 4.7. The $pK_a$ for the dependency of the $b_6f$ turnover to the lumen pH is conserved in all organisms and its value is comprised between 6 to 6.5. Therefore, in our conditions, a $pK_a$ of 4.7 measured in the external medium corresponds to a $pK_a$ value inside the thylakoid lumen of 6 to 6.5. Using this method, we assessed that the pH in the lumen was higher than the external medium pH by about 1.6 units (Figure 2.8.B).

In the green alga *C. reinhardtii*, NPQ can be induced in the dark by permeabilizing cells using nigericin and acidifying the medium using acetate (Dinc *et al.*, 2016; Tian *et al.*, 2019). Notably, the $pK_a$ for NPQ was of about 6.2 (Tian *et al.*, 2019). This is consistent with our measurements: the relationship between NPQ and the lumen pH in *P. tricornutum* (Figure 2.8.B) closely resembles that found in the green alga *C. reinhardtii* (Tian *et al.*, 2019). This suggests that NPQ strictly depends on lumen pH in the diatom *P. tricornutum*, both during induction or relaxation.

In this experiment, the lumen pH was lowered by permeabilizing cells to protons and adding acidity in the external medium. Since the thylakoids are comprised within the chloroplast stroma, protons reaching the lumen must have travelled through the stroma. Hence, there probably was no proton gradient across the thylakoid membrane in these conditions. NPQ requires thus only a low lumen pH and not a pH difference between the stroma and the lumen.

## 2.3 ESTIMATION OF THE LUMEN PH BASED ON NPQ

We fitted the data obtained from Figure 2.4, shifted the pH scale by 1.6 unit (Figure 2.8) and obtained the following dependency of NPQ to the lumen pH (Equation 2.1.):

$$NPQ/NPQ_{max} = 1 - \frac{1}{1+(6.3/pH)^n}\,;\; n = 13$$

***EQUATION 2.1.***

When NPQ values are comprised between 10% and 90% of $NPQ_{max}$, NPQ and lumen pH appear linearly correlated (Figure 2.9.A). Outside of this linear range, this relationship (leads to estimating non-physiological thylakoid lumen pH values below 5 or above 8. Using the linearity within this specified range, we were able to estimate the lumen pH during different light exposures (Figure 2.9.B and C) simply by using the NPQ value.

Several methods exist today to measure the pH of a given compartment. Most of them rely on expressing a fluorescent protein in the compartment of interest. Our technique, however, does not require any genetic engineering but instead takes advantage of an easy *in vivo* fluorescence measurement in wild-type diatom cells.

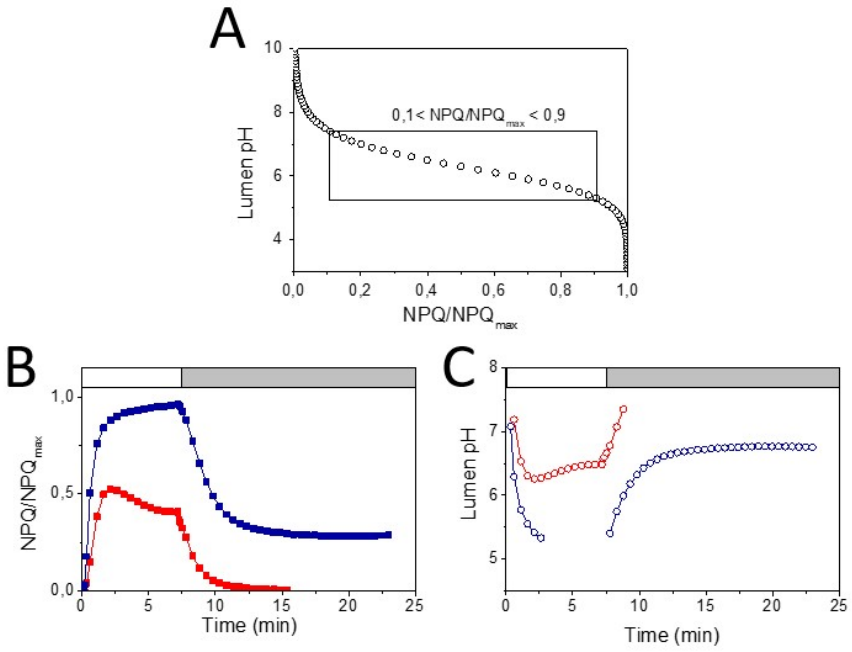


***FIGURE 2.9. ESTIMATION OF THE LUMEN PH FROM NPQ.***

*(A) Lumen pH can be estimated based on Equation 2.1. (B) NPQ normalized to $NPQ_{max}$ of* P. tricornutum *cells exposed to (red symbols) moderate high light (125 µmol.photons.m$^{-2}$, light box) followed by low light (30 µmol.photons.m$^{-2}$, grey box) or to (blue symbols) high light (383 µ mol.photons.m$^{-2}$, white box) followed by moderate high light (125 µmol.photons.m$^{-2}$, grey box). (C) Estimated lumen pH of the same* P. tricornutum *cells exposed to (red symbols) moderate high light followed by low light) or (blue symbols) high light followed by moderate high light.*

## 2.4 CONCLUSION

NPQ, i.e. in thermal dissipation of excess light energy, can be induced in the dark in the diatom *P. tricornutum* by adding acetic acid in permeabilized cells. We calibrated the pH-dependency of NPQ in WT *P. tricornutum* Pt1 cells and noticed that the quenching profile is shaped as a sigmoid.

The shape of this sigmoid is quite similar in the ecotype Pt4 that expresses constitutively lower amounts of LHCX1. Consequently, although this protein controls the extent of NPQ response, it does not appear as the main actor of the pH-sensitivity of NPQ in diatoms.

We corrected this pH profile using the kinetics of cytochrome $b_6f$ and determined a $pK_a$ for the thylakoid lumen of ~6.3. This value highly resembles the one found in *C. reinhardtii* cells (~6.2, (Tian *et al.*, 2019)). This indicates that just like in green algae and plants, NPQ in diatoms is triggered by a decrease in the lumen pH. The reversibility of this phenomenon when alkalinity is added suggests that NPQ could be entirely controlled by the value of the lumen pH. While *in vivo* an acidic lumen pH is always concomitant with the presence of a proton gradient across the thylakoid membrane, a pH difference between the thylakoid lumen and chloroplast stroma is not needed *per se* for NPQ induction.

We were finally able to predict the lumen pH based on NPQ measurements. This easily implemented technique could be used to characterize the pH response proteins involved in NPQ induction. In the case of *P. tricornutum*, characterizing is such a way mutants lacking either one of the LHCX isoforms or bearing point mutations in the possible pH-sensing residues could provide interesting insight on the role and activation kinetics of this protein family. Another study for which lumen pH prediction based on NPQ measurement could be useful would be the identification of the enzyme(s) diadinoxanthin de-epoxidase out of the four VDE homologues predicted in the *P. tricornutum* genome.

# 3 IDENTIFICATION OF A HOMOLOGUE OF KEA3 IN *P. TRICORNUTUM*

We have ascertained that a strict relationship exists between NPQ and the thylakoid lumen pH in *P. tricornutum*. Acidity in the thylakoid lumen results from the balance between proton influx and efflux across the membrane, therefore ion transporters are good candidates to modulate thylakoid lumen pH and thus NPQ. We thus sought for possible ion transporters. We report here the identification of a $K^+/H^+$ antiporter in *P. tricornutum*, homologue to the *A. thaliana* KEA3. We then constructed molecular tools to study its function in photosynthesis and physiology in diatoms.

## 3.1 THE KEA FAMILY IN *P. TRICORNUTUM*

### 3.1.1 The KEA family in photosynthetic eukaryotes

In order to identify a putative KEA3 homologue in *P. tricornutum*, the KEA proteins were blasted against the genomes of some selected members of the green lineage (the bryophyte *P. patens* and the green alga *C. reinhardtii*), of red algae (*C. crispus*, *P. umbilicalis*) and of stramenopiles (see Annex 9 for the list of accessions). Red algae were included since they are believed to be the ancestors of the secondary plastid present in stramenopiles (Falciatore *et al.*, 2020). Sequences were aligned with MUSCLE and a phylogenetic tree was constructed using the Phylogeny web tool (Figure 3.1) to identify the closest homologue of KEA3 in diatoms (Dereeper *et al.*, 2008, 2010; Wang *et al.*, 2020).

In the green lineage, homologs of the KEA4 to 6 subfamily are only found in the genome of multicellular plants (*A. thaliana*, *P. patens*) but are absent from the green alga *C. reinhardtii*. This subclade is present in unicellular extremophile red algae (*C. crispus, P. umbilicalis*) but absent in aquatic stramenopiles, including *P. tricornutum* (Chanroj *et al.*, 2012).

Our phylogenetic analysis also shows that no direct homologues of KEA1 and KEA2 can be found in *P. tricornutum.* The subclade formed by KEA1 and KEA2 is indeed only represented in the green lineage and absent in the red lineage (red algae and stramenopiles). These proteins are predicted to be addressed to the inner plastid envelope that derives from the original cyanobacterial symbiont, providing a possible explanation for the absence of KEA1-2 homologs in the red lineage (Chanroj *et al.*, 2012).

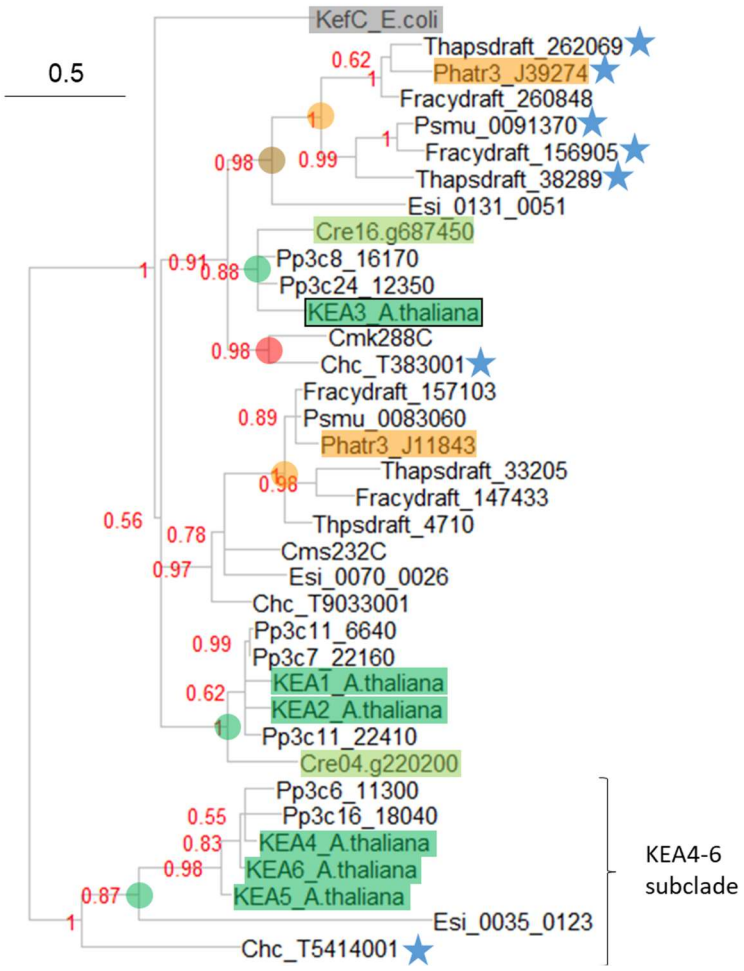


***FIGURE 3.1 ROOTED PHYLOGENETIC TREE OF THE KEA FAMILY IN SELECTED SPECIES FROM THE GREEN LINEAGE, STRAMENOPILES AND RED ALGAE.***

*The gene products discussed in this manuscript are highlighted. Dots highlight monophyletic families (red: red algae, brown: stramenopiles, golden: diatoms, green: green algae and land plants). Scale represents the number of substitutions per site. Bootstrap values (n= 100) are displayed in red. Branches with a support value below 0.5 were collapsed. Stars indicate proteins bearing an EF-hand (see below). All sequences accessions are available in Section 9.*

The KEA3-related family, however, is widely represented in all organisms studied. In the diatom *P. tricornutum*, two members of the KEA family appear as potential homologues of AtKEA3. Both genes are more closely related to AtKEA3 than to AtKEA1 and AtKEA2 based on sequence alignment (Figure 3.1). These two genes will thus be extensively studied in the following.

### 3.1.2 Functional protein domains in the KEA family in *P. tricornutum*

We identified functional protein domains in the primary protein sequence of members of the KEA3 family in *P. tricornutum* using the InterPro webtool (Mitchell *et al.*, 2019). They both contain a transmembrane cation/$H^+$ antiporter domain and a soluble RCK domain and

thus share typical features of plastidial $K^+/H^+$ exchanger with proteins of the *A. thaliana* subfamily KEA 1 to 3 (Figure 3.2). The cation/H+ antiporter domain is highly hydrophobic and contains from 9 to 11 transmembrane helixes depending on the prediction tool used (TMHMM or TMPred, (Rost, Fariselli and Casadio, 1996; Krogh *et al.*, 2001)). The RCK domain bears a conserved $NAD^+$ binding motif.

In addition, the amino acid sequence of the protein encoded by the gene Phatr3_J39274 also harbors an EF-hand. EF-hands are structural domains widely spread across all reigns of life. EF-hands fold around a calcium ion and chelate it with high affinity (Lewit-Bentley and Réty, 2000). The induced structural change is reversible when the local calcium concentration decreases.

The presence of an EF-hand in the primary sequence is a specific feature of red algae and stramenopiles KEA proteins as none is detected in green algae or plants (Figure 3.1). Calcium regulation of KEA activity could be a key feature of members of the red lineage. This hypothesis will be investigated in Section 4.6.

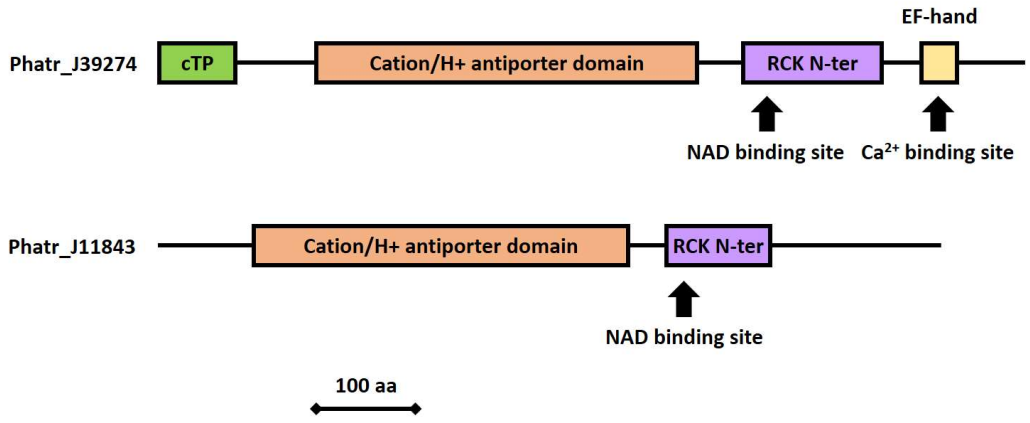


***FIGURE 3.2 PREDICTED DOMAINS IN THE PRIMARY SEQUENCES OF THE KEA FAMILY MEMBERS IN* P. TRICORNUTUM.**

*cTP: chloroplast transit peptide. RCK: Regulation of $K^+$ conductance domain.*

### 3.1.3 Putative subcellular targeting

The protein encoded by the gene Phatr3_J39274 displays a predicted chloroplast transit peptide (cTP) when analyzed with the tools Asafind, SignalP and Hectar (Gschloessl, Guermeur and Cock, 2008; Petersen et al., 2011; Gruber et al., 2015) (Table 3.1). Conversely, no cTP is predicted for the gene Phatr3_J11843. This does not necessarily mean that such a transit peptide would not exist: indeed, the *P. tricornutum* genome is yet poorly annotated and some predicted protein sequences might be incomplete. Nonetheless, the

presence of a putative chloroplast transit peptide in gene Phatr3_J39274 is another indication supporting its closest homology with AtKEA3.

| Gene accession | Asafind result | Signal P cleavage sit | Hectar result |
|---|---|---|---|
| Phatr3_J39274 | Plastid, high confidence | 17 | Chloroplast (0.8253) |
| Phatr3_J11843 | Negative | – | Other (0.7092) |
| Phatr3_J20657 | Plastid, high confidence | 37 | Chloroplast (0.9765) |

***TABLE 3.1. ASAFIND, SIGNALP AND HECTAR RESULTS FOR THE TWO KEA PROTEINS AND ATPC***

*ATPC: chloroplastic ATP synthase gamma chain, gene Phatr3_J20657, chloroplast control.*

## 3.2 EXPRESSION PATTERN OF THE KEA FAMILY IN *P. TRICORNUTUM*

The chloroplast proton motive force in *P. tricornutum* is fueled by the linear electron flow from PSII as well as redox power import from the mitochondrion (Bailleul *et al.*, 2015). Depending on light conditions, the contribution of the linear electron flow fluctuates, possibly resulting in different extent and composition of the proton motive force throughout the day. Since AtKEA3 in *A. thaliana* is believed to be a regulator of the chloroplast proton motive force (Armbruster *et al.*, 2014; Wang *et al.*, 2017), the expression of its homologue in *P. tricornutum* could be expected to be regulated by light conditions.

To test this hypothesis, data from already published transcriptomics datasets were analyzed (see Section 8.2 for methods). The expression profile of the members of the KEA family in *P. tricornutum* (Phatr3_J39274 and Phatr3_J11843) and *C. reinhardtii* (gene Cre16.g687450 and Cre04.g.220200) were compared. Comparing the expression pattern of *P. tricornutum* and *C. reinhardtii* genes seems more relevant than comparing *P. tricornutum* directly with *A. thaliana*. Even though *P. tricornutum* is equally evolutionary distant from *A. thaliana* as from *C. reinhardtii*, *P. tricornutum* and *C. reinhardtii* do share common characteristics that make their gene expression pattern more comparable. These algae are unicellular, have a single chloroplast and divide about once a day under optimal culture conditions, hence a need to duplicate all of their material within a relatively short time frame and regulate gene transcription accordingly.

In *C. reinhardtii*, two genes belong to the KEA family (Figure 3.1, highlighted in light green). One of them is closely related to KEA3 in *A. thaliana* (gene Cre16.g687450) and the other one is homolog to KEA1/2 (gene Cre04.g220200). Considering that both *C. reinhardtii* and *A. thaliana* belong to Viridiplantae, the distances between the *A. thaliana* and *C. reinhardtii* gene sequences are smaller. Homology between proteins is therefore more easily established between them than with a diatom.

Two relevant datasets were analyzed for *P. tricornutum*. In the first one, cells were acclimated to 16h:8h photoperiod (Chauton et al., 2013) (***FIGURE 3.3***.A). In the second one, cells were first acclimated to continuous white light, then placed in the dark for 48 h, and eventually switched back to continuous white light (Nymark et al., 2013) (Figure 3.3.B). The chosen dataset to explore the response of the KEA family in *C. reinhardtii* was the one of (Strenkert *et al.*, 2019), in which cells were acclimated to 12h:12h photoperiod (Figure 3.3.C).

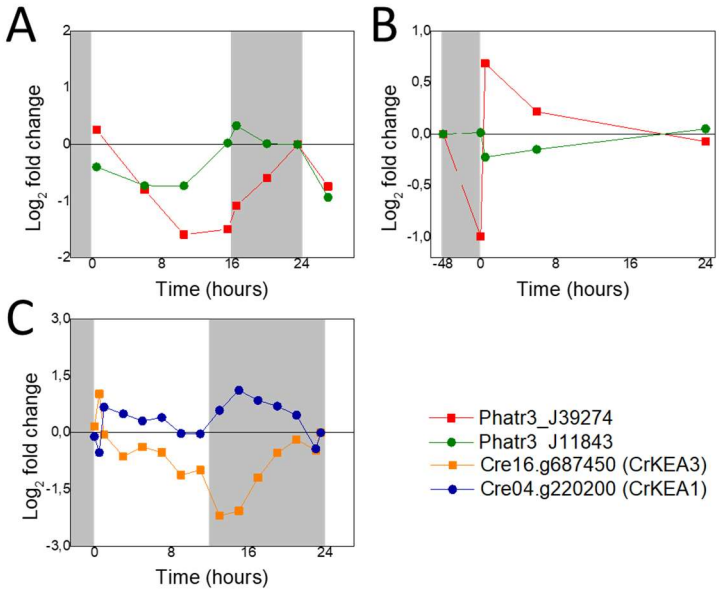


***FIGURE 3.3. MRNA ACCUMULATION IN RESPONSE TO LIGHT OF THE MEMBERS OF THE KEA FAMILY IN P. TRICORNUTUM AND C. REINHARDTII.***

*Grey boxes indicate darkness periods. (A) Log2 fold change upon exposure to 16h:8h photoperiod with 150 µmol.photons.m$^{-2}$ in* P. tricornutum *(data from* (Chauton *et al.*, 2013)*). (B) Log2 fold change upon adaption to 100 µmol.photons.m$^{-2}$ continuous light, followed by 48h of darkness and 100 µmol.photons.m$^{-2}$ 24h of continuous light in* P. tricornutum *(data from* (Nymark *et al.*, 2013)*). (C) Log2 fold change upon exposure to 12h:12h photoperiod with 200 µmol.photons.m$^{-2}$ in* C. reinhardtii *(data from* (Strenkert *et al.*, 2019)*).*

The mRNA accumulation of Phatr3_J39274 transcripts drops during the day by about 3-fold and recovers to its original levels during the night (Figure 3.3.A). On the opposite, Phatr3_J11843 transcript accumulation was quite stable during the day and increases slightly at the beginning of the dark period.

Adaption to darkness led to a decrease in Phatr3_J39274 expression and a switch to light caused a surge in Phatr3_J39274 transcript accumulation (Figure 3.3.B), followed by a fall in transcription up to reaching the levels corresponding to continuous light adaption after 24h of light exposure. A similar pattern was observed for other genes, especially the

photoprotection effectors Lhcx2 and Lhcx3. The expression of gene Phatr3_J11843 is very little affected by a switch to prolonged darkness and remains at similar levels as in continuous light.

In *C. reinhardtii*, the accumulation Cre16.g687450 transcripts decreased during the day and increased during the night (Figure 3.3.C). It peaked 30 minutes after light onset, just like Phatr3_J39274 following a switch to light. mRNA accumulation of the Cre04.g.220200 transcript seemed quite irresponsive to the light cycle, except for an increase in transcription at the beginning of the night.

Overall, the transcript accumulation pattern of genes Phatr3_J39274 and Cre16.687450 are strikingly similar, being repressed by light exposure, enhanced in the dark and booming upon a switch from darkness to light. The transcription of the other KEA family members Phatr3_J11843 and Cre04.g220200 are on the other hand little responsive to light.

## 3.3 IDENTIFICATION OF KEA3 IN *P. TRICORNUTUM*

The wide conservation of KEA family members across photosynthetic eukaryotes lead us to identify the Phatr3_J39274 gene product as the most probable thylakoid KEA3 in *Phaeodactylum tricornutum*. Several arguments support this identification:

(1) Gene Phatr3_J39274 is more closely related to AtKEA3 than gene Phatr3_J11843, even when considering only the most conserved cation/$H^+$ antiporter domain.
(2) Phatr3_J39274 gene product has a predicted chloroplast transit peptide.
(3) Gene Phatr3_J39274 shows a strong light induction pattern at the transcriptional level.

The gene Phatr3_J39274 was considered as the homologue of AtKEA3 and extensively studied. In the rest of the manuscript, the protein encoded by this gene will be called KEA3.

In order to study the function of this protein, mutants were constructed in *P. tricornutum* and characterized as for their involvement in photosynthesis.

## 3.4 MOLECULAR CHARACTERIZATION OF THE MUTANT LINES

### 3.4.1 Presentation of mutants

As a tool to study the role of KEA3 in *P. tricornutum*, a set of KO-mutants were constructed by CRISPR-Cas9 (G. Allorent, (Allorent *et al.*, 2018)). Details concerning mutant construction are available in Section 8.5.

Several knockout (KO) mutants were created. For practicality reasons, we used only a few of them on a routine. The two KO-mutants mostly used were named *kea3-1* and *kea3-2*. They stem from independent CRISPR events on two different target sites, both located in the cation/$H^+$ antiporter domain. An insertion of one nucleotide at position 484 *(kea3-1)* and a 457 bp deletion at position 558 (kea3-2) from the translation initiation base lead to truncated proteins (Figure 3.4). None of these truncated protein bears a full cation/$H^+$ antiporter domain.

The KO mutant *kea3-1* was complemented with the CDS of KEA3 fused with eGFP (Figure 3.4). Many complemented strains were obtained but only one was routinely used and named *kea3-1*/KEA3-eGFP (Figure 3.4). It was constructed by biolistics by inserting the CDS under the control of the Lhcf1 strong and light inducible promotor (Allorent *et al.*, 2018).

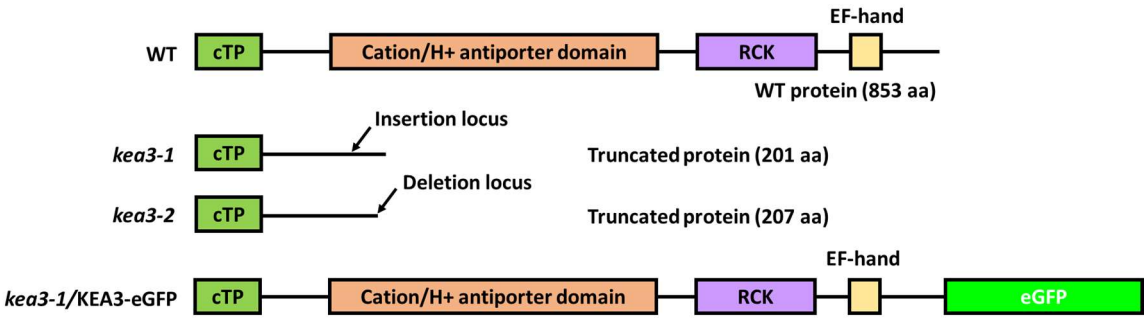


***FIGURE 3.4. CARTOON SHOWING THE PROTEIN DOMAINS OF THE WT, KO-MUTANTS* KEA3-1 *AND* KEA3-2 *AND A COMPLEMENTED STRAIN* KEA3-1*/KEA3-EGFP.***

*Light green box: cTP, putative chloroplast transit peptide. Orange box: cation/$H^+$ antiporter domain. Purple box: RCK domain. Dark green box: eGFP.*

## 3.4.2 Detection of KEA3 by immunolabelling

In order to characterize the mutants, we have produced specific antibodies directed against the KEA3 protein of *P. tricornutum*.

### *3.4.2.1 Production of anti-peptide antibodies*

The first strategy implemented to detect PtKEA3 was to produce anti-peptide antibodies. Two peptides were selected and their position is shown in Figure 3.5. Peptide 2 (sequence CVDPSLSDTALRPSRN) is specific of PtKEA3 (Phatr3_J39274), while Peptide 1 (sequence CFGGDLARKRKQREEA) is specific of both PtKEA3 and PtKEA1/2 (gene Phatr3_J11843). Considering this gene may be of interest for future developments in the laboratory, Peptide 1 was selected as well.

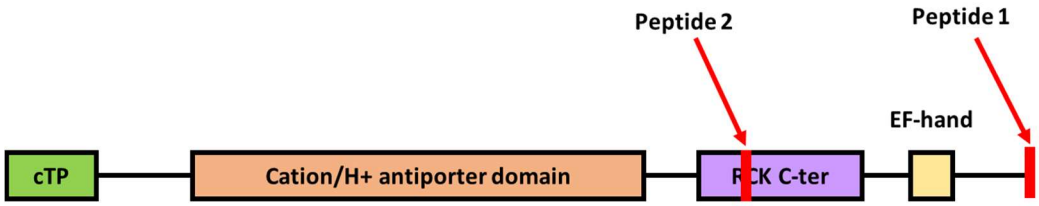


***FIGURE 3.5. POSITION OF THE TWO CHOSEN IMMUNOGENIC PEPTIDES IN KEA3.***

Two rabbits were immunized against the two peptides (Eurogentec, Speedy Rabbit). The serum from the rabbit that had triggered the strongest immune response was purified against each peptides. The pre-immune sera, final bleeds and purified antibodies were frozen at -80°C. Glycerol was added to the purified antibodies to optimize conservation.

### *3.4.2.2 Characterization of anti-peptide antibodies on total protein extracts*

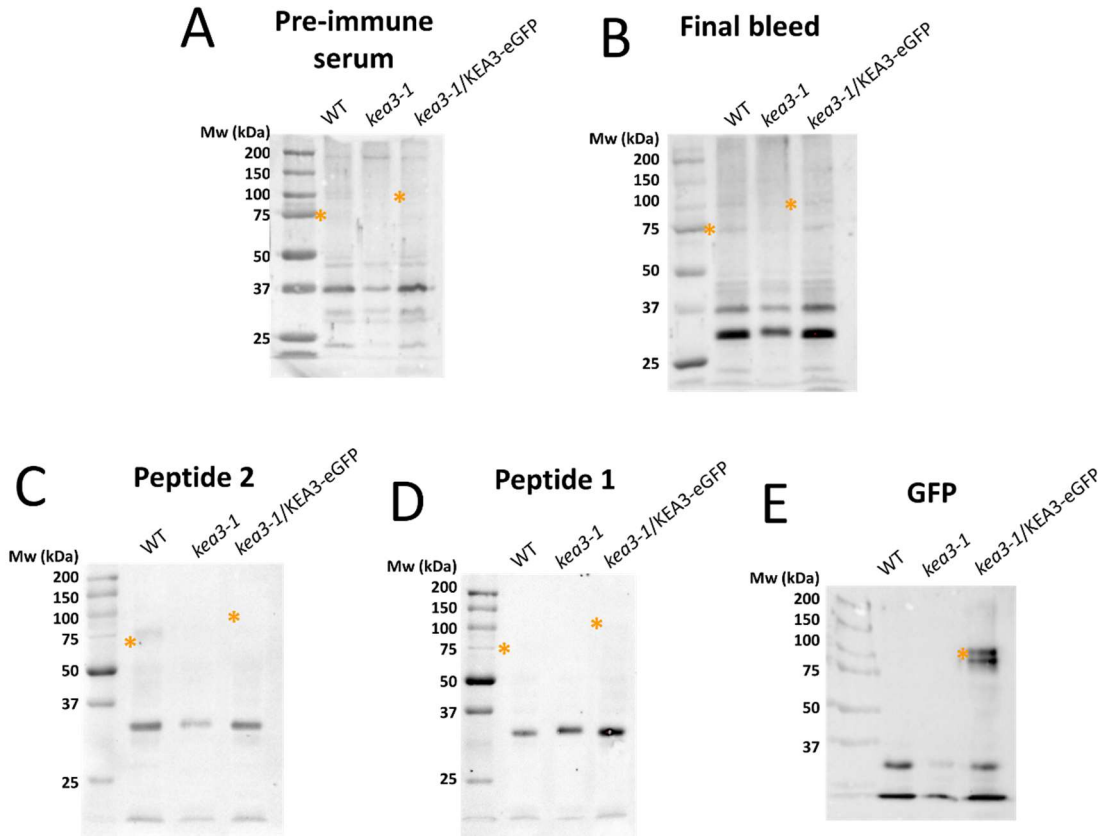


***FIGURE 3.6. CHARACTERIZATION OF THE ANTI-PEPTIDE ANTIBODIES ON TOTAL PROTEIN EXTRACTS.***

*SDS-PAGE of total protein extracts from WT,* kea3-1 *and* kea3-1*/KEA3-eGFP (50 µg protein/lane). Membranes were hybridized with (A) pre-immune serum (B) final bleed serum, (C) an antibody purified against Peptide 1 (1:1000), (D) an antibody purified against Peptide 2 (1:1000). Immunnodetection was performed as in Section 8.6. Expected sizes for KEA3 and KEA3-eGFP are highlighted with orange stars.*

The antibodies, pre-immune serum and final bleed were tested against total protein extracts from WT, KO-mutants and complemented mutants (Figure 3.6, see Section 8.6 and

Section 8.6.1.1). The expected apparent size of the WT KEA3 protein is about 75 kDa and that of fusion protein KEA3-eGFP produced by the complemented mutant about 100 kDa. None of these bands appeared on the membrane when blotted with pre-immune serum as expected (Figure 3.6.A). When revealing the membrane with an antibody directed against GFP, a band appeared at the size expected for the fusion protein KEA3-eGFP and none in the WT and KO-mutant lanes (Figure 3.6.E), proving that at least the complemented line did express that protein.

This approach was therefore ineffective to detect the KEA3 protein.

#### *3.4.2.3 Characterization of anti-peptide antibodies on membrane-enriched protein extracts*

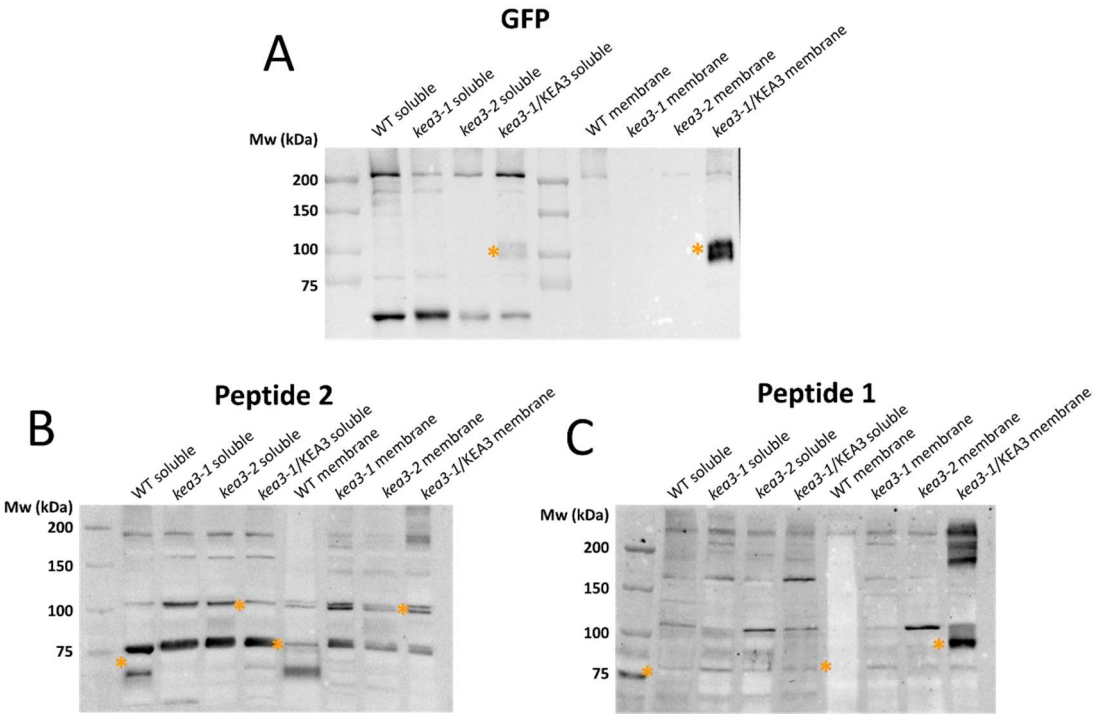


***FIGURE 3.7. CHARACTERIZATION OF ANTI-PEPTIDE ANTIBODIES WITH MEMBRANE-ENRICHED PROTEIN EXTRACTS.***

*SDS-PAGE of soluble and membrane-enriched protein extracts from WT,* kea3-1, kea3-2 *and* kea3-1*/KEA3-eGFP (50 µg total protein/lane). Membranes were hybridized with (A) an antibody against GFP, (B) an antibody purified against Peptide 2 (1:1000), (C) an antibody purified against Peptide 1 (1:1000). Immunnodetection was performed as in Section 8.6. Expected sizes of KEA3 and KEA3-eGFP are highlighted with orange stars.*

In order to circumvent this problem, we settled a new protocol to enrich the total extract with membrane proteins (see Section 8.6.1.2). KEA3 is indeed a highly hydrophobic protein due to its large transmembrane domain that is most likely to be associated with membranes

than other soluble proteins. This was verified in the case of the line *kea3-1*/KEA3-eGFP since the signal obtained from the membrane fraction was higher than in the soluble fraction (Figure 3.7.A), confirming that separating membranes from soluble proteins is a suitable way to improve the detection of KEA3.

The purified antibodies were also tested with this improved protein preparation protocol. Unfortunately, we observed many unspecific signals at the expected size of KEA3 (around 75 kDa) with both antibodies (Figure 3.7.B and C), making the antibodies unusable to detect the WT KEA3 protein.

We only observed a signal at the expected size for the fusion protein KEA3-eGFP in the membrane fraction of *kea3-1*/KEA3-eGFP when using the antibody against Peptide 1 (Figure 3.7.C, orange star) that might correspond to the fused protein.

#### *3.4.2.4 Production an antibody directed against the soluble part of KEA3*

Since the anti-peptide antibodies were not useful tools to detect KEA3, another strategy had to be used. Producing the full length recombinant protein in *E. coli* was impossible, possibly indicating that the full length protein is lethal for bacteria. We thus decided to use as an antigen the soluble sequence of the protein. This truncated part of the protein lacks the catalytic antiporter domain and ought not to induce any cytotoxicity (Figure 3.8).

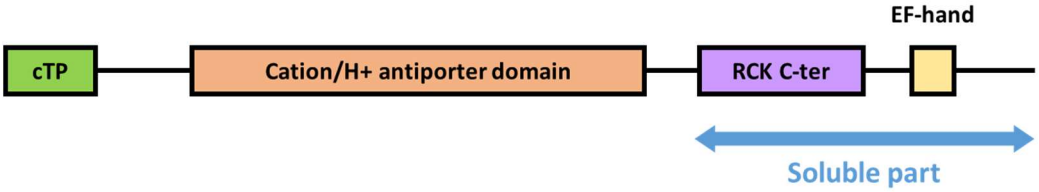


***FIGURE 3.8. THE SOLUBLE PART OF KEA3 CONSISTS OF THE TWO DOMAINS RCK AND EF HAND.***

The soluble part of KEA3 was recombinantly produced in *E. coli* (see Section 8.4.5). One guinea pig was immunized against the purified recombinant protein (Company name). The 42 days after immunization, the serum from the guinea pig was harvested and used for immunodetection. The antibody was then tested by blotting membrane-enriched protein extracts from the four strains studied (WT, the two mutants *kea3-1* and *kea3-2* and the complemented strain *kea3-1*/KEA3-eGFP) and *E. coli* cells overexpressing the antigen using pre-immune serum (Figure 3.9.A) and serum of the immunized guinea pig (Figure 3.9.B).

No bands at the expected size for KEA3 were detected using the pre-immune serum (Figure 3.9.A). A parasitic band around 100 kDa, corresponding to the expected size of the fusion protein, was detected in the four strains. As expected, no signal was detected in the two mutant lanes using the KEA3 antibody (Figure 3.9.B). A band was detected in the WT

protein extracts at the anticipated size of about 75 kDa, while the KEA3-eGFP fusion protein was detected at about 100 kDa. A large band around 37 kDa was detected in the *E. coli* sample, corresponding to the size of the soluble KEA3 fragment overproduced.

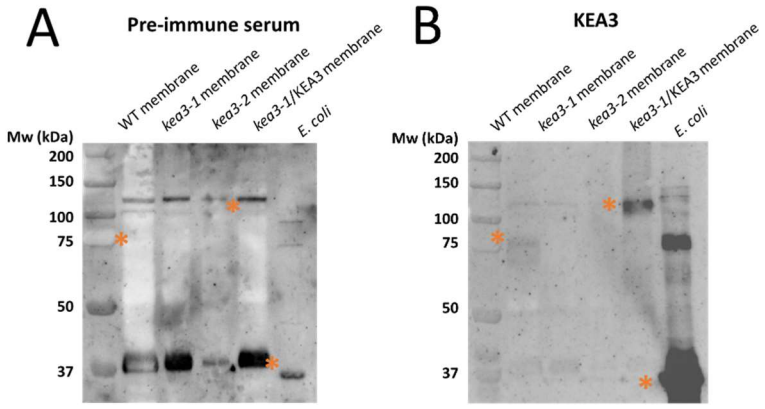


***FIGURE 3.9. CHARACTERIZATION OF THE ANTIBODY DIRECTED AGAINST THE SOLUBLE PART OF KEA3.***
*SDS-PAGE of membrane-enriched protein extracts from WT,* kea3-1, kea3-2 *and* kea3-1*/KEA3-eGFP (50 µg total protein/lane) and* E. coli *overexpressing the soluble part of KEA3 (1µg protein/lane). Membranes were hybridized (A) pre-immune serum (1:1000) (B) serum from the same guinea pig 42 days after immunization with the soluble part of KEA3 as an antigen (1:1000). Expected sizes for KEA3, KEA3-eGFP and the soluble part of KEA3 are highlighted by orange asterisks.*

The signal in the WT lane was quite low, hinting that KEA3 is probably lowly expressed under our standard growth conditions. The amount of KEA3 protein detected in the complemented strain *kea3-1*/KEA3-eGFP is higher than in the WT. This confirms that the complemented strain is also an overexpressor. In the following of this manuscript, this *kea3-1*/KEA3-eGFP strain will indifferently be called "complemented" or "overexpressor".

### 3.4.3 Expression pattern of KEA3 and in the WT and complemented strain

KEA3 was shown to have a light-dependent expression pattern, which could result in a different phenotype depending on the time of the day (see Section 3.2). Additionally, the complemented KO-mutant *kea3-1*/KEA3-eGFP expresses the fusion protein KEA3-eGFP under the control of the Lhcf1 protein. It is thus an overexpressor.

We have thus investigated the expression pattern of Lhcf1 in WT *P. tricornutum* in and compared it to Kea3 in the two *P. tricornutum* datasets previously studied (Chauton *et al.*, 2013; Nymark *et al.*, 2013). Lhcf1 transcription is enhanced in the light and repressed in the dark. A switch from dark to light does not trigger a fast induction of transcription of Lhcf1, unlike in Kea3 (Figure 3.10).

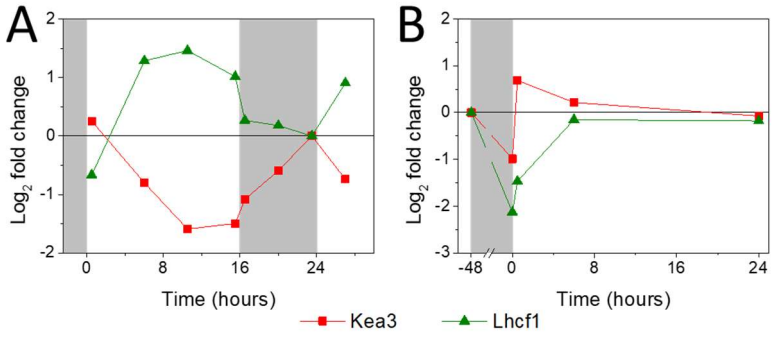


***FIGURE 3.10. TRANSCRIPTION OF GENES KEA3 AND LHCF1 IN RESPONSE TO LIGHT IN* P. TRICORNUTUM.**

*Grey boxes indicate darkness periods. (A) Log2 fold change upon exposure to 16h:8h photoperiod with 150 µmol.photons.m-2 (data from* (Chauton *et al.*, 2013)*). (B) Log2 fold change upon adaption to 100 µmol.photons.m-2 continuous light, followed by 48h of darkness and 100 µmol.photons.m-2 24h of 7continuous light (data from* (Nymark *et al.*, 2013)*).*

The native Kea3 promotor and the Lhcf1 promotor of the overexpressing strain are both regulated by light but in opposing ways. Consequently, the expression of the KEA3 protein in the WT and the complemented strain *kea3-1*/KEA3-eGFP where the expression of the fusion protein is under the control of the Lhcf1 promotor may vary differently depending on light intensity and on the light cycle.

The transcription of Kea3 appears regulated by light (Figure 3.10). Yet the transcription of Kea3 may also be under circadian regulation as under day/light cycles it follows a seemingly cyclic expression. A major actor of the circadian clock has recently been discovered in *P. tricornutum* (Annunziata *et al.*, 2019). It would thus be interesting to verify if the expression of Kea3 is under the control of the transcription factor RITMO by performing qPCR analysis on KO-mutants lacking the said transcription factor.

## 3.5 CELL GROWTH OF MUTANT STRAINS

We compared growth rates in our KO and overexpressing mutants. Three sets of experiments were run. Cells were grown under the standard conditions used for all experiments in this manuscript. The strain *kea3-2* grew slower than all other lines, however such was not the case for the KO-mutant *kea3-1* that had a similar growth rate as the WT (Figure 3.11). We therefore conclude that deleting the KEA3 gene does not affect growth in these conditions.

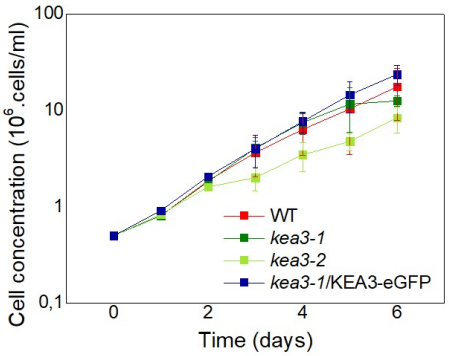


***FIGURE 3.11. CELL GROWTH OF WT, KEA3-1, KEA3-2 AND THE OVEREXPRESSING STRAIN KEA3-1/KEA3-EGFP.***

*N=3 independent experiments, Mean ± SD.*

In *A. thaliana*, the absence of KEA3 did not induce any growth phenotype in standard conditions (Armbruster *et al.*, 2016; Wang *et al.*, 2019), while a very slight decrease of the growth rate could only be observed under fluctuating light conditions (i.e. cycles of 1 minute of high light followed by 5 minutes of low light). (Armbruster *et al.*, 2016).

## 3.6 LOCALISATION OF KEA3

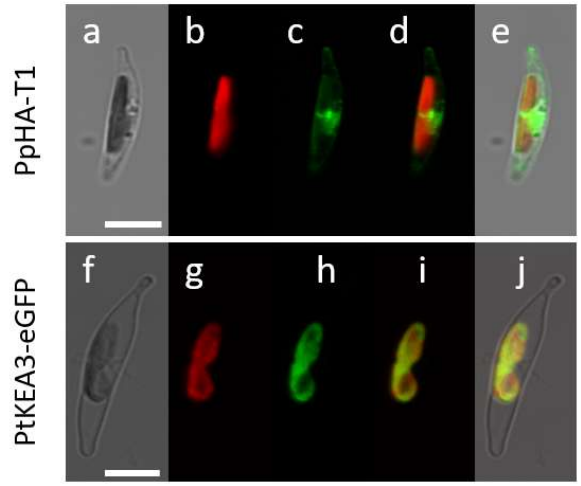


***FIGURE 3.12. LOCALIZATION OF EGFP (A-E) AND FULL-LENGTH KEA3-EGFP FUSION PROTEIN (F-J) EXPRESSED IN P. TRICORNUTUM.***

*(a, f) Bright field, light microscopy images; (b, g) chlorophyll, chlorophyll auto-fluorescence; (c, h) eGFP, GFP fluorescence; (d, e, i, j) merged, merged channels. The scale bar represents 5 µm. Collaboration with H. Hu.*

Although KEA3 is predicted to be targeted to the chloroplast (see Section 3.1.2), this must be verified experimentally. Cells have been transformed with the fusion protein KEA3-eGFP by electroporation according to the protocol from (Zhang and Hu, 2014) under the control

of the Lhcf1 promotor (H. Hu, Wuhan, China, in collaboration). These strains were imaged using confocal microscopy. Another strain was constructed by the same method as a control expressing eGFP under the control of the Lhcf1 promotor.

When expressed recombinantly in *P. tricornutum*, eGFP is targeted to the cytosol (Figure 3.12. a-e). When fused to KEA3, the eGFP fluorescence colocalizes with chlorophyll autofluorescence (Figure 3.12. f-j).

KEA3 is therefore expressed in the chloroplast of *P. tricornutum*. This plastid is quite complex as it is surrounded by four membranes (Flori *et al.*, 2016). The fluorescence pattern of eGFP fusion proteins addressed to any of these four membranes often encircles chlorophyll autofluorescence (Moog *et al.*, 2015; Liu *et al.*, 2016). Such is not the case for the fusion protein KEA3-eGFP (Figure 3.12. f-j). This protein is thus most likely targeted to the thylakoid membrane.

## 3.7 CONCLUSION

The gene Phatr3_J39274 was identified as the most likely homologue of *A. thaliana* KEA3 in the diatom *P. tricornutum*. Additionally, it has the same regulation pattern regarding light as the homologue of KEA3 in the green alga *C. reinhardtii*, i.e. its transcription is induced in the dark and decreases in the light. The resulting protein is likely targeted to the thylakoid membrane.

A set of KO-mutants and overexpressors were constructed and characterized. These strains have further been used to unveil the pH-dependency of NPQ in diatoms.

# 4 REGULATION OF PHOTOPROTECTION BY THE TRANSPORTER KEA3 IN *P. TRICORNUTUM*

In *A. thaliana,* KEA3 was shown to be involved in NPQ induction and relaxation kinetics (Armbruster *et al.*, 2014, 2016; Wang *et al.*, 2017). To test if the protein KEA3 may be playing a similar role in diatoms, the photoprotective response of WT, KO-mutants and complemented strains were compared in various light conditions.

## 4.1 USE OF NIGERICIN TO CHARACTERIZE KEA3 MUTANTS

Nigericin is an ionophore catalyzing K+/H+ exchange across biological membranes. Used at low concentrations, it modifies the composition of the proton motive force by decreasing ΔpH and partially compensating it with ΔΨ. At higher concentrations, it dissipates both components of the proton motive force and acts as an uncoupler (Ahmed and Booth, 1983; Pu, Wang and Chen, 1995). Therefore, if used at low concentrations, e.g. 0.05 to 2 µM in *E. coli* (Ahmed and Booth, 1983), the transport activity of nigericin could mimic that of KEA3 (Figure 4.1). In *A. thaliana,* infiltration of low doses of nigericin in *kea3* KO-mutants successfully restored the WT phenotype (Armbruster *et al.*, 2014). Since both nigericin and KEA3 catalyze $K^+/H^+$ exchange, nigericin could be a powerful tool to characterize the role of KEA3 in diatoms.

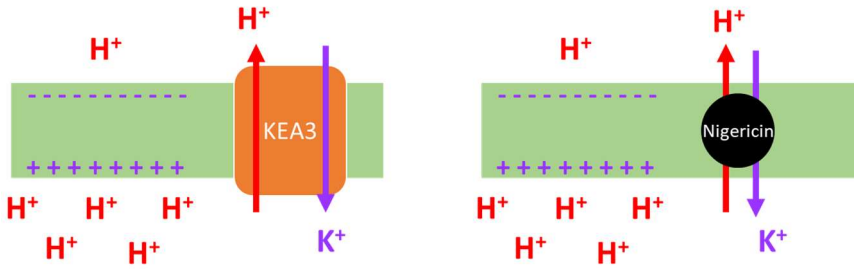


***FIGURE 4.1. FUNCTIONAL EQUIVALENCE BETWEEN NIGERICIN AND KEA3 IN RESPONSE TO A PROTON GRADIENT ACROSS A BIOLOGICAL MEMBRANE.***

In order to determine the proper nigericin concentration to characterize the mutants described in Section 3, we have measured photosynthetic parameters of *P. tricornutum* WT and mutants in the presence of various concentrations of nigericin (Figure 4.2). NPQ was induced in dark-adapted *P. tricornutum* cells as explained in Section 8.8.1.

Cells were exposed to high light (1227 µmol.photons.m$^{-2}$). Since this light was considerably higher than the growth light (40 µmol.photons.m$^{-2}$), NPQ was induced and reached ~2 units in about 5 minutes in standard conditions, meanwhile the efficiency of PSII dropped from ~0.7 in the dark to ~0.03. Following high light exposure, cells were then exposed to low light (30 µmol.photons.m$^{-2}$) and NPQ relaxed within 15 minutes while $\Phi_{PSII}$ recovered up to ~0.6. NPQ was relaxed in low light because it was shown to be very slow in the dark in *P. tricornutum* (Ruban *et al.*, 2004; Goss *et al.*, 2006) (see Section 4.4).

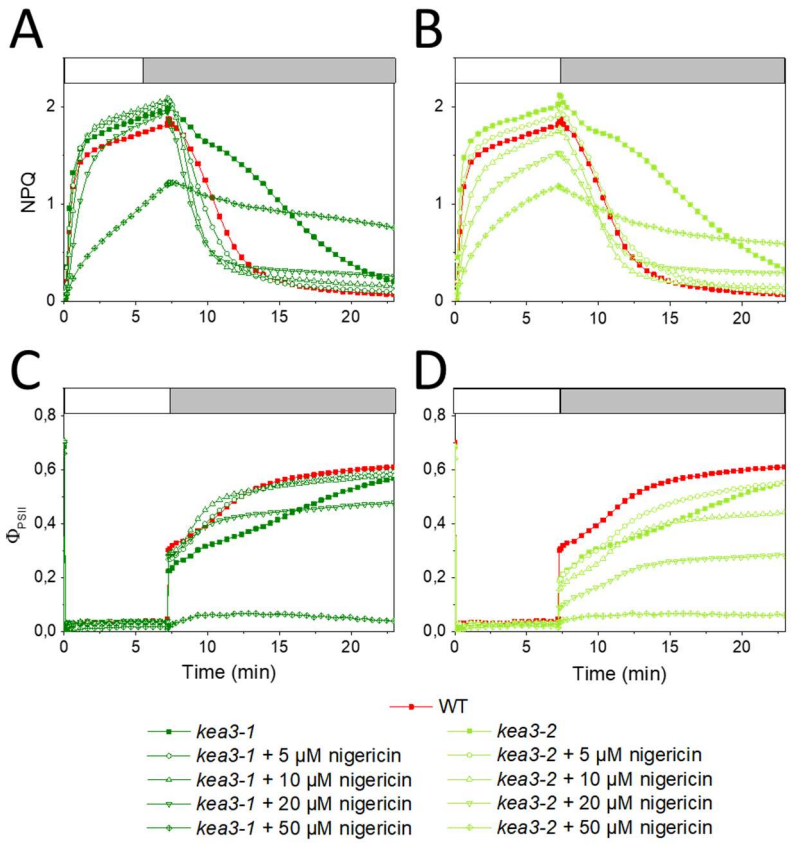


***FIGURE 4.2. EFFECT OF NIGERICIN ON KEA3 KO MUTANTS.***

*NPQ was induced in high light (1200 µmol.photons.m$^{-2}$, white box), followed by relaxation in low light (30 µmol.photons.m$^{-2}$, grey box) in WT* P. tricornutum *cells and in the two mutants (A, C)* kea3-1 *and (B, D)* kea3-2 *in the presence of various doses of nigericin ranging from 5 to 50 µM. (A, B) NPQ and (C, D) $\Phi_{PSII}$ traces are shown. One representative experiment.*

Although nigericin is added in the external medium of cells, it does penetrate across thylakoid membranes as increasing doses of nigericin have an effect on PSII fluorescence. Both mutants are affected in their fluorescence kinetics as compared to the WT: NPQ relaxation and $\Phi_{PSII}$ recovery are slower in the mutants (Figure 4.2).

At 50 µM nigericin, $\Phi_{PSII}$ does not recover in low light while NPQ remains high even after 15 minutes of relaxation in low light. This is a signature of photoinhibition (qI), hinting that this dose of nigericin induces toxic and possibly non-specific effects e.g. disruption of cytoplasmic pH.

NPQ relaxation and $\Phi_{PSII}$ recovery in low light in the mutant accelerate in the presence of small doses of nigericin (5 to 10 µM) up to reaching similar kinetics as in the WT. These doses therefore complement the phenotype of the KO-mutants without promoting photoinhibition since the steady-state $\Phi_{PSII}$ reached after 15 minutes of low light is the same with or without these small doses of nigericin. The concentration of 10 µM of nigericin was chosen to conduct the rest of experiments since it efficiently complements KO-mutants.

## 4.2 EFFECTS OF KEA3 AT DIFFERENT LIGHT INTENSITIES ON NPQ KINETICS

### 4.2.1 KEA3 does not affect photoprotective capacities

#### *4.2.1.1 KEA3 leaves the maximum NPQ capacity unchanged*

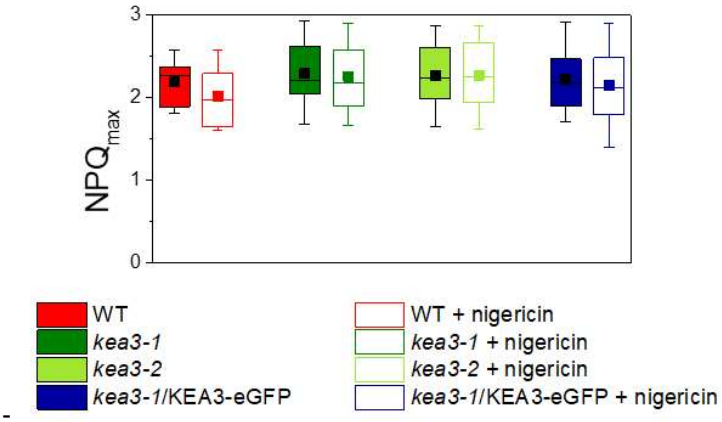


***FIGURE 4.3. $NPQ_{MAX}$ IS UNAFFECTED BY THE PRESENCE OF KEA3.***

*Maximum NPQ levels reached during 7 minutes of illumination at 1200 µmol.photons.m$^{-2}$ in WT, two KO-mutants (*kea3-1 *and* kea3-2*) and one complemented strain (*kea3-1*/KEA3-eGFP) with and without 10 µM nigericin. N = 15 independent biological replicates. Middle line: median line. Whiskers: extreme values. Squares: mean value. Box: 2$^{d}$ and 3$^{rd}$ quartiles.*

When *P. tricornutum* cells are illuminated for 7 minutes with high light (1200 µmol.photons.m-$^{2}$), they reach a maximum NPQ, which will be called $NPQ_{max}$ in the rest of this manuscript. $NPQ_{max}$ varies between the different biological samples, independently of the genotype or the light treatment (Figure 4.3). In the presence of nigericin, $NPQ_{max}$ is slightly lower in the WT than in control conditions, although this difference not significant.

Except for this, $NPQ_{max}$ was not affected in the two KO-mutants and in the overexpressing strain in control conditions and with nigericin (Figure 4.3). KEA3 thus mostly affects NPQ kinetics and not the extent of NPQ capacity.

It appears thus reasonable to normalize each acquisition to $NPQ_{max}$ of the control to smoothen the effect of biological variations and access to otherwise hidden information.

In low light grown *P. tricornutum* cells, the maximum NPQ is correlated with the expression of LHCX1 that varies during the day (Bailleul *et al.*, 2010; Taddei *et al.*, 2016). Additionally, very tiny differences in cell concentration between different biological replicates result in different light exposure perceived by each individual cell, triggering different extents of NPQ response. Experimental precautions were undertaken to minimize these variations as for timing and cell concentration during measurement, yet these were not sufficient to remove all discrepancies. We therefore attributed them to natural variations occurring between independent biological samples.

#### *4.2.1.2 Photosynthetic complexes are unaffected by the presence of KEA3*

$NPQ_{max}$ is controlled by the expression of the different LHCX isoforms (Bailleul *et al.*, 2010; Taddei *et al.*, 2016, 2018; Buck *et al.*, 2019). Western blot analysis revealed that the accumulation of LHCX proteins was not affected in the WT, KO mutants and overexpressing lines (Figure 4.4), providing a rationale for the unchanged $NPQ_{max}$.

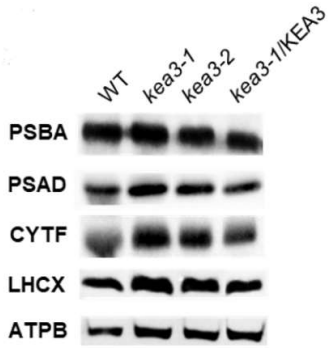


***FIGURE 4.4. ACCUMULATION OF PHOTOSYNTHETIC COMPLEXES AND LHCX IN WT AND MUTANT STRAINS.***

*Total protein extracts from WT, KO-mutants* kea3-1 *and* kea3-2 *and overexpressor* kea3-*1/kea3-eGFP were analysed by immunodetection using antisera directed against PSBA (Photosystem II D1 protein, 25 µg), Cyt f ($b_6f$ complex PETA protein, 50 µg), PSAD (Photosystem I subunit, 20 µg), LHCX (20 µg). ATPB (ß subunit of ATP synthase mitochondrial and chloroplastic, 20 µg) is used as loading control.*

Similarly, none of the main photosynthetic complexes (PSI, PSII or cytochrome $b_6f$) were affected in protein accumulation in the KEA3 mutants or the overexpressor. We can thus

conclude that the photosynthetic architecture of KEA3 mutants is most likely identical to that of the WT.

### 4.2.2 KEA3 slows down NPQ induction in high light

During the first minutes of high light onset following dark-adaption, NPQ induction is very fast as 75% of NPQmax is reached in about 2 minutes (Figure 4.5). During that period, NPQ induction is faster in both KO-mutants than in the WT, itself faster than the overexpressor strain. The NPQ induction rate in the KO-mutants can be decreased to WT-like levels with the addition of an appropriate amount of nigericin (Figure 4.5), thus performing a chemical complementation of the KO-mutants.

This indicates that KEA3 is active in high light during NPQ induction through $K^+/H^+$ exchange by evacuating protons from the lumen, as evidenced by the chemical complementation of the mutants by nigericin. However in high light KEA3-dependent proton transport, even when the protein is overexpressed (Figure 4.5.C), is not sufficient to affect $NPQ_{max}$.

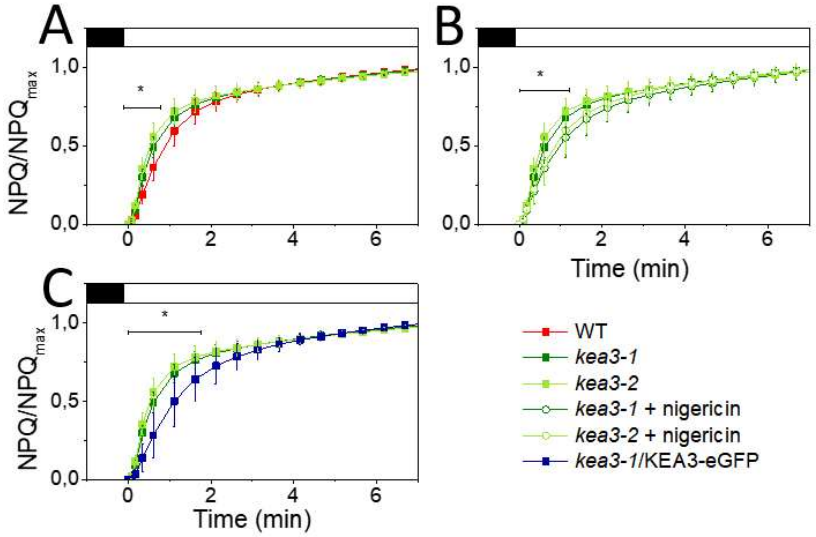


***FIGURE 4.5. NPQ INDUCTION IN HIGH LIGHT.***

*WT, two KO-mutants with and without 10 µM nigericin addition (*kea3-1 *and* kea3-2*) and one overexpressor strain (*kea3-1*/KEA3-eGFP). P. tricornutum cells were dark-adapted (black box), exposed to high light (1200 µmol.photons.m$^{-2}$, white box) and then to low light (30 µmol.photons.m$^{-2}$, grey box). N = 15 independent biological replicates, Mean ± SD. Asterisks indicate statistically significant differences between resp. WT, KO-mutants with nigericin or overexpressor with both of the KO-mutants ($p < 0.05$). No differences were detected between the two mutant lines either with or without nigericin addition.*

### 4.2.3 KEA3 affects the extent of photoprotection in moderate high light

When exposing WT cells to moderate light (about 3 times the growth light, Figure 4.6), NPQ is also induced at about half $NPQ_{max}$. observed in high light (Figure 4.6) Both mutants induce more NPQ (0.75 $NPQ_{max}$) than the WT and the overexpressor at moderate high light. In the presence of nigericin, NPQ in the mutants decreases to WT-like levels, while the WT and complemented mutant lines are less sensitive to nigericin addition.

Moderate high light induces different extents of photoprotection depending on the presence of KEA3. Not only is KEA3 active under these conditions, but these experiments also show that the induced NPQ response quantitatively depends on $K^+/H^+$ exchange, and thus of the dynamics of the proton motive force.

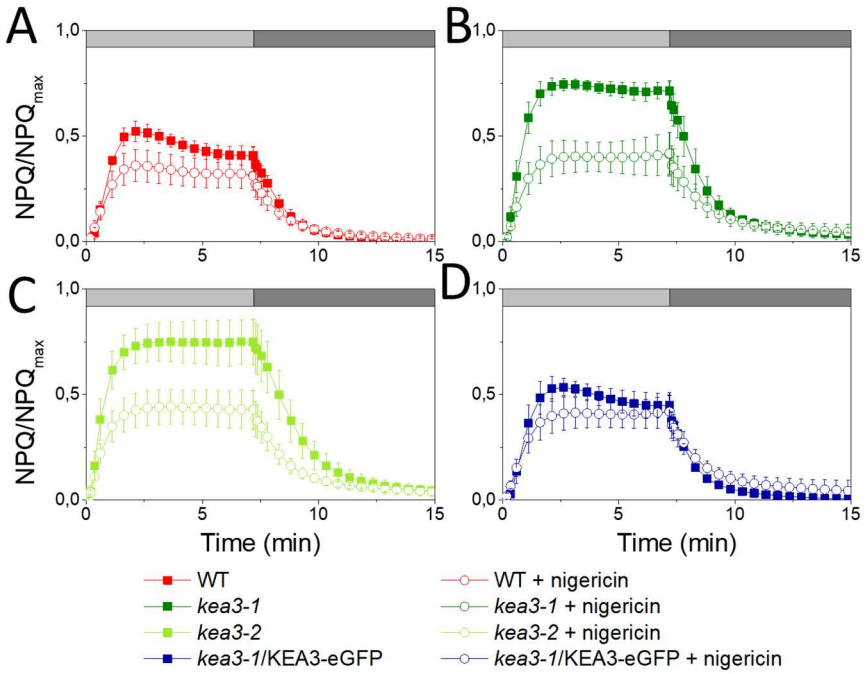


***FIGURE 4.6. NPQ INDUCTION IN MODERATE HIGH LIGHT.***

*NPQ was induced in (A) WT, KO-mutants (B)* kea3-1 *and (C)* kea3-2 *and (D) overexpressor mutant* kea3-1*/KEA3-eGFP cells at to moderate light (125 µmol.photons.m$^{-2}$, light grey box) followed by relaxation in low light (30 µmol.photons.m$^{-2}$, dark grey box).*

### 4.2.4 KEA3 affects NPQ relaxation kinetics in low light

To study NPQ relaxation, NPQ was induced in high light (1200 µmol.photons.m$^{-2}$) in the four strains studied with or without nigericin. When $NPQ_{max}$ was reached, the light was switched to low light (30 µmol.photons.m$^{-2}$). NPQ then relaxed.

Nigericin accelerates NPQ relaxation in the WT (Figure 4.7.A). NPQ relaxation in both mutant lines *kea3-1* and *kea3-2* is significantly slower than in the WT (Figure 4.7.B), while

10 µM nigericin addition accelerates NPQ relaxation in both mutant lines to WT-like levels (Figure 4.7.C) and thus chemically complements the KO phenotype. NPQ relaxation in the overexpressor is slower than in both WT lines and, unlike in the WT and KO-mutants, insensitive to nigericin addition (Figure 4.7.D and E).

Therefore, KEA3 accelerates NPQ decay in low light in a quantitative manner: the higher the amount of KEA3 protein expressed, the faster NPQ relaxation.

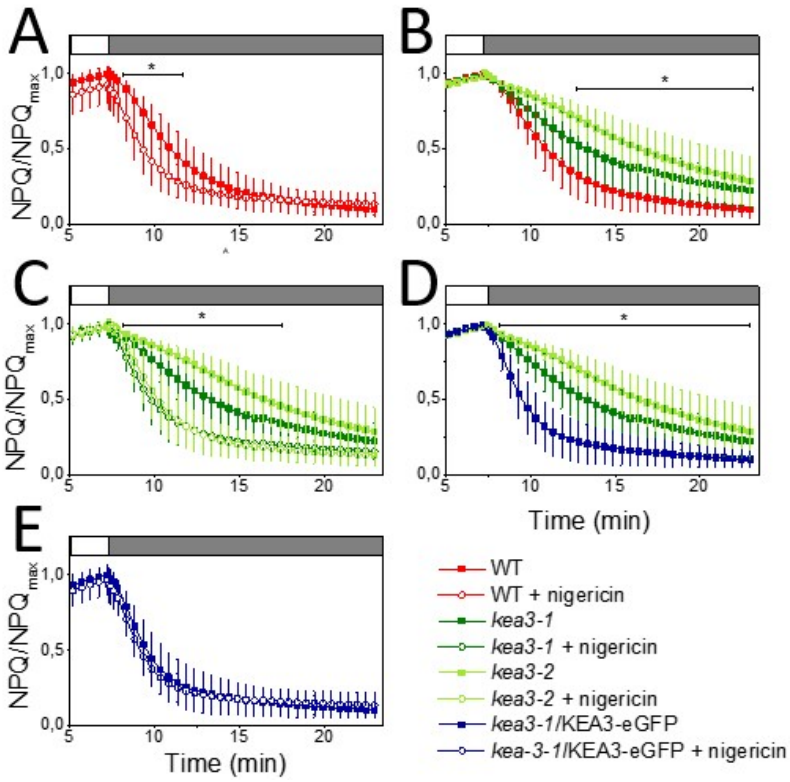


***FIGURE 4.7. NPQ RELAXATION KINETICS IN LOW LIGHT.***

*NPQ was induced to NPQmax for 7 minutes at high light (1200 µmol.photons.m$^{-2}$, white box) and relaxed in low light (30 µmol.photons.m$^{-2}$, grey box) in WT, KO-mutants* kea3-1 *and* kea3-2 *and overexpressor* kea3-1*/KEA3-eGFP with and without 10 µM nigericin. N = 15 independent biological replicates, Mean ± SD. Asterisks indicate statistically significant differences between samples either the WT, the overexpressor or both of the KO-mutant strains ($p < 0.05$).*

## 4.3 KEA3 MODULATES LIGHT UTILIZATION IN *P. TRICORNUTUM*

Having established that KEA3 is involved in modulating the speed of NPQ induction (Figure 4.5) and relaxation (Figure 4.7) but also the extent of NPQ at steady state at moderate high light (Figure 4.6), we have investigated the influence of the presence of KEA3 on light utilization on a wide panel of light intensities (Figure 4.8).

The Relative Electron Transfer Rate (rETR) is a proxy for the speed of electron transfers across the linear electron chain, and is therefore a good parameter to monitor photosynthetic efficiency (see Section 1.4.2).

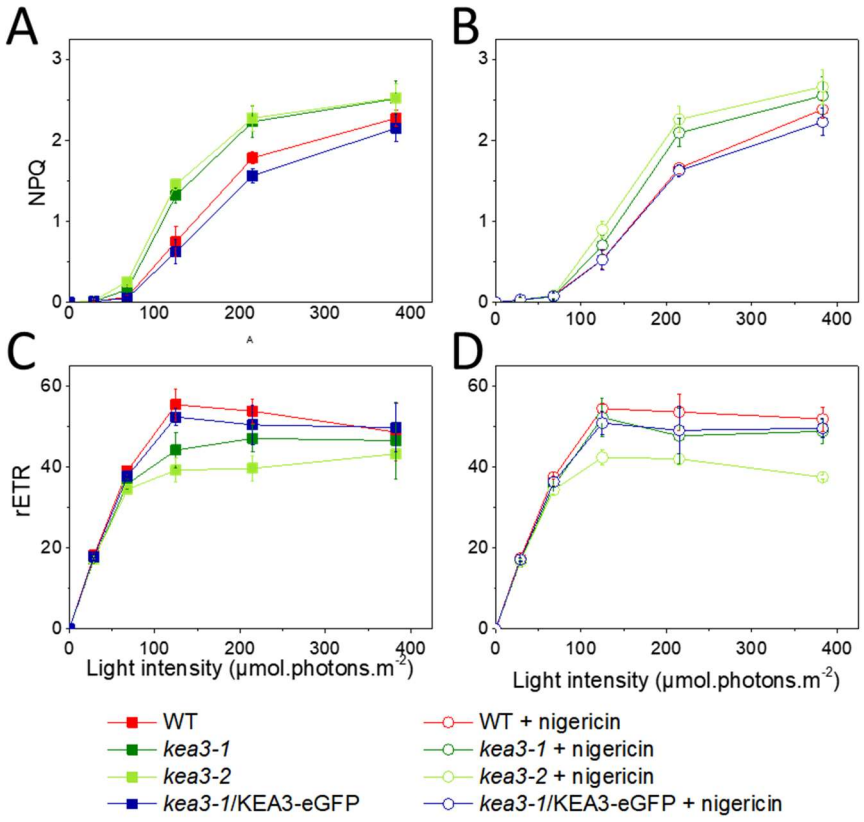


***FIGURE 4.8. KEA3 AND NIGERICIN MODULATE LIGHT UTILIZATION IN P. TRICORNUTUM.***

*Cells were exposed to the indicated light intensity. NPQ (A, B) and rETR (C, D) were measured at steady state in the absence (A, C) or in the presence (B, C) of 10 µM nigericin. N=3 independent biological replicates. Mean ± s.e.m.*

At low light intensities (0 to 70 µmol.photons.m$^{-2}$), neither NPQ nor rETR are affected by the presence of KEA3 or nigericin (Figure 4.8). However, at moderate high light intensities (125 to 200 µmol.photons.m$^{-2}$), the KO-mutants reach higher NPQ values than the WT. This is partially reversed by the addition of 10 µM nigericin, while rETR for the KO-mutants becomes saturated, i.e. KO-mutants reach their maximum electron transfer capacity. At high light (400 µmol.photons.m$^{-2}$ and above), all cell lines reach a similar $NPQ_{max}$ while the maximum rETR value for KO-mutants is lower than for the WT and overexpressor. Adding nigericin to the KO-mutants restored the maximum rETR value in the mutant *kea3-1* but not in the mutant *kea3-2* (Figure 4.8.B). However, this mutant was also shown to grow slower than all the other cell lines (see Section 3.5) and the absence of ETR recovery even in the presence of nigericin is probably due to a defect in the mutant itself rather than to a

toxic effect of nigericin. Thus, KEA3 limits the rate of electron transfer at high light intensities but not in low light.

The presence of KEA3 is able to shift NPQ induction or rETR saturation to higher light intensities. However, this difference observed between the four strains studied does not stem from an acclimation to high light as has often been observed (Serôdio and Lavaud, 2011) since the maximum NPQ capacity of all the strains is similar. KEA3 thus controls light utilization in *P. tricornutum* and especially the shift from a light harvesting state to a photoprotective state within the photosystem antennae.

## 4.4 KEA3 IS INACTIVE DURING NPQ RELAXATION IN THE DARK

Unlike in plants or green algae, NPQ relaxation in diatoms is very slow in the dark (Ruban *et al.*, 2004; Goss *et al.*, 2006). Since KEA3 accelerates NPQ relaxation in low light (see Section 4.2.4), we have investigated whether it could also play the same role in the dark.

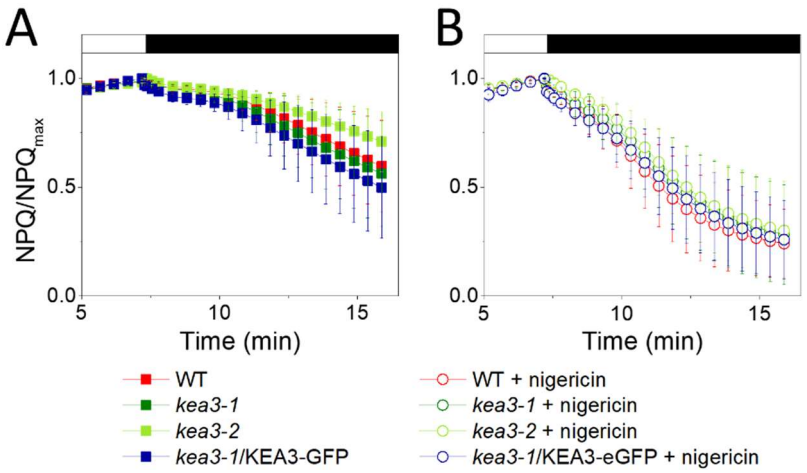


***FIGURE 4.9. NPQ RELAXATION KINETICS IN THE DARK.***

*NPQ was induced to $NPQ_{max}$ for 7 minutes in high light (1200 µmol.photons.m$^{-2}$, white box) and then relaxed in the dark in the WT, KO-mutants* kea3-1 *and* kea3-2 *and the overexpressor mutant* kea3-1*/KEA3-eGFP, with and without 10µM nigericin. N = 5 independent biological replicates, Mean ± SD.*

No statistically significant differences were detected in the relaxation speed of KEA3 KO or overexpressor mutants strains compared to the WT for a dark-relaxation of NPQ (Figure 4.9, $p > 0.05$). Nigericin addition accelerated NPQ relaxation in all strains, up to a speed comparable to NPQ relaxation in low light (Figure 4.8). KEA3 is therefore not involved in accelerating NPQ relaxation in the dark; however nigericin addition fastened it up. This indicates that the slow NPQ relaxation speed in the dark observed in diatoms is due to a slow relaxation of the proton gradient. The absence of differences is relaxation speed

between the four genotypes studied hints that KEA3 is probably not involved in this proton transfer. We thus deduce that KEA3 is not active in the dark.

In diatoms, NPQ relaxation is tightly dependent on the epoxidation of the pigment diatoxanthin into diadinoxanthin. Notably, NPQ is proportional to the de-epoxidation state (DES) of these pigments (Lavaud *et al.*, 2002). In order to verify that KEA3 did not alter this relationship, we induced NPQ at several levels in the four mutant lines in the presence or absence of nigericin (Figure 4.10, see Section 8.7 for experimental details) and noticed that the proportionality between NPQ and DES is conserved. This result is in line with a previous study that showed that uncoupling the thylakoid proton gradient did not affect the relationship between pigments and de-epoxidation state (Goss *et al.*, 2006).

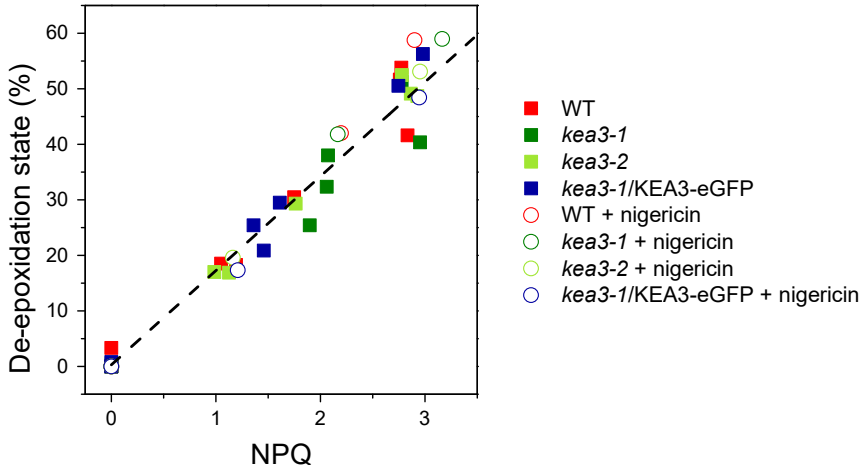


***FIGURE 4.10. NPQ REMAINS PROPORTIONAL TO THE DE-EPOXIDATION STATE OF THE PIGMENTS IN THE FOUR LINES STUDIED AND IN THE PRESENCE OF NIGERICIN.***

NPQ and the de-epoxidation state (DES) of the xanthophyll cycle were proportional no matter if the KEA3 protein or nigericin were present. We can therefore assume that NPQ relaxation in the dark still was correlated with DES, as stated in (Goss *et al.*, 2006).

We have shown that KEA3 is involved in modulating NPQ levels depending on the light intensity while it is inactive during NPQ relaxation in the dark. Since NPQ and the DES remain proportional no matter if KEA3 is present, KEA3 is also involved is modulating the DES. However, the KEA3-dependent regulation of the xanthophyll cycle takes place upstream of the PSII antenna quenching process.

## 4.5 KEA3 MODULATES THE PROTON MOTIVE FORCE

A major regulator of NPQ is the proton motive force and most precisely its chemical component ΔpH (see Section 1.4.4). By regulating the p.m.f., KEA3 could therefore affect downstream the extent of NPQ and DES.

To check whether KEA3 is involved in regulating the proton motive force, cells were adapted to conditions in which the NPQ phenotype of KO-mutants was altered compared to WT, i.e. moderate high light where the strains have a different NPQ level (see Section 4.2.3, Figure 4.11) and high light since the following relaxation in low light had different kinetics depending on the strain(see Section 4.2.4, Figure 4.11). They were then shifted to dark and relaxation of the electric field generated across the thylakoid membrane (ΔΨ) was measured using the ECS method (Witt, 1979; Bailleul *et al.*, 2015). By plotting the linear versus quadratic components of the ECS signal, one can estimate the fraction of ΔΨ remaining after ~ 80 ms of switch to darkness (see Section 8.8.2 for experimental details). Nigericin dissipates the ΔpH component of the proton motive force and thus converts it into ΔΨ (Ahmed and Booth, 1983; Pu, Wang and Chen, 1995). A rise in the ΔΨ in the presence of nigericin can therefore be interpreted as the signature of a dissipated ΔpH. This experiment was performed in the four cell lines studied, with and without nigericin, in high and moderate high light (Figure 4.11).

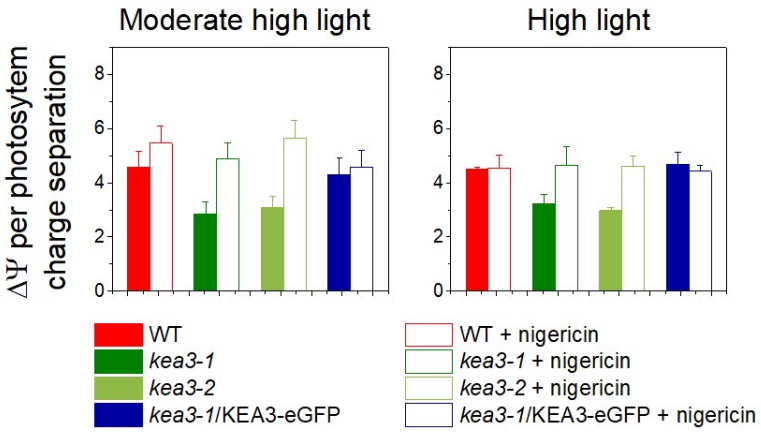


***FIGURE 4.11. EVALUATION OF COMPOSITION OF THE PROTON MOTIVE FORCE IN THE WT AND MUTANT LINES USING THE ECS METHOD.***

*Cells were acclimated to moderate high light (125 µmol.photons.m$^{-2}$) or to high light (1200 µmol.photons.m$^{-2}$) before measurement with and without 10 µM nigericin. The ΔΨ component of the proton motive force was normalized on the signal produced by one charge separation per photosystem induced by a single turnover flash. N = 3 independent biological replicates. See Section 8.8.2 for methods.*

In the two KO lines lacking KEA3, the ΔΨ is lower than in the WT and complemented strain and increases upon addition of nigericin, confirming that a ΔpH is indeed present in these strains under high or moderate high light (Figure 4.11). Because the ECS signals correspond to absorption changes of pigments embedded into the thylakoid membrane, the effect of nigericin on the KO mutants confirms that the ΔpH present in these lines spans the

thylakoid membrane. This experiment thus consolidates the localization of KEA3 determined by confocal imaging (see Section 3.6).

Unlike in the mutants, nigericin did not induce a significant rise in ΔΨ in the WT and in the cell line overexpressing KEA3 (Figure 4.11), suggesting that the amplitude of the ΔpH was lower in these lines. However, concluding that no ΔpH was present in these lines would be a mistake. Indeed, nigericin-dependent conversion of ΔpH into ΔΨ is prompt to energetic leaks, i.e. not all the energy stored in the form of ΔpH is readily converted into ΔΨ (Ahmed and Booth, 1983). If the ΔpH present in the WT and overexpressing lines were substantially smaller than in the KO mutants, the ECS method might not be sensitive enough to detect the small changes in ΔΨ in WT and overexpressing lines.

Cell lines expressing KEA3 have a higher ΔΨ component than KO lines lacking KEA3 in the absence of nigericin. This suggests that the functional homology between KEA3 and nigericin goes further than expected: just like nigericin, KEA3 does not just dissipate ΔpH but transforms its energy into ΔΨ. A possible mechanism for this conversion will be debated in the Discussion section.

In the model plant *Arabidopsis thaliana* (Armbruster *et al.*, 2014, 2016; Correa-Galvis *et al.*, 2020), KEA3 is believed to act principally on the ΔpH component of the proton motive force. Before this work, the only protein known to affect the proton motive force in diatoms was the mitochondrial alternative oxidase AOX (Bailleul *et al.*, 2015).

## 4.6 Regulation of KEA3 by calcium

We have shown that KEA3 dissipates the proton gradient across the thylakoid membrane in the light (Section 4.2) but not in the dark (Section 4.4). It ensues that the activity of KEA3 must be regulated.

A distinctive feature of KEA3 homologues from the green and the red lineage is the presence of an EF-hand in sequences from most red algae and stramenopiles investigated (see Section 3.1.2). An EF-hand is a small protein domain able to reversibly bind calcium with high affinity (Figure 4.12.A). Calcium binding induces a structural change as the two helixes fold around the coordinated calcium ion (Yap *et al.*, 1999). These domains are often found by pairs, however sometimes like in KEA3 only one of these motifs is present. In an example found in the literature (Zhou, Frey and Yang, 2009) calcium binding on an EF-hand induced dimerization of a protein (Figure 4.12.B). Such could also be the case for KEA3. Dimerization is all the more expected in KEA3 as transporters bearing a RCK domain are often found as oligomers (Roosild *et al.*, 2009).

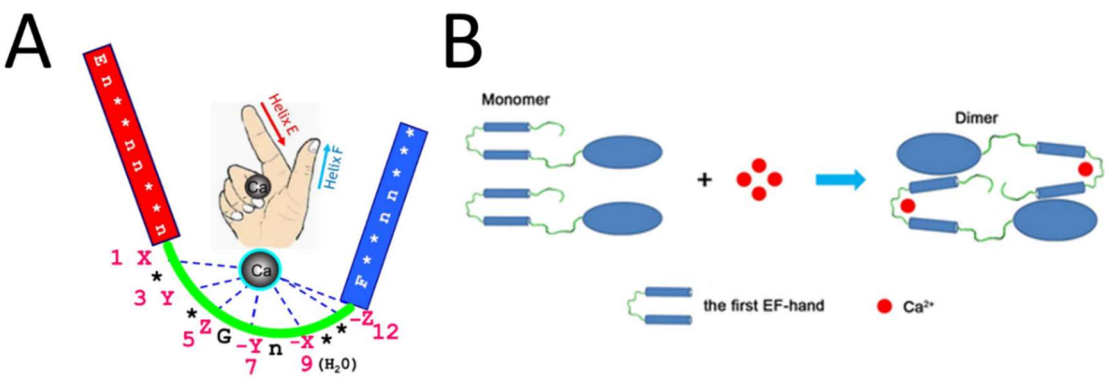


***FIGURE 4.12. STRUCTURAL CHANGES INDUCED BY CALCIUM BINDING ON AN EF-HAND.***

*(A) Cartoon of the canonical EF-hand motif, containing a helix-loop-helix topology. $Ca^{2+}$ can be coordinated by oxygen atoms born by residues in the loop. Adapted from* (Zhou, Frey and Yang, 2009). *(B) Calcium binding on an EF-hand induced dramatic structural changes, including in this case dimerization of the human MICU2. From* (Li *et al.*, 2016).

We have thus investigated whether calcium could be involved in regulating $K^+/H^+$ exchange in KEA3.

### 4.6.1 KEA3 binds calcium in vitro

In order to assess if KEA3 is able to bind calcium, we performed an SDS-PAGE analysis on total protein extracts from the overexpressor *kea3-1*/KEA3-eGFP. Detection of the fusion protein KEA3-eGFP is indeed easier than the WT KEA3 protein since such can be done using a highly sensitive, commercial antibody targeted against GFP. Total protein extracts were separated under denaturing conditions (see Section 8.6 for experimental procedures) in acrylamide gels either standard (Figure 4.13.A), supplemented with calcium (Figure 4.13.B), supplemented with the calcium chelator EGTA (Figure 4.13.C) or with the divalent cation magnesium (Figure 4.13.D).

A smear appears on top of the signal corresponding to the fusion protein at the expected size of 100 kDa in control conditions (Figure 4.13.A). The smear disappears in the presence of calcium (Figure 4.13.B). In the presence of the calcium chelator EGTA, the equilibrium between the two bands is shifted towards the higher molecular weight (Figure 4.13.C). The smear is unaffected by the addition of magnesium (Figure 4.13.D), showing that this effect is specific for calcium ions and not for divalent cations in general.

The observed bandshift of the fusion protein in the presence of calcium can be explained by the structural changes triggered by calcium binding on an EF-hand. The binding of Ca2+ to an EF-hand is often so strong that it remains even under the denaturing conditions encountered in a SDS-PAGE. When calcium is bound, the folding of the domain makes the

protein more hydrophobic and results in an electromobility shift of around 15 kDa (Ishitani *et al.*, 2000). This bandshift is of the same order of magnitude as in our experiment (Figure 4.13), confirming that the fusion protein KEA3-eGFP is able to bind calcium *in vitro*, which ought to have implications on the function of the protein *in vivo*.

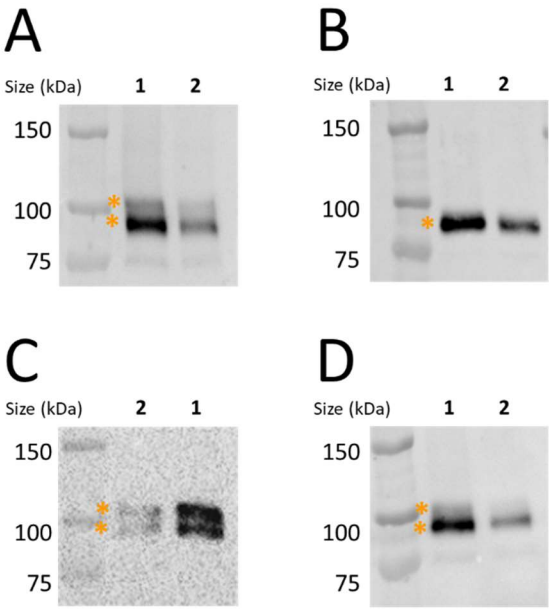


***FIGURE 4.13. KEA3 BINDS CALCIUM* IN VITRO.**

*SDS-PAGE of total protein extracts from two different* kea3-1*/KEA3-eGFP overexpressing strains (lanes 1 and 2) with an antibody directed against eGFP in (A) control conditions (B) the presence of 1mM $CaCl_2$ (C) 10mM EGTA and (D) 1mM $MgCl_2$. Orange starts highlight bands corresponding to the fusion protein KEA3-eGFP.*

### 4.6.2 Construction of an EF-hand mutant

In order to address further this question, we have constructed new mutants of KEA3 lacking the EF-hand and investigated its physiology.

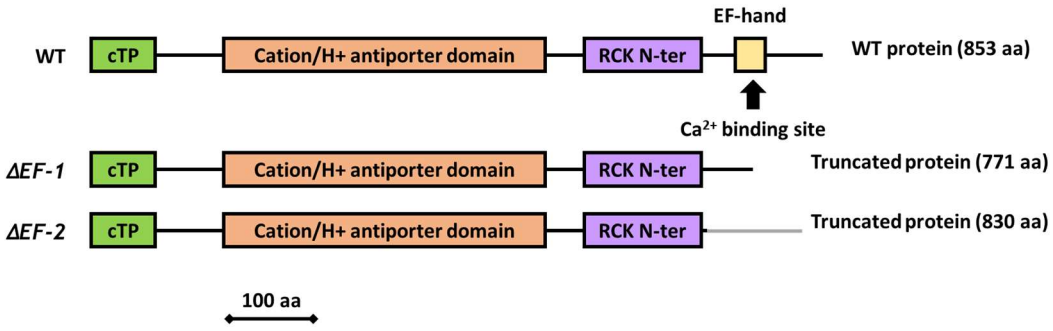


***FIGURE 4.14. CARTOON OF THE PROTEIN DOMAINS OF THE WT AND THE TWO MUTANTS LACKING THE EF-HAND.***

*The aberrant protein sequence of the mutant ΔEF-2 is displayed in grey.*

These mutants were constructed using the CRISPR-Cas9 technique and biolistic transformation (Allorent *et al.*, 2018) (see Section 8.5). They derive from two independent transformations and two different CRISPR-Cas9 target sites (Figure 4.14). A 8 bp deletion in the CDS of the mutant *ΔEF-1* caused a frameshift and the appearance of an early stop codon before the calcium binding loop (Figure 4.14). In the mutant *ΔEF-2*, an off-frame 9 bp deletion resulted in a modified primary sequence (in grey in Figure 4.14). Both mutants thus lack the calcium binding site and the EF-hand domain of KEA3.

### 4.6.3 NPQ phenotype of EF-hand deprived mutants (preliminary results)

We tested the phenotype of the mutant *ΔEF-1* in a transition from high light to low light and moderate high light to low light. The mutant *ΔEF-1* had a similar $NPQ_{max}$ value as the other strains (not shown). When shifted from high light to low light, NPQ relaxation in the mutant *ΔEF-1* is faster than both KO-mutants but seemingly slower than the WT (Figure 4.15.A). Besides, when exposed to moderate high light, NPQ induction in the ΔEF-1 mutant reaches ~0.4 NPQmax, a value comprised in-between the WT (~0.2 NPQmax) and the KO-mutants (~0.5 to 0.7 NPQmax, Figure 4.15.B). In these two situations, 10 µM nigericin addition in the mutant lacking an EF-hand reversed the phenotype to the WT situation (not shown). In a transition from high light to dark, the speed of NPQ relaxation in the WT, KO and *ΔEF-1* mutants was similar (not shown).

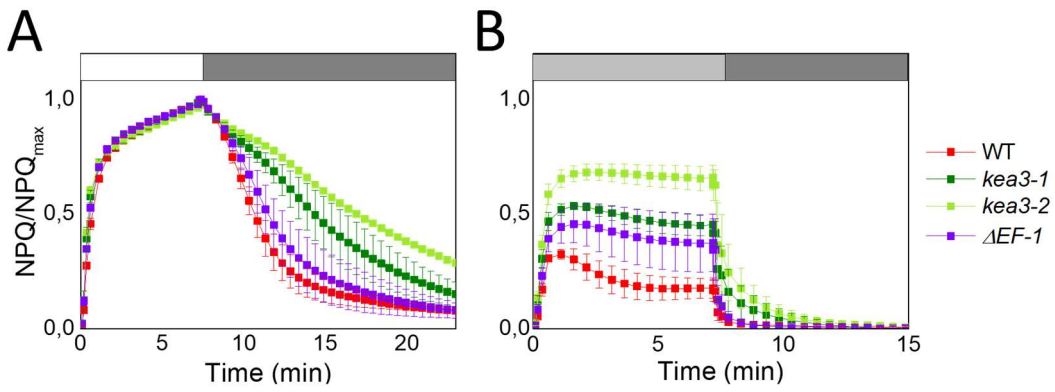


***FIGURE 4.15. NPQ PHENOTYPE OF THE MUTANT LACKING AN EF-HAND.***

*WT, KEA3 KO-mutants* kea3-1 *and* kea3-2 *and one mutant lacking the EF-hand* ΔEF-1 *were exposed to (A) high light (1220 µmol.photons.m$^{-2}$, white box) followed by relaxation in low light (30 µmol.photons.m$^{-2}$, dark grey box) and (B) moderate high light (125 µmol.photons.m$^{-2}$, light grey box) followed by relaxation in low light (30 µmol.photons.m$^{-2}$, dark grey box). NPQ was normalized to $NPQ_{max}$. N=3 independent biological replicates. Mean ± s.e.m. Preliminary results.*

In a transition from high light to low light and in moderate high light (Figure 4.15), the mutant *ΔEF-1* has an intermediate phenotype between the WT and the KO-mutants, while the truncated KEA3 protein it bears is inactive in the dark, just like the WT. This suggests

that the EF-hand deprived KEA3 protein could be less active than the full-length protein. EF-hand domains are often involved in dimerization (Li *et al.*, 2016), hence a lower KEA3 activity as the *ΔEF-1* truncated KEA3 protein could be defective in dimerization. Since no differences were encountered between the WT, *ΔEF-1* and KEA3-KO mutants, the EF-hand ought not to be involved in the regulation of KEA3 activity in the dark.

These preliminary data must be interpreted with caution as few replicates were performed and the mutant *ΔEF-2* has not been included in the study yet.

## 4.7 CONCLUSION

Using a set of KO mutants and an overexpressor, we have investigated the role of the newly identified $K^+/H^+$ antiporter KEA3 and established that it is involved in the regulation of photoprotection in *P. tricornutum*. We have been using an appropriate dose of the ion exchanger nigericin that effectively complements the KO-mutants.

We have studied the role of KEA3 in different light transitions. The presence of this antiporter slows down NPQ induction in high light, decreases NPQ level in moderate high light and accelerates NPQ relaxation in low light. Overall, KEA3 modulates light utilization in an intensity dependent manner, i.e. the presence of KEA3 delays the saturation of electron transfer and induction of photoprotective mechanisms. However, KEA3 appears inactive in the dark.

KEA3 is able to bind calcium through its EF-hand domain. A mutant lacking this domain displayed an intermediate phenotype between the WT and the two KO-mutants, hence possibly a lower activity of the truncated protein. This could be due to a defect in dimerization.

KEA3 does not alter the mechanisms of photoprotection *per se*, especially since the proportionality relationship between NPQ and DES is conserved. KEA3 instead controls the trigger of photoprotection, i.e. the proton motive force. We have evidenced that in the presence of KEA3, the ΔpH component of the p.m.f. is decreased and converted into ΔΨ. Since we had previously demonstrated that NPQ depends univocally of the lumen pH in *P. tricornutum*, the modulation of photoprotection and light utilization by KEA3 can be understood only through its effects on the thylakoid lumen pH.

Using KEA3 as a tool, we thus attempted to model the dependency of NPQ to the lumen pH in order to further validate our conclusions.

# 5 MODELLING NPQ DEPENDENCY TO PH

We have shown previously that NPQ is strictly dependent on the lumen pH in *P. tricornutum*. The $K^+/H^+$ antiporter KEA3 therefore regulates NPQ by fine-tuning the composition of the p.m.f.

In diatoms, NPQ and the de-epoxidation state are proportional (Lavaud *et al.*, 2002) and disrupting the thylakoid proton gradient with either KEA3 or nigericin does not affect this relationship. Since the xanthophyll cycle results from the competition between two enzymatic reactions (de-epoxidation catalyzed by a diadinoxanthin de-epoxidase DDE and epoxidation catalyzed by a diatoxanthin epoxidase DEP, see Section 1.4.3.2), NPQ can be viewed as the result of this enzymatic equilibrium.

In order to formally verify our conclusions regarding pH, we have built different scenarios to model this regulation.

## 5.1 KINETIC MODELLING OF NPQ

### 5.1.1 First order kinetic model and theoretical frame

We have applied a model developed by B. Bailleul and L. Blommaert (Blommaert *et al*, in preparation) to our conditions. This model describes NPQ dynamics upon a change of light intensity by evaluating the rate constants for the enzymes DDE and DEP.

This model is based on three hypothesis:

(1) No photoinhibition takes place. If this condition is met, NPQ consists only of qE as state transitions are absent in diatoms (Owens, 1986).

(2) The amount of diatoxanthin (Dt) is always proportional to NPQ. In particular, no diadinoxanthin neo-synthesis should take place within the time of measurement, i.e. the size of the xanthophyll pool size XP remains constant.

(3) The enzyme kinetic constants are of first order for their respective substrate, i.e.

$$\begin{cases} v_{epox} = k_{epox}.[Dt] \\ v_{de-epox} = k_{de} \quad .[Dd] \end{cases}$$

***EQUATION 5.1***

*$v_{expox}$, $v_{de\text{-}epox}$ are respectively the rate of epoxidation and de-epoxidation and $k_{epox}$ and $k_{de\text{-}epox}$ their time constants.*

The rate of *[Dt]* creation can thus be expressed as:

$$\frac{d[Dt]}{dt} = v_{de-epox} - v_{epox} = k_{de-epox}.[XP] - \left(k_{epox} + k_{de-epox}\right).[Dt]$$

***EQUATION 5.2***

*[XP] is the xanthophyll pool, i.e. [XP] = [Dd] + [Dt].*

By integrating this equation with respect to time, we obtain:

$$[Dt](t) = \frac{[XP]}{1 + \frac{k_{epox}}{k_{de-ep}}} - A.e^{-(k_{epox}+k_{de-epox}).t}$$

***EQUATION 5.3***

*A is a constant.*

Considering that NPQ is proportional to the de-epoxidation state, i.e. $^{[Dt]}/_{[XP]} = \alpha.NPQ$, we obtain:

$$NPQ(t) = \frac{1}{\alpha}.\frac{1}{1 + \frac{k_{epox}}{k_{de-epox}}} - B.e^{-(k_{epox}+k_{de-epox}).t}$$

***EQUATION 5.4***

*B is a constant.*

Accordingly, in this model, the relaxation or induction speed is determined by the sum $k_{epox} + k_{de-epox}$ while steady state NPQ depends on the ratio $^{k_{epox}}/_{k_{de-epox}}$.

## 5.1.2 Verification of hypothesis

For Equation 5.4 to be valid, all the hypothesis aforementioned must first be validated: absence of photoinhibition, proportionality between NPQ and DES and constant xanthophyll pool size for all strains and conditions investigated.

### *5.1.2.1 Absence of photoinhibition*

We were not able to induce NPQ at the same high light intensity as previously (1200 µmol.photons.m$^{-2}$, see Section 4) since especially in the KO-mutant strains this light intensity would induce incomplete relaxation of NPQ in low light (30 µmol.photons.m$^{-2}$, see Section 4.2.4), i.e. photoinhibition or qI.

When cells underwent a transition from 400 µmol.photons.m$^{-2}$ to 30 µmol.photons.m$^{-2}$ (Figure 5.1), NPQ relaxed to zero. Therefore, this high light intensity did not induce any

irreversible photoinhibition even in the mutants and was deemed suitable to perform the rest of experiments.

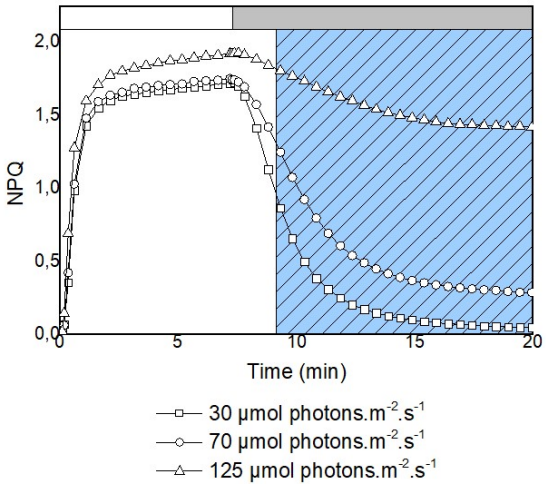


***FIGURE 5.1. EXPERIMENTAL SETUP.***

*NPQ induction and relaxation in the mutant kea3-1 exposed to high light (400 µmol.photons.m$^{-2}$, white box) followed by relaxation at the indicated light intensity (grey box). Only the hatched part was considered for fitting.*

The experimental process was as follows: NPQ was induced to $NPQ_{max}$ at 400 µmol.photons.m$^{-2}$ and eventually relaxed at a specified light intensity. In every strain, both the steady-state NPQ value reached at the end of the relaxation phase and the time constant for the relaxation depend on the light intensity (Figure 5.1).

#### *5.1.2.2 Proportionality between DES and NPQ*

We had quantified diatoxanthin and diadinoxanthin content of cells (see Section 4.4) and verified that the relationship between NPQ and DES remained the same in all the strains and was not affected by the addition of nigericin. We were therefore able to express NPQ as $NPQ = \alpha . {[Dt]}/{[XP]}$, and estimated α = 0.21.

Neo-synthesis of diadinoxanthin, i.e. increasing of the xanthophyll pool size takes does not happen before 40 minutes to hours of high light illumination (Mewes and Richter, 2002; Lavaud, Rousseau and Etienne, 2004; Blommaert *et al.*, 2017), therefore the setup presented here (Figure 5.1) should not induce any rise in the xanthophyll pool size. Therefore, NPQ and DES were always proportional.

### 5.1.3 Experimental results

All verifiable hypothesis being verified, we applied the method described above to the four strains studied in this manuscript (WT, KEA3 KO-mutants and KEA3 overexpressing strain)

in the presence or absence of nigericin and calculated. Since at the beginning of the relaxation phase the NPQ curve is not shaped like an exponential but rather as a sigmoid, the first two minutes were not taken into account in the fitting (Figure 5.1, hatched part). The NPQ relaxation curves were fitted using the equation $y = y_0 + Ae^{-t/\tau}$. The parameters $k_{epox}$ and $k_{de\text{-}epox}$ were identified from Equation 5.5 as:

$$\begin{cases} y_0 = \frac{1}{\alpha}.\frac{1}{1+\frac{k_{epox}}{k_{de-epox}}} \\ \frac{1}{\tau} = k_{epox} + k_{de-epox} \end{cases}$$

***EQUATION 5.5***

Hence:

$$\begin{cases} k_{de-epox} = \frac{\alpha.y_0}{\tau} \\ k_{epox} = \frac{1-\alpha.y_0}{\tau} \end{cases}$$

***EQUATION 5.6***

The four strains had very similar $k_{de\text{-}epox}$ for all light intensities (Figure 5.2), since no significant differences were detected. Similarly, the parameter $k_{de\text{-}epox}$ was not affected by the addition of nigericin, but rather increased with increasing light intensity. This hints that the de-epoxidase is not affected by pH. On the opposite, the two KO strains *kea3-1* and *kea3-2* had significantly lower $k_{epox}$ than the WT and the overexpressing strain, suggesting that the epoxidase activity depends on pH. Addition of nigericin in these two strains increased $k_{epox}$ to similar levels as for the WT in control conditions.

This would suggest that increased thylakoid $K^+/H^+$ exchange through either KEA3 or nigericin does not directly affect the rate of DDE but instead the rate of DEP. This result is surprising since experimental evidence have shown that DDE in *P. tricornutum* and its homolog in plants VDE are sensitive to pH (Bratt *et al.*, 1995; Jakob, Goss and Wilhelm, 2001; Grouneva *et al.*, 2006). To our knowledge, no *in vitro* study has yet been published on the influence of pH on the activity of DEP or ZEP.

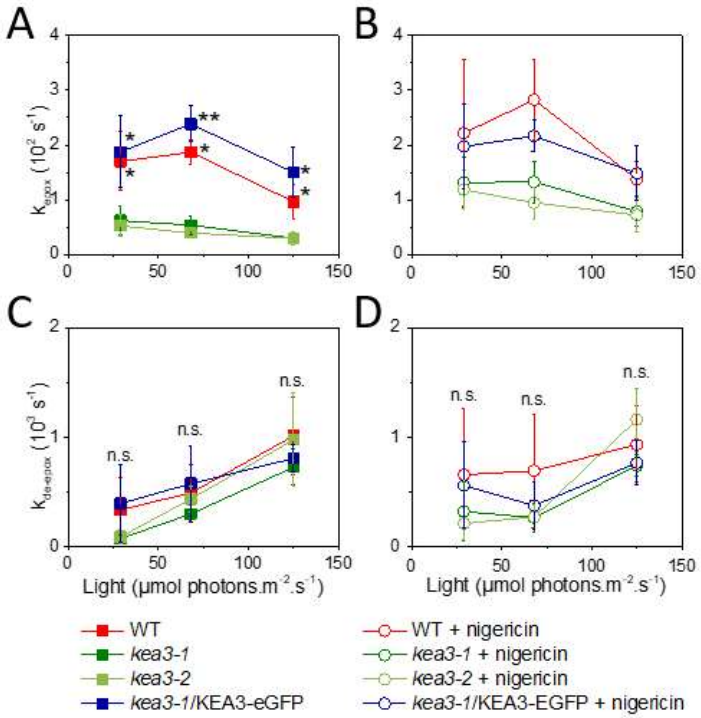


***FIGURE 5.2. ESTIMATION OF EPOXIDATION AND DE-EPOXIDATION RATES AT DIFFERENT LIGHT INTENSITIES IN THE FOUR STRAINS STUDIED.***

*Cells were exposed to high light (400 µmol.photons.m$^{-2}$) followed by relaxation at the indicated light intensity. The parameters $k_{epox}$ and $k_{de\text{-}epox}$ were estimated after fitting of the NPQ curves according to Figure 5.1 for WT, KO-mutants* kea3-1 *and* kea3-2 *and overexpressor* kea3-1*/KEA3-eGFP with and without 10 µM nigericin. N = 6 independent biological replicates. Mean ± SD. Asterisks indicate statistically significant differences between samples either the WT or the overexpressor to both of the KO-mutant strains (*: p < 0.05; **: p<0.01).*

### 5.1.4 Possibility of a pH-dependency of DEP

The experiment presented in Figure 5.2 suggests that DEP activity in diatom is modulated by pH. The gene encoding DEP has not yet been characterized experimentally in *P. tricornutum*, therefore the subchloroplastic localization of the enzyme in diatoms is still undetermined. The most likely option would be for this enzyme to be localized on the stromal side of the thylakoid membrane just like in plants.

In this case, its pH-sensitivity would indicate that the pH of the stroma in diatoms becomes alkaline upon high light exposure. Indeed, previous reports have indicated that the thylakoid lumen acidification is mirrored upon high light exposure by an alkalization of the stroma (Werdan, Heldt and Milovancev, 1975; Oja, Laisk and Heber, 1986). Since a proton is required for the epoxidation reaction, even a slight alkalization of the stroma could decrease DEP activity and thus the apparent time constant of DEP $k_{epox}$.

However, we have demonstrated previously (see Section 2) that NPQ can be induced and reversed in the dark by the sole addition of acid or alkalinity and that NPQ is univocally dependent on the lumen pH. In this experiment, potassium hydroxide was added to the external medium, therefore the stroma was necessarily more alkaline than the thylakoid lumen. This is incompatible with the idea that an alkaline stroma would be required for NPQ induction. Consequently, the DEP cannot be both localized in the stroma as expected from the literature and activated by an alkalization of the stroma as suggested from the model.

Another possibility to explain this apparent contradiction would be that DEP would be localized in the thylakoid lumen, although this would be unlikely as ZEP has been found in the stroma of *A. thaliana*. It would thus be deactivated by low pH in the thylakoid lumen and activated by neutral pH, consistently with the lumen pH dependency of NPQ previously determined. This model predicts that DDE would not be pH-sensitive, which is inconsistent with previous studies in plants and diatoms (Bratt *et al.*, 1995; Jakob, Goss and Wilhelm, 2001; Grouneva *et al.*, 2006) that do highlight an activation of DDE by acidic pH.

Predicting a first order kinetics for each substrate for DDE and DEP leads to unexpected conclusions that contradict either the literature or previous data from this very study. We therefore deemed that this kinetic assumption did not properly describe our system.

## 5.2 MODELLING OF THE XANTHOPHYLL CYCLE WITH MICHAELIS-MENTEN KINETICS

### 5.2.1 Simple Michaelis-Menten kinetics

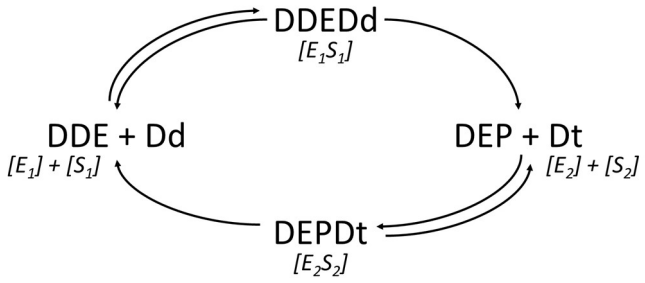


***FIGURE 5.3. HYPOTHETICAL KINETIC SCHEME OF THE XANTHOPHYLL CYCLE IN P. TRICORNUTUM.***

We tried to re-analyze the same data (see Section 5.1) using a more complex kinetic model. We thus chose to use the classical frame of Michaelis-Menten kinetics, that it to say considering that the formation of the enzyme-substrate complex is a reversible reaction

while the unbinding of the product from the enzyme is irreversible (Figure 5.3). Such was done both for DDE and DEP.

According to this model, the rate of formation of diatoxanthin can be described by the following equation:

$$\frac{d[Dt]}{dt} = \frac{v_{m,DDE}.([XP] - [Dt])}{K_{m,DDE} + ([XP] - [Dt])} - \frac{v_{m,DEP}.[Dt]}{K_{m,DEP} + [Dt]}$$

***EQUATION 5.7***

*$v_{m,\,DDE}$, $v_{m,DEP}$ are the respective maximum activity of each enzyme and $K_{m,DDE}$ and $K_{m,DEP}$ their Michaelis affinity constants. [XP] is the xanthophyll pool, i.e. [XP] = [Dd] + [Dt].*

Since NPQ is proportional to the de-epoxidation state as previously, i.e. $NPQ = \alpha.{}^{[Dt]}/_{[XP]}$:

$$\frac{dNPQ}{dt}(t) = \frac{v_{m,DDE\ app}.\left({}^{1}/_{\alpha} - NPQ(t)\right)}{K_{m,DDE\ app} + 1 - \alpha.NPQ(t)} - \frac{v_{m,DEP\ app}.NPQ(t)}{K_{m,DEP\ app} + \alpha.NPQ(t)}$$

***EQUATION 5.8***

$$v_{m\ app} = {}^{v_m}/_{[XP]}\ and\ K_{m\ app} = {}^{K_m}/_{[XP]}.$$

This differential equation cannot be solved analytically. As a consequence, we tried to solve the coefficients $v_{m,\,app}$ and $K_{m,\,app}$ numerically by using four different time points for a given NPQ trace as a system of four equations. The value obtained for $v_{m,\,app}$ and $K_{m,\,app}$ were dependent on the time points chosen. Since these values were not constants, this indicates that the simple Michaelis-Menten model described here is not suitable to describe the kinetics of DDE and DEP.

### 5.2.2 pH dependency of Michaelis-Menten parameters

Previous studies (Bratt *et al.*, 1995; Grouneva *et al.*, 2006) have stated that the kinetics of DDE and its plant homologue VDE are activated by pH. In particular, the rate of partially purified VDE has been measured in the presence of a fixed concentration of its substrate violaxanthin and various concentrations of ascorbate. At very low pH, the activity of VDE drops, probably due to a denaturation of the enzyme. However, at higher pH compatible with the thylakoid lumen, the maximum activity of VDE, linearly depends on pH at a given concentration (Figure 5.4). This value would correspond to $v_{m,DDE\ app}$ in our model.

Replacing the term $v_{m,DDE\ app}$ by a term comprising pH such as $v_{m,DDE\ app} - \beta.pH$ in Equation 5.8 would take the pH-dependency of VDE into account. However, it would imply making the hypothesis that the ascorbate concentration remains constant in the thylakoid lumen

during NPQ induction and decay that is to say ascorbate is always in excess for the de-epoxidation reaction. In a previous report, addition of ascorbate to *P. tricornutum* cells before illumination increased the final diatoxanthin content of these cells without significantly altering the NPQ value (Lavaud and Kroth, 2006), meaning that ascorbate is this case was limiting for diadinoxanthin de-epoxidation. Henceforth taking into account the pH-dependency of DDE cannot be done by replacing $v_{m,DDE\ app}$ by a $v_{m,DDE\ app} - \beta.pH$ in Equation 5.8.

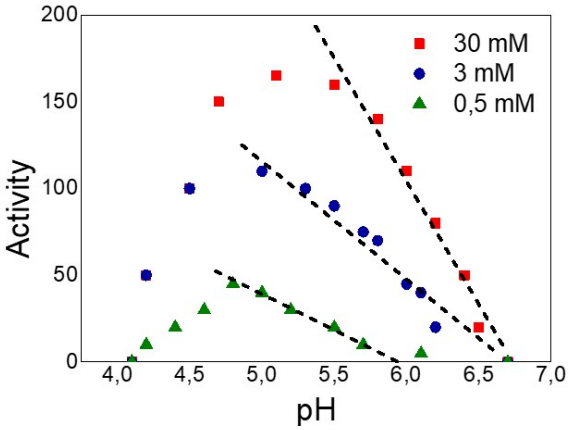


***FIGURE 5.4. MAXIMUM SPECIFIC ACTIVITY OF PARTIALLY PURIFIED VDE IN THE PRESENCE OF VARIOUS ASCORBATE CONCENTRATIONS (30 MM, 3 MM AND 0.5 MM) AS A FUNCTION OF PH.***

*The data was retrieved by graphical reading of* (Bratt *et al.*, 1995)*. Lines were drawn to model the dependency of DDE activity for pH values compatible with the thylakoid lumen.*

Besides, since ascorbate can be a limiting substrate, modelling the activity of DDE would require some knowledge of the ascorbate concentration in diatoms thylakoids. Such has never been done in diatoms and this would be a technical challenge.

We conclude from this that modelling NPQ dependency to pH seems even more complex than all the models that we have investigated. A strategy to circumvent this problem will be presented in the Discussion Section below.

# 6 DISCUSSION AND PERSPECTIVES

In this manuscript, we have described how non-photochemical quenching of PSII is dependent on the value of the lumen pH in *P. tricornutum*. We have identified the $K^+/H^+$ antiporter KEA3 as one of the key players of the regulation of the lumen pH and thus NPQ. We can thus refine the model for the regulation of photoprotection in diatoms.

## 6.1 NPQ IS A UNIVOCAL FUNCTION OF LUMEN PH IN DIATOMS

### 6.1.1 Mimicking NPQ in the dark

Intrinsically, NPQ mechanisms aim at dealing with excessive light conditions. We have however been able to induce it in the dark in permeabilized cells (see Section 2.1.1), simply by modifying the external pH.

In *P. tricornutum*, PSII becomes quenched in the dark but only after a prolonged period of about 24h (Jakob, Goss and Wilhelm, 1999), with no effects on PSII quenching visible within the first hours of dark adaption. Since cells had been placed in the dark for at most 45 minutes following light exposure (see Section 2.1.1 and 8.8.1.1), the quenching observed does not result from a "dark adapted" state. We thus considered that the quenching observed rather mimics the "classical" NPQ response to high light illumination.

### 6.1.2 Clarifying pH control of NPQ

When *P. tricornutum* cells were partially permeabilized to protons using low doses of the $K^+/H^+$ exchanger nigericin, modifying the pH of the external medium resulted in quenching or unquenching PSII. Using the catalytic rate of the $b_6f$ complex as a probe, we have been able to estimate the lumen pH as a function of the external pH in these permeabilized cells (Section 2.2). It ensues that NPQ univocally depends on the value of the lumen pH, that is to say lowering the lumen pH immediately triggers NPQ induction while neutralizing the lumen pH causes NPQ decay. Reciprocally, the value of the lumen pH can be predicted using a very simple NPQ measurement.

The idea that NPQ is pH-dependent in diatoms is not new in itself (Jakob, Goss and Wilhelm, 1999, 2001; Mewes and Richter, 2002; Lavaud, Rousseau and Etienne, 2004; Ruban *et al.*, 2004; Goss *et al.*, 2006; Grouneva *et al.*, 2006; Lavaud and Kroth, 2006; Goss and Jakob, 2010; Cruz *et al.*, 2011). However, it has never been reported before to be univocal. Previous reports had stated that a low lumen pH was no longer needed once diatoxanthin

had been formed (Goss *et al.*, 2006), while we have shown that increasing the lumen pH immediately resulted in NPQ decay.

We have been able to use NPQ measurements as a probe to infer the thylakoid lumen pH. This method is valid within the range where the relationship between the lumen pH and NPQ is almost linear, i.e. when the lumen pH is comprised between ~5.4 to 7.2. This powerful, easy-to-handle tool could be used to decipher the pH-sensitivity of photoprotective mechanisms in diatoms in various conditions.

### 6.1.3 A model for NPQ dynamics in *P. tricornutum*

In the green lineage as in diatoms, NPQ requires the simultaneous presence of effector pigments and activated effector protein. The main difference between diatoms and the green lineage is that in the green lineage NPQ decay follows the kinetics of the proton gradient decay since the activation and deactivation of PSBS and LHCSR is controlled by the lumen pH (Ruban *et al.*, 2004; Niyogi and Truong, 2013; Ballottari *et al.*, 2016; Ruban, 2016; Tian *et al.*, 2019).

In order to construct a model for NPQ in diatoms, we have simulated the behavior of NPQ in the green lineage and in diatoms. Each of the effector was modelled as a single exponential function while NPQ was modelled as the product of both quenchers (Figure 6.1). We have simulated two series of high light illumination followed by relaxation in the dark or in low light respectively for the green lineage or *P. tricornutum*.

In the frame of the model previously established for the green lineage (Figure 6.1), we simulated the activation of both quenchers (PSBS/LHCSR and zeaxanthin, LHCX proteins and diatoxanthin, respectively) with an exponential dependency to time.

A "memory effect" has been evidenced in the green lineage (Ruban *et al.*, 2004; Allorent *et al.*, 2013; Matuszyńska *et al.*, 2016). In high light conditions, both the protein effector PSBS/LHCSR are activated by protonation while violaxanthin is de-epoxidized into antheraxanthin and zeaxanthin. In the dark, the protein effector is deactivated quite fast while the xanthophyll cycle is slowly relaxing. NPQ relaxation thus follows the deactivation kinetics of PSBS/LHCSR. Upon a second high light illumination, NPQ induction is faster as the xanthophyll cycle that was kinetically limiting in the first round of illumination is already de-epoxidized (Figure 6.1).

Such is not the case in diatoms: no memory effect has ever ben evidenced while the amount of diatoxanthin formed and NPQ are strongly correlated (Lavaud, Rousseau and Etienne, 2004; Ruban *et al.*, 2004; Johnson *et al.*, 2008). We have demonstrated that NPQ is strongly

correlated to the lumen pH through the activation and de-activation of the xanthophyll cycle.

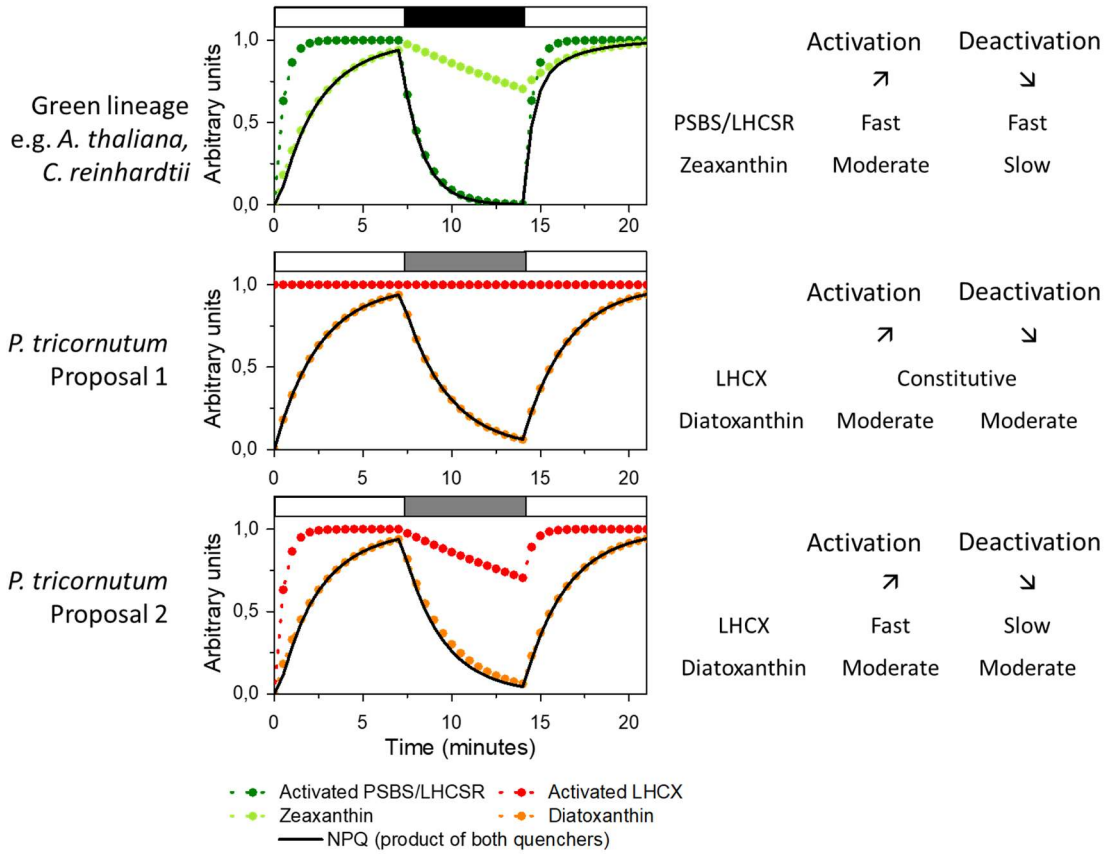


***FIGURE 6.1. SIMULATION OF THE KINETICS OF NPQ EFFECTORS IN THE GREEN LINEAGE AND IN DIATOMS.***

*Activation speeds for each effector during the NPQ induction (white box, upward arrow) or decay (black or dark grey box, downward arrow) are shown on the right. NPQ is calculated as the product of the quenchers.*

The only way for the model to respect the proportionality between NPQ and the amount of diatoxanthin is by maintaining the level of activated LHCX at a constant level (Figure 6.1, Proposal 1) or fast activated and slowly deactivated (Figure 6.1, Proposal 2). Indeed, in the frame of Proposal 2, since the amount of activated LHCX remains close to the maximum except in the first minutes of high light onset, NPQ and diatoxanthin still appear proportional. Both proposals are coherent with the literature and with the findings of this manuscript.

Some of the conserved acidic residues from *C. reinhardtii* LHCSR1 and LHCSR3 involved in pH-sensing and protein activation (Ballottari *et al.*, 2016) are conserved the LHCX proteins (Taddei *et al.*, 2016), suggesting that these might play the same role in diatoms. The question whether these residues control the activation of the LHCX proteins could be solved

by creating knock-downs of all the isoforms, (Buck *et al.*, 2019) and complementing these knock-downs with mutated genes missing a few of the conserved residues.

### 6.1.4 Refining NPQ model in diatoms

#### *6.1.4.1 Diatoxanthin formation is kinetically limiting in NPQ induction*

Since NPQ always remained proportional to the de-epoxidation state, it ensues that the enzymatic reactions leading to the formation of both diadinoxanthin and diatoxanthin are tightly pH-controlled in *P. tricornutum*. If the LHCX proteins are indeed activated instead of constitutively active (Figure 6.1, Proposal 2), the activation of the LHCX proteins could be due to pH. This activation is however not be visible in the pH-profile of NPQ (see Section 2). Therefore, activation of the LHCX1 protein is not a kinetically limiting step.

The dependency of NPQ to lumen pH that we have established has the classical sigmoidal shape of pH-jump-dependent phenomena. In particular, this special relationship has a single $pK_a$. As NPQ and the de-epoxidation of the xanthophyll cycle are proportional in *P. tricornutum*, the $pK_a$ is probably due to an activation of de-activation of the enzymes involved. From this, we can deduce that the kinetically limiting step in NPQ formation and decay is xanthophyll conversion.

We can therefore refine the present model for NPQ formation and induction in *P. tricornutum*:

(1) The kinetics of NPQ induction and decay are determined by the lumen pH through a tight control of the de-epoxidation and epoxidation rates of the xanthophyll cycle.
(2) The LHCX proteins are involved in controlling the maximum extent of NPQ but not its dynamics, or if such is the case, to a lesser extent than their functional homologues LHCSR/PSBS in the green lineage

Since NPQ in *P. tricornutum* is even more dependent on the variation of the lumen pH than in the green lineage, understanding proton fluxes inside the thylakoid lumen is of paramount importance when studying photoprotection in diatoms.

#### *6.1.4.2 Perspective: Modelling of NPQ, the xanthophyll cycle and pH*

Modelling the enzymatic conversion of diatoxanthin and diadinoxanthin by classical kinetic approaches showed that the actors currently identified cannot alone explain the dynamics of NPQ (see Section 5). In particular, we believe that the dynamics of ascorbate in the thylakoid lumen are of paramount importance to understand this enzymatic conversion.

By integrating the data presented in this manuscript into a model of photosynthesis (Matuszyńska *et al.*, 2016), we wish to validate our approach and conclusions. A collaboration is ongoing with A. Matuszyńska (Heinrich-Heine University, Düsseldorf, Germany) to study these aspects. It consists in adapting the previously published model to the case of diatoms (e.g. no or little activation of the LHCX proteins by pH, proportionality between NPQ and de-epoxidation state) and aims at reproducing the KEA3 phenotype by simply changing the "proton leak" parameter. If the reconstruction of the data succeeds, this will mean that the proposed model correctly describes NPQ kinetics in *P. tricornutum*.

## 6.2 MODULATION OF NPQ BY AN ION TRANSPORTER

The $K^+/H^+$ exchange antiporter KEA3 first was identified in the land plant *Arabidopsis thaliana* (Armbruster *et al.*, 2014). Its homologues are highly conserved across photosynthetic eukaryotes, including the remotely related diatom *Phaeodactylum tricornutum*. We have constructed KO-mutants for KEA3 using the CRISPR-Cas9 technique and complemented them with a copy of the *P. tricornutum* KEA3 gene fused with eGFP. We have then characterized this mutant from a photosynthetic perspective.

### 6.2.1 KEA3 controls NPQ dynamics in light transitions

The presence of the KEA3 protein does not affect $NPQ_{max}$ reached under saturating light but rather the kinetics of NPQ relaxation and induction. In all conditions investigated where the lack of KEA3 had an effect, nigericin addition complemented the phenotype of the KO-mutants (see Section 4.2). We have verified that KEA3 is indeed a trans-thylakoid proton pump in *P. tricornutum* since the presence of KEA3 or the addition of nigericin caused a decrease in the electric field across the thylakoid membrane (see Section 4.5). Having previously evidenced that NPQ induction and decay is controlled by the value of the lumen pH, the KEA3 phenotype can be interpreted in term of variation of the lumen pH value.

Upon a transition from dark to high light (see Section 4.2.2), NPQ induction is faster in KO-mutants lacking KEA3 and speeded up by the addition of nigericin. This indicates that during this transition KEA3 dissipates a part of the proton gradient formed, and therefore slows down NPQ induction.

Upon a transition from high light to low light (see Section 4.2.4), NPQ decay is slower in the KO-mutants than in the WT and the overexpressor strain and can be accelerated by the addition of nigericin. Before the transitions, all cell lines had reached about the same $NPQ_{max}$ value, associated with a low thylakoid lumen value. The presence of KEA3 speeds up NPQ decay, once more by accelerating the dissipation of the proton gradient.

One of the most striking phenotypes associated with the KEA3 mutation is the different NPQ levels reached under moderate high light (see Section 4.2.3). Indeed, while in WT and overexpressor strains NPQ was induced to a low level (about 0.4 $NPQ_{max}$), both mutants yielded high NPQ values (about 0.75 $NPQ_{max}$). NPQ could be decreased to WT-like levels by the addition of nigericin. In this particular condition, KEA3 was therefore changing the steady-state value of the thylakoid lumen pH and thus the extent of NPQ. It is worth noting that the values were stable over time, i.e. in both the WT and the KO-mutant strains an equilibrium between the proton fluxes was reached.

In a more general manner, the presence of KEA3 partially dissipates the proton gradient and results in smoothing NPQ induction response towards higher light intensities (see Section 4.3).

### 6.2.2 Role of KEA3 in a transition from light to dark

#### *6.2.2.1 The proton gradient controls NPQ decay in the dark*

NPQ in diatoms is well-known to relax slowly in the dark (Goss *et al.*, 2006). Dark relaxation following high light exposure was the only case when the presence of KEA3 or nigericin had a different effect: while nigericin successfully increased NPQ relaxation rate, the decay speed was identical in the WT, KO-mutant and overexpressor (see Section 4.4).

NADPH is a mandatory co-factor for the enzymatic conversion of diatoxanthin into diadinoxanthin that enables NPQ relaxation. It is a product of photosynthesis and therefore has been hypothesized to be the limiting factor for NPQ relaxation in the dark (Goss *et al.*, 2006). However, the fact that nigericin accelerated NPQ decay suggests that at least in the experimental conditions used here, the relaxation of the proton gradient, and not NADPH, was limiting.

However, KEA3 did not release the proton gradient in the dark, unlike in the light, and probably was inactive. This raises the question of a possible control of KEA3 activation or deactivation.

#### *6.2.2.2 Perspective: Activation and deactivation of ATP synthase in diatoms*

Another and main actor of proton gradient relaxation is the chloroplast ATP synthase. We have evidenced that in the dark, ATP synthesis plays a minor role in the equilibration of protons across the thylakoid membrane. Hence, the ATP synthase could be deactivated in the dark in *P. tricornutum*, and possibly even function as an ATP-ase (Bailleul *et al.*, 2015).

In plants and green algae, the chloroplast ATP synthase is deactivated in the dark due to a redox control of its activity through the formation of disulfide bounds on the γ subunit

between two conserved cysteine residues (Fischer and Gräber, 1999; Hisabori *et al.*, 2002; Kohzuma *et al.*, 2013; Hahn *et al.*, 2018). However, these cysteine residues are not conserved in *P. tricornutum* (Figure 6.2, yellow highlights). This suggests that the mechanism for ATP synthase control in diatoms is different from plants and green algae and possibly closer to cyanobacteria. A novel gating mechanism of the ATP synthase has recently been discovered in the cyanobacterium *Thermosynechococcus elongatus* (Murakami *et al.*, 2018). It involves the insertion of a loop from the γ subunit of ATP synthase that prevents the rotation of the β subunit (Figure 6.2, green box), just like in the mitochondrial ATP synthase (Campanella *et al.*, 2009). A similar mechanism could govern the activation and deactivation of the ATP synthase in diatoms.

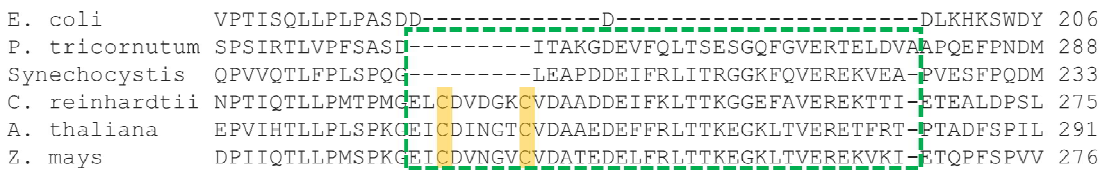


***FIGURE 6.2. PROTEIN ALIGNMENT OF THE ATP SYNTHASE Γ SUBUNITS OF SEVERAL ORGANISMS.***

*For photosynthetic eukaryotes (*P. tricornutum*,* C. reinhardtii*,* A. thaliana *and* Z. mays*) only the chloroplastic ATP synthase was considered. The two cysteine residues involved in redox control of the ATP synthase in the green lineage are highlighted in yellow. The specific loop found only in photosynthetic organisms is circled in green.*

### 6.2.3 Regulation of KEA3 activity in *P. tricornutum*

KEA3 in *P. tricornutum* was shown to be active in the light and inactive in the dark. This raises the question of a possible regulation of KEA3 activity.

The primary sequence of KEA3 bears one functional domain (the cation/$H^+$ antiporter domain) and two regulatory domains (the regulator of $K^+$ conductance domain and the EF-hand). Both of these domains could thus potentially explain the regulation of KEA3 function.

#### *6.2.3.1 Perspective: Regulation of KEA3 through the RCK domain*

The protein KEA3 in *A. thaliana* and *P. tricornutum* as well as their bacterial counterpart KefC possess two main protein domain: one cation/$H^+$ antiporter domain and one regulator of $K^+$ conductance (RCK) domain. This RCK domain is localized on the stromal side of thylakoids in *A. thaliana* (Wang *et al.*, 2017) and on the inner side of the plasmic membrane in *E. coli* (Miller *et al.*, 2000; Fujisawa, Ito and Krulwich, 2007). Both of these locations are topologically equivalent to the inside of the cell. It is thus reasonable to assume that the RCK domain of KEA3 is also localized on the stromal side in *P. tricornutum*.

The RCK domain controls AtKEA3 activity: proteins bearing a truncated RCK domains are less effective than full ones (Armbruster *et al.*, 2016; Tsujii *et al.*, 2019). In *A. thaliana,* KEA3 is active in low light and inactive in high light (Armbruster *et al.*, 2014; Wang *et al.*, 2017; Dukic *et al.*, 2019). An overactive allele of KEA3 was however found to be active in high light (Wang *et al.*, 2017; Wang and Shikanai, 2019). This hints that the regulation of KEA3 activity is different in plants and in diatoms.

In KefC, the RCK domain is involved in binding regulatory metabolites such as NADH and glutathione and the ancillary protein KefF (Fujisawa, Ito and Krulwich, 2007; Roosild *et al.*, 2009; Lyngberg *et al.*, 2011). No clear homologue of KefF can be detected in the genomes of *A. thaliana* or *P. tricornutum*, therefore the gating mechanism of KefC by KefF is expected not to be transposable to KEA proteins.

In *E. coli*, binding of NADH on KefC inhibits $K^+$ transport (Fujisawa, Ito and Krulwich, 2007). However, in the dark when KEA3 is inactive the linear electron chain does not produce any NAD(P)H. It ensues that the inhibitory effect of NADH on KefC activity is not identical for NAD(P)H and KEA3 in diatoms.

Besides, RCK domains are known to dimerize and even oligomerize to activate $K^+$ transport (Jiang *et al.*, 2002; Roosild *et al.*, 2002). This could provide a rationale for the lower activity reported in AtKEA3 isoforms bearing truncated RCK domains (Armbruster *et al.*, 2016) and could also be a conserved regulatory feature in *P. tricornutum.*

However, the role of these motifs cannot be properly studied unless the protein is crystalized *in vitro* and studied using electrophysiology (Carraretto *et al.*, 2013). Another approach to study the role of the RCK domain could be to recombinantly express the protein in *E. coli*. The full-length AtKEA2 protein is unfortunately toxic to bacteria (Kunz *et al.*, 2014) and our attempts to produce recombinantly the *P. tricornutum* KEA3 protein in *E. coli* were unsuccessful. Recombinant expression of KEA3 in an organism such as yeast (Tsujii *et al.*, 2019) could be a way to study the role of the RCK domain in the regulation of KEA3 activity.

#### *6.2.3.2 Perspective: Diatoms, calcium fluxes and photosynthesis*

The second regulatory motif of KEA3 is an EF-hand, a small structural domain that is able to reversibly bind calcium ions with high affinity. This domain in *P. tricornutum* KEA3 is indeed able to bind calcium *in vitro* on a denaturing SDS-PAGE (see Section 4.6.1). We have constructed mutants of KEA3 lacking this domain (see Section 4.6.2) and investigated the phenotype of one of them in a different light transitions (see Section 4.6.3). Preliminary results indicate that the truncated protein is constitutively less active than the full-length

one. Since EF-hand domains often interact by pair, the lower activity of the truncated protein could be explained by a defect in protein dimerization.

Although this is an interesting finding, this approach does not provide any insight on the role of calcium ions *per se* in the regulation of KEA3. Another strategy to study the role of a possible calcium activation of KEA3 would be to complement one of the KO-mutants with a modified EF-hand either constitutively unable to bind calcium and thus locked in an "open" conformation. Indeed, one of the most conserved amino-acid residues in the calcium binding loop of EF-hands is a glycine residue in position 6 as this small residues enables the folding of the two helixes around the bound calcium ion. By changing this amino acid to valine, which is alkaline too but has a longer side-chain, the EF-hand would lose its capacity to bind calcium, as verified with an InterPro analysis (Mitchell *et al.*, 2019). The plasmid for transformation has been constructed and awaits transformation.

More importantly, this approach would provide very valuable information on calcium fluxes in diatoms induced by illumination. *P. tricornutum* cells have been shown to respond to perturbations in their environment by calcium release inside the cytoplasm (Falciatore *et al.*, 2000). Isolated chloroplasts of wheat or spinach import calcium during illumination, while calcium could be involved in energy distribution between photosystems or even thylakoid membrane stacking, which are typical responses to high light exposure (reviewed in (Brand and Becker, 1984)). The role of calcium ions in diatom's photosynthesis is yet a new, unexplored and exciting field.

### 6.2.4 Mode of action of KEA3 in *P. tricornutum*

The flux of protons getting inside the lumen is mostly due to linear electron flow since cyclic electron flow is minor in diatoms (Bailleul *et al.*, 2015). Protons can get out of the lumen through various pumps. The most well-known of these is the chloroplastic ATP synthase. Our data evidenced here that KEA3 is also involved in regulating proton accumulation inside the thylakoid lumen.

Upon a transition from dark to high light, the combined rates of ATP synthase and KEA3 are slower than the rate of the linear electron flow (Figure 6.3.A). The resulting rise in the lumen pH induces NPQ at its maximum level ($NPQ_{max}$).

When cells are moved from dark to moderate high light, the rate at which protons are pumped in (by the linear electron flow) and out (by the ATP synthase and KEA3) of the lumen is of the same order of magnitude (Figure 6.3.B). The pH inside the lumen thus stems from an equilibrium between the two fluxes, and thus so does NPQ.

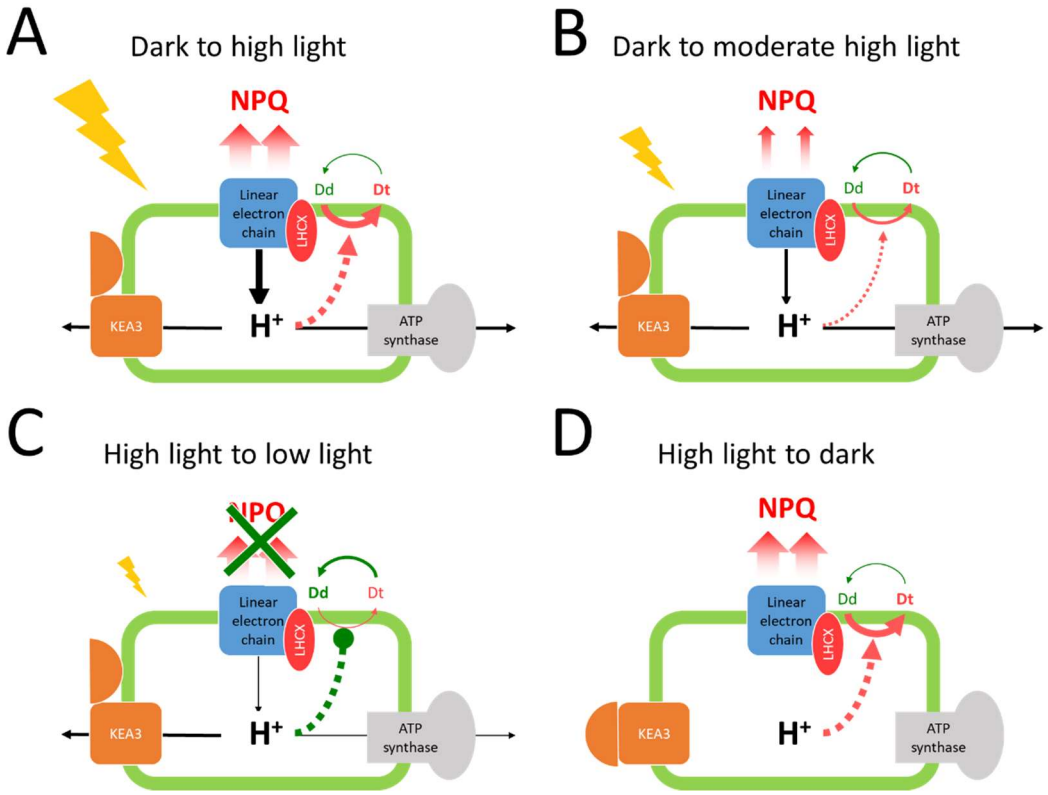


***FIGURE 6.3. MODEL FOR KEA3 ACTIVITY IN SEVERAL LIGHT TRANSITION.***

*(A) Dark to high light. (B) Dark to moderate high light. (C) High light to low light. (D) High light to dark.*

When *P. tricornutum* cells are shifted from high light to low light, the protons that have been accumulated inside the lumen are evacuated through KEA3 and the ATP synthase (Figure 6.3.C). The rate of proton pumping through the linear electron is too low to counteract the proton drain from the thylakoid lumen. NPQ relaxation is all the more fast as the proton gradient is quickly dissipated.

When *P. tricornutum* cells are moved from high light to dark, both KEA3 (likely gated by the stroma-localized RCK domain) and the electron transfer chain are inactive (Figure 6.3.D). The ATP synthase might remain functioning, but at a very low rate that does not efficiently dissipate the proton gradient. It may also be completely inactive and functioning instead as an ATPase (Bailleul *et al.*, 2015). The slow dissipation of the ΔpH would thus be due mostly to leaks in the thylakoid membrane due to other ion channels and transporters.

## 6.3 ENERGETICS OF THE PROTON MOTIVE FORCE

### 6.3.1 Energy conversion by KEA3

Often in this manuscript has it been stated that KEA3 "dissipates" the ΔpH component of the proton motive force. Although this is technically true, this wording could be misleading as it implies that $K^+/H^+$ transport KEA3 is a wasteful process.

Indeed, when measuring the extent of the electric field in the WT, KO-mutants and complemented strains (see Section 4.5) we observed that the KO-mutants had a higher ΔΨ, which increased to WT-like levels in the presence of 10 µM nigericin. Therefore KEA3, just like nigericin (Ahmed and Booth, 1983), is able to convert chemical energy in the form of a proton gradient into electrical energy. KEA3 is thus not an energy dissipating valve but rather an energy converter.

A possible mechanism explaining the energetic neutrality of KEA3 could involve an ion counterflux following KEA3 activity.

Being a $K^+/H^+$ exchanger, KEA3 equilibrates the sum of the chemical potential of $K^+$ and $H^+$ ions ($\mu_{K+} + \mu_{H+}$) on both sides of the thylakoid membrane. The concentration of potassium ions in leaves chloroplasts ranges from 40 mM to 200 mM (Robinson and Downton, 1984; Demmig and Winter, 1986). At a pH as low as 5.4, which is the lower physiological limit in the thylakoid lumen, the proton concentration is ~7 mM. Assuming that these potassium ions would be equally distributed between the stroma and the lumen, the concentration in $H^+$ ions would be insignificant as compared to the concentration in $K^+$ ions. Henceforth KEA3-mediated $K^+/H^+$ exchange could completely eliminate the proton gradient without perturbing the concentration of $K^+$ ions. If such were the case, KEA3 could only dissipate ΔpH and not affect ΔΨ.

Our experiments however show that both nigericin and KEA3 are able to convert ΔpH into ΔΨ. Hence, we must conclude that proton transport through KEA3 causes significant changes in potassium concentration across the thylakoid membrane. It ensues that the concentration of potassium ions is lower in the thylakoid lumen than in the stroma. More importantly, the conversion of ΔpH into ΔΨ following KEA3 activity is only possible if other, yet unidentified, thylakoid ions channels and transporters were catalyzing a counterflux. This counterflux would not necessarily involve potassium ions but could stem for the export of cations from the thylakoid lumen or import of anions from the chloroplast stroma.

The only two thylakoid ion pumps yet characterized in diatoms are KEA3 and the ATP-synthase. Studying other thylakoidal ion channels and transporters in diatoms is a new,

unexplored field that could help to understand the intricate picture of ion fluxes in thylakoid sacks in response to environmental variations.

### 6.3.2 Perspective: Regulation of the proton motive force by a network of ion channels

In the recent years, a few ion channels and transporters regulating the proton motive force in chloroplasts have been identified in the model plant *A. thaliana* (Szabò and Spetea, 2017). Among these, the $K^+$ channel TPK3 (Carraretto *et al.*, 2013) and the $Cl^-$ channels CLCe (Herdean, Nziengui, *et al.*, 2016) and VCCN1/2 (Duan *et al.*, 2016; Herdean, Teardo, *et al.*, 2016) have all been suggested to affect the proton motive force in plants. In particular, the CLCe and VCCN channels have been shown to independently regulate photosynthesis (Dukic *et al.*, 2019).

Therefore, finding homologues of these three transporters in *P. tricornutum* could provide very useful information on the regulation of the proton motive force in diatoms, especially if double mutants lacking both KEA3 and one of these other channels were constructed. We have thus searched for their homologues in *P. tricornutum*.

We have selected other putative regulators of the proton motive force by crossing the annotated *P. tricornutum* transporters and channels from the Membrane Transport Database (Elbourne *et al.*, 2017) with their predicted localization from Hectar (Gschloessl, Guermeur and Cock, 2008). We have included genes predicted to be targeted to the chloroplast but also genes displaying a secretion signal peptide. Indeed, since *P. tricornutum* is a secondary endosymbiont, the proteins bearing these motifs are either targeted to the chloroplast envelope or to the extracellular medium. As seems very unlikely that membrane transporters would be secreted, we assume that all transporters bearing a secretion signal peptide are actually targeted to the chloroplast.

The list of these potential candidates is available in Annex 9.2.

# 7 CONCLUSION: AN INTEGRATIVE MODEL OF NPQ REGULATION BY PH AND KEA3 IN *P. TRICORNUTUM*

Diatoms are one of the most successful clade of oceanic plankton. This is due to their efficient photoprotection mechanisms that allow them to be flexible to changing environmental conditions. In the model species *Phaeodactylum tricornutum*, we have demonstrated that the signal triggering the induction of photoprotection is the acidification of the thylakoid lumen in case of excess light conditions. Since the pH control of NPQ induction is univocal, measuring NPQ could be a way to estimate the lumen pH in *P. tricornutum*.

Additionally, we have refined the model for NPQ induction in *P. tricornutum*. While in both the green and the red lineage NPQ is dependent on the thylakoid lumen pH, the resulting kinetic interplay between the different effectors of photoprotection is different. In particular, the reversible conversion of diatoxanthin into diadinoxanthin is the main target for kinetic modulation of NPQ, while the kinetics of LHCX activation/deactivation are not preeminent for this regulation. We eventually aim modelling the role of the pH and xanthophyll cycle in NPQ induction *in silico* to further validate the model.

In conditions of excess light, the thylakoid lumen gets acidified by proton pumping through the linear electron chain. Since the pH of the lumen controls the extent of photoprotection, it ensues that the controlling the lumen pH could be a manner for *P. tricornutum* to balance the competition between photoprotection and photochemistry.

We have identified the $K^+/H^+$ antiporter KEA3 and constructed a set of KO-mutants and complemented strains. Using these tools, we have determined that KEA3 is involved in modulating the NPQ response of diatoms by converting the ΔpH component of the proton motive force into ΔΨ, thereby not leading to any energy loss. By doing so, KEA3 delays NPQ induction and accelerates NPQ relaxation in the light while maintaining the ATP output. Since KEA3 controls proton homeostasis in the lumen, thus modulates the extent of photoprotection at moderate high light.

KEA3 however appeared inactive in the dark. This hints that the activity of the protein may be regulated depending on environmental conditions. This control of KEA3 activity could be achieved through one of the two regulatory domains it bears. A promising hypothesis is

that the EF-hand is involved in enhancing KEA3 activity, possibly by promoting dimerization.

KEA3 is the first ion channel ever characterized in a diatom, and the first regulator of the proton motive force in *P. tricornutum* belonging neither to chloroplast nor mitochondrial the electron transport chain. Even though KEA3 is a major regulator of photoprotection in diatoms, our study has revealed that it is most likely part of a wide, yet unknown, network of thylakoid ion channels and transporters.

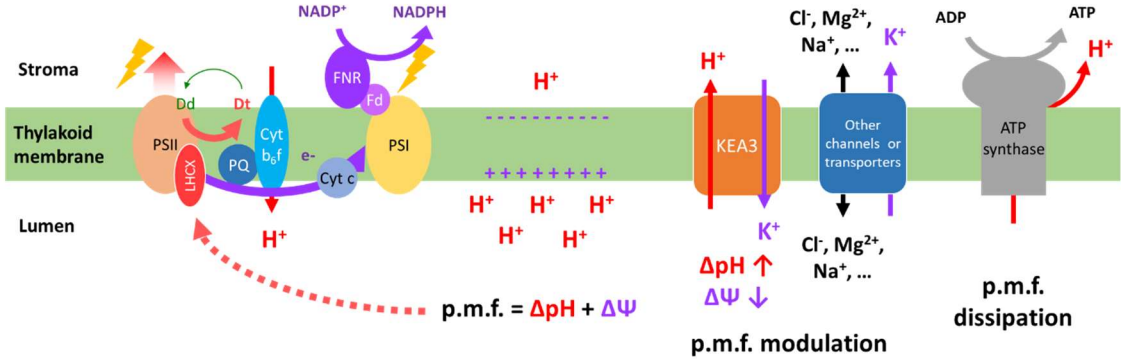


***FIGURE 7.1. ION FLUXES AND PHOTOPROTECTION EFFECTORS ACROSS THE THYLAKOID MEMBRANE IN P. TRICORNUTUM.***

# 8 MATERIALS AND METHODS

## 8.1 ANALYSIS OF PROTEIN SEQUENCES

### 8.1.1 Phylogenetic tree construction

Phylogenetic trees were constructed using the **Phylogeny** web tool (Dereeper *et al.*, 2008, 2010) with the following parameters: "A la Carte" Mode; Alignment – MUSCLE; Curation – GBLOCKS (options: allow gap positions within the final blocks; allow less strict flanking positions); Phylogeny – PhylML (Bootstrapping procedure, number of bootstraps = 100) + aLRT.

The tree was plotted in R (R foundation for statistical analysis, Vienna, Austria) using the **Treeio** package (Wang *et al.*, 2020).

### 8.1.2 Analysis of protein sequences

Protein domains were detected using the **InterPro** web tool (Mitchell *et al.*, 2019).

Transmembrane helixes were detected using the **TMHMM** (Krogh *et al.*, 2001) and **TMPred** (Rost, Fariselli and Casadio, 1996).

Transit peptides for *P. tricornutum* genes were detected using **Asafind**, **SignalP** and **Hectar** (Gschloessl, Guermeur and Cock, 2008; Petersen *et al.*, 2011; Gruber *et al.*, 2015).

## 8.2 ANALYSIS OF TRANSCRIPTOMIC DATASETS

Transcriptomic datasets are very valuable sources of information when studying an unknown gene. Although the function of most genes products of *P. tricornutum* remain until today unknown, a large number of transcriptomics studies have already been conducted that all provide precious clues on the behavior of a certain gene candidate (here, the KEA family) depending on growth conditions. These data are very helpful to orientate research towards the most promising directions.

The transcriptomic datasets that have been analyzed in this manuscript were obtained from two different techniques (microarray and RNA-sequencing), each requiring a different treatment.

### 8.2.1 Microarray datasets

Among the microarray datasets involving the response of *P. tricornutum* genes to light, we chose the tons that included data on the response of the two genes of interest (Phatr3_J39274 and Phatr3_J11843). Two datasets satisfying that condition were chosen involving *P. tricornutum* genes (Chauton *et al.*, 2013; Nymark *et al.*, 2013) were downloaded from the **GEO** database under the accession numbers GSE42514 and GSE42039.

When performing a microarray study, several hybridization probes are designed for each gene. This is why these datasets come in two files: the first one is named 'family' and the second one 'series matrix'. The 'family' file contains all the information linking each probe identifier to the gene it was designed for. The 'series matrix' file contains the response of each probe to all the conditions investigated in the study. The 'series matrix' file had already been transformed using the quantile-normalization method by the authors of the studies. The background had not been corrected for.

Using R (R foundation for statistical analysis, Vienna, Austria), each probe identifier in the 'series matrix' table was assigned to the gene it detected. Sometimes, the same gene was detected by several probes. We chose to keep only the probe that provided the highest values in order to minimize the effect of background noise. The different biological replicates were replaced by the median value for each condition (the median being less sensitive to noise than the mean). We thus obtained a table containing one robust expression value for each gene in each condition.

### 8.2.2 RNA-sequencing dataset

The dataset describing the response of genes from the green alga *C. reinhardtii* during a day (Strenkert *et al.*, 2019) was presented as metric Fragment Per Kilobase of transcript per Million mapped reads (FPKM). This dataset was already normalized and only provided one value per gene and per condition; therefore it was used as such without any modifications.

## 8.3 DIATOM CULTURE CONDITIONS

### 8.3.1 Diatom culture in liquid cultures

Wild-type, KO-mutants and complemented strains were grown in ESAW (Enriched Seawater, Artificial Water) liquid medium (Berges, Franklin and Harrison, 2001), supplemented in nitrogen and phosphorus (10 times more than the standard medium), enabling to reach higher cell density. The subsequent medium (Table 8.1) is named ESAW 10N 10P in the followings. Cells were grown at 20°C under continuous shaking (100 rpm)

und semi-continuous illumination (12h:12h photoperiod) at a light intensity of 40 µmol.photons.$m^{-2}$ in a INFORS multitron growth cabinet (INFORS, Switzerland).

Cells were harvested in mid-exponential phase when reaching the cell density of 5 million/mL from 1 to 4 hours maximum after the light had been switched on.

| | Final (M) | | Final (M) |
|---|---|---|---|
| NaCl | $3{,}63.10^{-1}$ | Fe-EDTA | $6{,}55.10^{-6}$ |
| $Na_2SO4$ | $2{,}50.10^{-2}$ | $Na_2EDTA.2H_2O$ | $8{,}30.10^{-6}$ |
| KCl | $8{,}03.10^{-3}$ | $ZnSO_4.7H_2O$ | $2{,}54.10^{-7}$ |
| $NaHCO_3$ | $2{,}07.10^{-3}$ | $CoSO_4.7H_2O$ | $5{,}69.10^{-8}$ |
| KBr | $7{,}25.10^{-4}$ | $MnSO_4.4H_2O$ | $2{,}42.10^{-6}$ |
| $H_3BO_3$ | $3{,}72.10^{-4}$ | $Na_2MoO_4.2H_2O$ | $6{,}12.10^{-9}$ |
| NaF | $6{,}67.10^{-5}$ | $Na_2SeO_3$ | $1{,}00.10^{-9}$ |
| $MgCl_2.6H_2O$ | $4{,}71.10^{-2}$ | $NiCl_2.6H_2O$ | $6{,}27.10^{-9}$ |
| $CaCl_2.2H_2O$ | $9{,}14.10^{-3}$ | $CuSO_4.5H_2O$ | $3{,}92.10^{-8}$ |
| $SrCl_2.6H_2O$ | $8{,}18.10^{-5}$ | Thiamin HCl (vitamin B1) | $2{,}96.10^{-7}$ |
| $NaNO_3$ | $5{,}49.10^{-3}$ | Cycobalamin (vitamin B12) | $1{,}48.10^{-9}$ |
| $NaH_2PO_4.H_20$ | $2{,}24.10^{-4}$ | Biotin (vitamin H) | $4{,}09.10^{-9}$ |

***TABLE 8.1. COMPOSITION OF THE ESAW 10N 10P MEDIUM.***

### 8.3.2 Diatom culture on agar plates

Mutant selection was performed on agar plates (agar 1% (w/v) in ESAW 10N 10P) supplemented with an antibiotic if required, at a light intensity of 20 µmol.photons.$m^{-2}$ at 18°C in a vertical light chamber (Sanyo plant growth chamber, Sanyo Japan).

### 8.3.3 Diatom storage

Wild-type and mutant strains were kept for storage in liquid ESAW 10N 10P supplemented with the proper antibiotics in the same conditions as agar plates.

## 8.4 MOLECULAR CLONING

### 8.4.1 DNA cloning

Plasmids of interest were constructed using Gibson assembly (Gibson et al., 2009). Briefly, template plasmids were linearized using appropriate restriction enzymes. DNA to be inserted was amplified by PCR with overlapping ends. These DNA fragments were then assembled in the presence of a 5' exonuclease, a DNA polymerase and a DNA ligase.

### 8.4.2 Contents of used plasmids

Several types of plasmids were constructed in this study for different purposes (Table 8.2).

| | Antibiotic resistance in *E. coli* | Other content |
|---|---|---|
| pKsdiaCas9_sgRNA | Carbenicillin | Cas9 and guide RNA expressed in *P. tricornutum* |
| pKsdiaCas9_sgRNA_ZeoR | Carbenicillin | Zeocin resistance, Cas9 and guide RNA expressed in *P. tricornutum* |
| pPHA_gene_BlastiR | Carbenicillin | Blasticidin resistance and gene of interest under the control of the Fcp promotor |
| pTA_MOB | Gentamycin | CEN/ARS yeast conjugative element expressed in *E. coli* |
| pPtBR11_gene_BlastiR | Carbenicillin | Blasticidin resistance and protein of interest under the control of the histone 4 promotor (pH4) |
| pET-28a_gene-his | Kanamycin | Gene of interest fused with His tag in under the control for the LacI promotor expressed in *E. coli* |

***TABLE 8.2. MAIN CHARACTERISTICS OF THE FAMILIES OF PLASMIDS USED IN THIS STUDY.***

### 8.4.3 Plasmid transformation in *E. coli*

In most cases, plasmids were used to transform Top10 *E. coli* competent cells (Invitrogen) with heat shock treatment according to the manufacturer's instructions. In case of a double transformation with two plasmids (e.g. pTA-MOB and pPtBR11), the protocol was adapted to leave a longer recovery time between transformation and selection by the two antibiotics.

The vector pET was transformed in Rosetta *E. coli* competent cells (Novagen) according to the manufacturer's instructions.

### 8.4.4 DNA sequencing

Plasmid DNA from *E. coli* cells was harvested and purified using a plasmid DNA extraction kit (Macherey-Nagel).

To select mutant strains in *P. tricornutum*, a few cells from single colonies were harvested from an agar plate using a sterile toothpick. The toothpick bearing algae was placed inside a ready-made PCR mix. The PCR was purified from a gel using a gel extraction kit (Macherey-Nagel).

PCR fragments and plasmids were sent for sequencing to (Eurofins Genomics, Netherlands and Macrogen Europe, Germany) following their instructions.

### 8.4.5 Recombinant production of the soluble part of KEA3

In order to produce an antibody directed against KEA3, we first produced a part of KEA3 that was expected not to be cytotoxic as in (Graindorge *et al.*, 2010). The *kea3* gene was cloned into the expression vector pET-28 starting from base 1749 (C. Giustini and G. Mangeonjean). The vector was eventually cloned into *E. coli* cells Production of the protein fragment was induced with IPTG. Bacteria were harvested and pelleted by centrifugation and eventually lysed by sonication. The recombinant protein fraction was purified on a nickel affinity column. The purity of the sample was verified on SDS-PAGE.

## 8.5 DIATOM GENETIC ENGINEERING

Two techniques have been used to generate *P. tricornutum* mutants: biolistics transformation and bacterial conjugation.

### 8.5.1 Biolistic transformation

#### *8.5.1.1 Principle of the biolistic transformation*

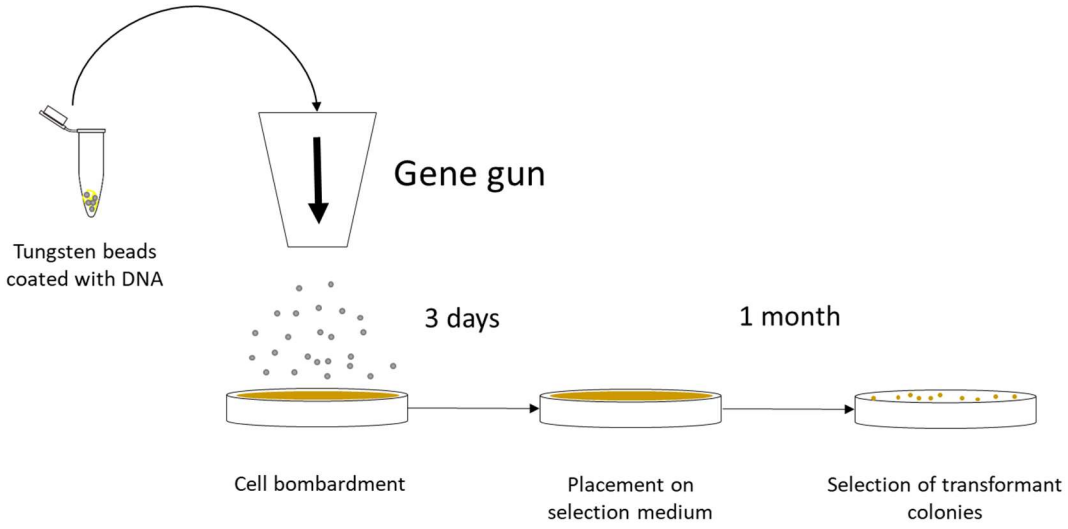


***FIGURE 8.1. SCHEME OF THE BIOLISTIC TRANSFORMATION OF DIATOMS.***

The biolistic transformation consists in bombarding plated diatoms with tungsten beads coated with a plasmid. The DNA content of the plasmid integrates inside of the genome of *P. tricornutum* and is expressed by the nucleus machinery. All of the biolistic transformations were performed as described in the article by Allorent et al (Allorent *et al.*, 2018). A typical yield for that kind of transformation is about 50 to 100 transformants per

plate (Figure 8.1). In the case of CRISPR-Cas9 transformation notably not all transformants are mutants, therefore the actual yield is more of 5 to 10 mutants per plate.

#### *8.5.1.2 Generation of KO-mutants*

The Cas9 protein participates in a bacterial defense system against pathogens. A guide RNA recognizes a specific sequence in the DNA of a pathogen. The Cas9 endonuclease then creates a double strand break in the DNA. Random errors in the repair eventually lead to inactivation of important genes in the pathogen through the apparition of frameshifts and early stop codons.

The CRISPR-Cas9 system has been adapted for *P. tricornutum* in the laboratory by G. Allorent and C. Giustini. All steps were therefore performed as in (Allorent *et al.*, 2018).

The first step is to identify CRISPR target sites that must fulfill two conditions: (1) they must exhibit the recognition motif for the Cas9, i.e. 5'-G(19bps)NGG-3' (2) they must be specific for the gene so as to avoid off-target gene editing. Adapters (Table 8.3) were designed and integrated in the plasmid pKSdiaCas9_sgRNA (AddGene) or the derived pKSdiaCas9_sgRNA_ZeoR plasmid (Table MM.2) and used for biolistics transformation.

| Mutant | DNA strand | Adapters sequence (5'-3') | Plasmid and experimenter |
|---|---|---|---|
| *kea3-2* | Forward | TCGAGGGGCAATCCTGGGACCCAA<br>AAACTTGGGTCCCAGGATTGCCCC | pKS_diaCas9; G. Allorent |
| *kea3-2* | Forward | TCGAGACATTGAACTCGGGGACGT<br>AAACACGTCCCCGAGTTCAATGTC | pKS_diaCas9; G. Allorent |
| *ΔEF-1* | Forward | TAGGGCTGGAAATGTACCAAGCCA<br>AAACTGGCTTGGTACATTTCCAGC | pKS_diaCas9_ZeoR; C. Seydoux |
| *ΔEF-2* | Reverse | TAGGGGCGGATCGGGGCAATTCAT<br>AAACATGAATTGCCCCGATCCGCC | pKS_diaCas9_ZeoR; C. Seydoux |

***TABLE 8.3. LIST OF ADAPTERS USED TO CONSTRUCT THE MUTANTS DESCRIBED IN THIS STUDY.***

#### *8.5.1.3 Mutant screening*

Mutant colonies were selected on plates. Their DNA was amplified by PCR using primers located 100 to 200 bp away from the expected cutting site. Amplicons were sequenced and compared to WT sequence (Figure 8.2). Most transformants colonies were a mixture of wild-type and mutant strains. When necessary, pure clones were isolated by several streaking steps.


***FIGURE 8.2. MUTANT DETECTION.***

*Aligned chromatograms of WT, transformant and isolated mutant. The mutant here is* ΔEF-1. *It displays a 8 bps deletion, causing a frameshift.*

## 8.5.2 Transformation by bacterial conjugation

### *8.5.2.1 Principle of bacterial conjugation*

An alternative strategy to transform diatom cells by bacterial conjugation has been used to transform *P. tricornutum* cells, in order to increase the transformation yield and speed up the process. Bacteria are able to exchange genetic material between one another by close physical contact. Such transfers have been optimized to enable genetic engineering of eukaryotes, including *P. tricornutum* (Karas *et al.*, 2015; Diner *et al.*, 2016). The protocol described below is adapted from the procedure by (Diner *et al.*, 2016).

Diatoms are mixed in close contact with *E. coli* cells containing both the pTA-MOB plasmid allowing the expression of the conjugative machinery in *E. coli* and the pPtBR11 vector containing the gene to be expressed in the diatom. The conjugation protocol yielded a high number of transformants (about 200 per plate) in about three weeks.

### *8.5.2.2 Heterogeneity in gene expression on conjugation transformed cells*

Two transformants obtained by conjugation with the construct pPtBR11_mOrange_ZeoR (named hereafter *mOrange-5B* and *mOrange*-6A) were screened by PCR. In both of them, the gene *mOrange* was correctly amplified. However, when analyzed with immunoblotting, only one out of the two strains did express the *mOrange* protein at the expected size, which was also verified by confocal imaging (not shown).

This argues against the use of the conjugation protocol for mutant generation, since detection of mutants by immunoblotting or phenotyping is more time extensive than by

PCR and requires either an antibody to be available or a phenotype to be properly characterized beforehand.

### 8.5.3 Comparison between the two transformation strategies available in the laboratory

The advantages and drawbacks of the two gene editing techniques presented above are summarized in Table 8.4 below.

| | Biolistic transformation | Bacterial conjugation |
|---|---|---|
| Advantages | Similar expression level for all transformants<br>Screening by PCR | No alteration of the original genome<br>Suitable for transient expression<br>High number of transformants<br>Fast recovery of transformants |
| Drawbacks | Possible damages to the genome due to the bombardment<br>Insertion locus is not controlled<br>Handling of toxic material (tungsten beads)<br>Many colonies are a mixture of WT and mutant | Screening needs to be performed by assessing the actual protein expression or mRNA transcription (functional analysis, Northern blot, Western blot, etc…)<br>The episome may not remain stable in *P. tricornutum* throughout generations |

***TABLE 8.4. ADVANTAGES AND DRAWBACKS OF TRANSFORMING P. TRICORNUTUM CELLS USING BIOLISTICS OR CONJUGATION IN THE LABORATORY.***

## 8.6 PROTEIN ANALYSIS

### 8.6.1 Preparation of protein extracts

#### *8.6.1.1 Preparation of total protein extracts*

Total protein was isolated from cell cultures in mid-exponential phase in Hepes 50mM, EDTA-free protein inhibitor cocktail (Prote@se, Roche, Switzerland). Cell walls were mechanically disrupted by four cycles of liquid nitrogen freezing/thawing and by vortexing in the presence of micro glass beads (Sigma Aldrich, 425-600 µm). After removing unbroken cell material and beads by centrifugation (7500 g, 30 seconds), the crude protein extract was precipitated for 20 minutes at -20°C on 80% (v/v) acetone. After centrifugation (15000 g, 20 minutes), the pellet was resuspended for 5 minutes at 4°C in 50 mM Tris, pH 7.6, 2% SDS supplemented with protein inhibitor. The suspension was again centrifuged to eliminate insoluble particles and the supernatant was kept as **total protein extract**.

#### *8.6.1.2 Preparation of membrane-enriched protein extracts*

To enrich extracts in soluble proteins or membrane protein, the following procedure was applied: the flow-through obtained after centrifugation in the presence of micro glass beads was centrifuged for 90 seconds at 13200 rpm at 4°C.

(1) The supernatant resulting from the centrifugation separating membrane proteins was enriched in soluble proteins. It was resuspended in 50 mM Tris, pH 7.6, 2% SDS supplemented with protein inhibitor cocktail (Prote@se, Roche, Switzerland) and used as **soluble protein extract**.

(2) The pellet resulting from this centrifugation was washed with Hepes 50 mM NaCl 500 mM and centrifuged for 90 seconds at 13200 rpm at 4°C. The supernatant was discarded. The washing procedure was repeated a second time. Eventually, the pellet was resuspended in 50 mM Tris, pH 7.6, 2% SDS supplemented with protein inhibitor cocktail (Prote@se, Roche, Switzerland) and used as **membrane protein extract**.

### 8.6.2 Protein quantification

Protein concentration was determined by BCA protein assay (Pierce, France) following the supplier's instruction with a BSA as standard.

### 8.6.3 Separation of proteins by electrophoresis (SDS-PAGE)

Electrophoresis was carried out according to the protocol by Laemmli (Laemmli, 1970).

### 8.6.4 Transfer

The separated proteins were transferred onto either a nitrocellulose or a PVDF membrane (previously soaked for 10 min in methanol before transfer). Transfer was performed at a constant voltage (115 V) for 75 min in 20 mM Tris, 153 mM glycine, 0.08 SDS, 20% ethanol (for nitrocellulose) or methanol (for PVDF) (Flori *et al.*, 2017).

The membrane is blocked in TBS-Tween 0.1% (v/v) supplemented with 5% w/v powder milk either 1h at room temperature or overnight at 4°C. In case the protein to be detected was GFP, the blocking solution was TBS-Tween 5% following supplier's instructions (Milteny Biotech, Germany).

### 8.6.5 Immunodetection of proteins

The membrane was washed with TBS-Tween 0.1%(v/v). The primary antibody was diluted in TBS-Tween 0.1% (1:1000 to 1:25000) and incubated with the membrane overnight at 4°C. The membrane was washed with TBS-Tween and incubated with a secondary antibody

directed against either rabbit or guinea pig (BioRad, USA) and diluted 1:10000 in TBS-Tween. The membrane was washed with TBS-Tween and placed in the presence of an electroluminescence substrate for the HRP protein coupled to the secondary antibody (Clarity Western Blot, BioRad, USA). Imaging is performed following manufacturer's instruction with a Chemidoc (BioRad, USA).

## 8.7 PIGMENT ANALYSIS

### 8.7.1 Pigment extraction

The protocol was established by M. Kuntz (Allorent *et al.*, 2013). 25 millions of *P. tricornutum* cells were harvested by centrifugation at 4°C and resuspended in 100 µL of ice-cold Methanol, Tris-HCl 10 mM, pH 7.4. Pigment extraction was carried out under argon atmosphere, on ice and in the dark to prevent pigment degradation. Pigments were extracted 3 times with 100 µL methanol until their complete solubilization in the organic phase (white pellet). All supernatants were pooled and dried under argon flux to allow complete evaporation of methanol. The extracts were further used for HPLC analysis.

To prevent modification of the pigment pool during centrifugation, an alternative protocol was used to avoid the centrifugation step. This latter protocol was mainly used for the determination of the de-epoxidation state ($D.E.S. = \frac{[Diatoxanthin]}{[Diatoxanthin] + \{Diadinoxanthin\}}$).

To perform pigment analysis, *P. tricornutum* cells (25 millions) were harvested and immediately frozen with liquid nitrogen. The sample was then lyophilized overnight. The resulting powder was extracted twice with 1 mL methanol in the dark, on ice and under argon atmosphere. The supernatants were dried under argon flux and further used for HPLC analysis.

### 8.7.2 HPLC analysis

Pigments in the dried supernatant were resuspended in 100 µL DMF and injected on a HPLC (Varian ProStar 800, Varian, USA), coupled to a diode detector. They were separated on a C18 column (Macherey-Nagel, France) extracted in the following solvents, in order (1) a mixture of 80% methanol and 20% water with a final ammonium acetate concentration of 0.1 M (2) 90% acetonitrile 10% water (3) 100% ethyl acetate. Pigments were identified according to their retention time and absorption spectrum as described in (Allorent et al, 2013).

## 8.8 ANALYSIS OF PHOTOSYNTHETIC ACTIVITY *IN VIVO*

### 8.8.1 Fluorescence measurements

#### *8.8.1.1 Principle of the measurement and main parameters*

Two devices have been used to perform photosynthetic measurements: a camera and a pulse amplification modulation fluorometer (PAM).

#### *8.8.1.2 Fluorescence measurements at the Pulse Amplification Modulator (PAM) fluorometer*

For these measurements, cells were concentrated to reach a cell density of 15 million cells/mL. They were measured inside the chamber of a Hansatech Oxygen meter (Hansatech, UK). The sample was illuminated from the side by a continuous white light. Cells were kept under constant agitation and constant temperature 19°C.

Fluorescence was induced using a red light of 100 kHz frequency. The contribution to global fluorescence of the white light and the measuring light can thus be easily separated by signal de-modulation i.e. considering only the component of 100 Hz frequency for fluorescence records.

#### *8.8.1.3 Fluorescence measurements in multi-well plates with a Speed Zen imaging fluorometer*

An imaging fluorometer (Speedzen 3, JbeamBio, France) enables to perform the same physiological measurement but in a multiplexed manner. 200 µL of cell suspension is harvested at 5 million cells/mL in exponential phase and placed on a 96-wells plate. If needed, the appropriate amount of inhibitor was added to the well. Cells rested in the dark for about ten minutes before measurement.

The sample was illuminated from the top by a red light of tunable intensity. Fluorescence was induced using short, blue pulses. While measuring fluorescence, the red light was turned off to avoid artifacts. Fluorescence was recorded using a highly sensitive and fast camera (Orca 4-Flash, Hamamatsu, Japan).

#### *8.8.1.4 Comparison between the two devices*

The camera and the PAM each have their advantages and drawbacks summarized in Table 8.5. below. Although in principle these two devices measure the same thing, in practice each of them is appropriate for a type of experiment.

| | PAM | Camera |
|---|---|---|
| Measurement in physiological state | Cells are kept agitated. | The cells may settle down. |
| | The cuvette is connected to a bath to control temperature. | The device tends to heat when used for a long time. |
| | Cells are concentrated prior to recording, possibly affecting their physiological state. | Cells are directly taken from their culture flask. |
| Practicality and reproducibility of data | The user needs to change lights manually. | Illumination sequences are set by the user before the measurement and can be re-used for reproducibility. |
| | Inhibitors and chemicals can be added throughout the measurement. | Inhibitors can only be added before the measurement. |
| | Samples must be recorded one by one. | Several different samples (inhibitor concentration, strain, etc.) can be measured at the same time. |

***TABLE 8.5 COMPARISON BETWEEN FLUORESCENCE MEASUREMENTS AT THE PAM OR AT THE CAMERA.***

#### *8.8.1.1 NPQ induction by acid shift in the dark*

The experiments involving NPQ induction by a pH-shift in the dark (see Section 2) were conducted using the PAM fluorometer. Before and after every addition of chemical, the pH was monitored.

Cells were concentrated to reach 15 million cells/ml and resuspended in fresh ESAW medium. $NPQ_{max}$ was measured by exposing cells to high light (1200 µmol.photons.$m^{-2}$) for a few minutes (generally about 8). NPQ was then relaxed in low light (30 µmol.photons.$m^{-2}$). The light was switched off and 20µM nigericin was added. Several doses of acetic acid (100 mM stock) or potassium hydroxide (10 mM stock) were added to the cell suspension.

### 8.8.2 Electrochromic shift measurements

During photosynthetic reactions, the water-splitting reaction, as well as proton transfer across the thylakoid membrane during plastoquinone-mediated electron transfer, ATP synthase activity, contribute to the buildup of an electric field (ΔΨ) across the thylakoid membrane. This electric field can be measured using the electrochromic shift (ECS) signal. These data provide information on the composition and dynamics of each the components of the photosynthetic chain (Bailleul et al., 2015).

#### *8.8.2.1 Principle*

The orbital energies of a molecule placed in an electric field are shifted proportionally to the intensity of the field (Stark effect). The electric field induced by photosynthetic reactions (ΔΨ) therefore causes a shift in the absorption band of the chlorophylls and carotenoids embedded in the thylakoid membrane protein complexes (Witt, 1979). This band shift is called electrochromic shift (ECS). The amplitude of the ECS is directly dependent on the intensity of the electric field (Figure 8.3).

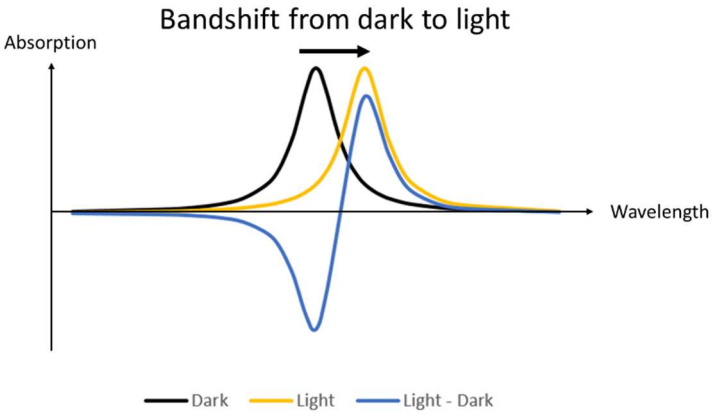


***FIGURE 8.3 PRINCIPLE OF AN ECS SPECTRUM.***

*When shifted from dark (black) to light (black), the induced electric field causes a displacement in the absorption spectrum. This displacement is proportional to the intensity of the electric field. The difference between the dark spectrum and the light spectrum (blue) is called the ECS spectrum.*

An ECS spectrum is thus a differential spectrum between dark and light (Figure 8.3).

#### *8.8.2.2 ECS spectrum in P. tricornutum*

The ECS spectrum of *P. tricornutum* has been described in (Bailleul *et al.*, 2015). It exhibits two main peaks: the first one at 520 nm, which varies linearly with the electric field (linear ECS), and the second at 565 nm, which varies in a quadratic manner to the field (quadratic ECS). At the same time, some molecules shift spectrum between their oxidized and reduced state in the light (e.g. PSI and cytochromes), in parallel to the establishment of the ECS. A simple measurement enables to quantify the oxidation state of each of these components, simultaneously. The signal deriving from the cytochromes corresponds to both cytochrome $b_6f$ and cytochrome $c_6$ (the soluble carrier replacing plastocyanin in *P. tricornutum*).

Since the peak of the cytochromes is located in between the peaks of linear ECS and quadratic ECS, it needs to be deconvoluted to properly estimate the extent of the signal. The deconvolution of the parameters that can be estimated with the ECS method is summarized in Table 8.6 below.

| Name | Calculation | Comment |
|---|---|---|
| Cyt | $A_{554} - 0.4 * (A_{520} + A_{565})$ | Signal proportional to the oxidation of cytochromes( $b_6f$ and $c_6$) |
| $ECS_{lin}$ | $A_{520} - 0.25 * Cyt$ | Signal proportional to $\Delta\Psi$ |
| $ECS_{qd}$ | $A_{565} + 0.15 * Cyt$ | Signal proportional to $\Delta\Psi^2$ |
| P700 | $A_{705}$ | Signal proportional to the oxidation of PSI |

***TABLE 8.6 LIST OF ECS PARAMETERS AND THEIR INTERPRETATION.***

### *8.8.2.3 Experimental setup*

All spectroscopic measurements were performed using a JTS-10 spectrophotometer (Biologic, France).

This instrument is equipped with several LED sources of tunable intensity (Figure 8.4). The measuring light flux (on the left side) is split in two by a semi-dichroic mirror. A blank is made in the dark by adjusting the shutter so that the signal received on the reference and the detector are at the same level. The sample is then illuminated by a chosen actinic light of pre-established sequence. The wavelength received on the detector is selected by interference filters (3 to 8 nm bandwidth). An external source of light can also be added (red light or laser).

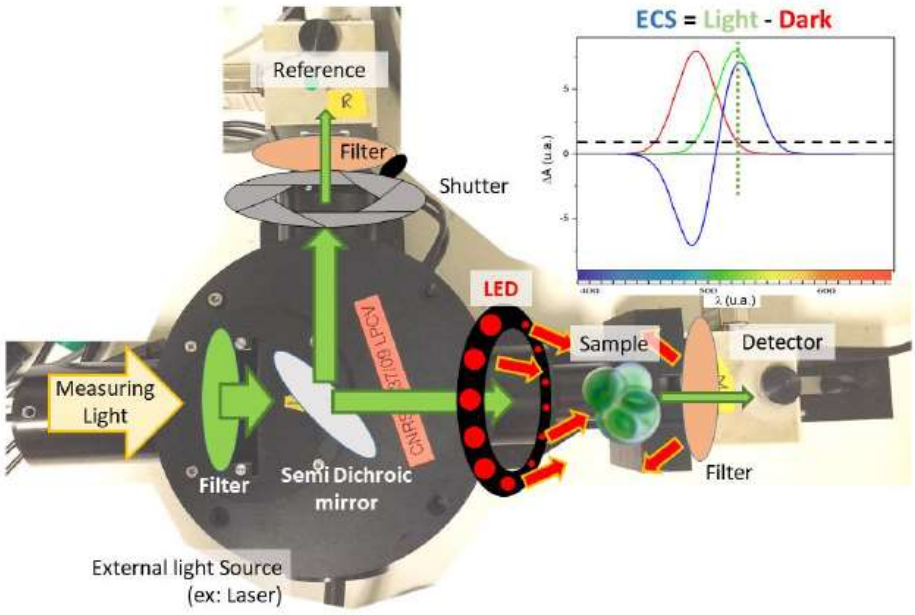


***FIGURE 8.4 A JOLIOT TYPE SPECTROPHOTOMETER.***

*Green arrows represent the path of the measuring light. Red arrows represent the path of the LED source that illuminate the sample. Adapted from D. Dal Bo.*

The point of using a laser flash is that this pulse is both saturating (it activates all photosystems in the sample) and very short (only one charge separation per photosystem is performed).

## 8.9 STATISTICAL ANALYSIS

Statistical analysis were performed using R 3.6.2 (R foundation for statistical analysis, Vienna, Austria). Significant differences between groups were analyzed using a Kruskal and Wallis test followed by a Dunn test corrected for multiple comparisons by the Benjamini-Hochberg procedure. Threshold for significance was set to $p < 0.05$.

# 9 ANNEXES

## 9.1 HOMOLOGUES OF KEA3

Protein sequences of members of the KEA family *A. thaliana* and from KefC in *E. coli* were retrieved from Uniprot. Members of the KEA family in other species were detected using the tool BLASTp. AtKEA1, AtKEA3 and AtKEA4 were used as query sequences. The organisms searched for were *Physcomitrella patens (taxid:3218)*, *Chlamydomonas reinhardtii (taxid:3055)*, *red algae (taxid:2763)*, *stramenopiles (taxid:33634).*

While the genome annotation of *A. thaliana*, *P. patens* and *C. reinhardtii* is well annotated, such is not the case for most read algae and stramenopiles. Many protein sequences retrieved from this search were incomplete or obviously truncated. This is why only a few species were selected: *Chondrus crispus* and *Cyanidioschoyzon merolae* for red algae and *Ectocarpus siliculosus* (brown, multicellular alga), *Nannochloropsis gaditana* (eustigmatophyte), *Thalassiosira pseudonana* (centric diatom), *Fragiliaropsis cylindrus* (araphid pennate diatom), *Pseudo-nitszchia multistriata* (toxic, raphid pennate diatom), *Phaeodactylum tricornutum* (raphid pennate diatom). The list of either gene or protein identifier corresponding to the protein sequences used is available in Table 9.1.

| Organism | Protein name in the tree | Accession | Database used |
|---|---|---|---|
| *A. thaliana* | KEA1 (A. thaliana) | *Q9ZTZ7* | Uniprot |
| *A. thaliana* | KEA2 (A. thaliana) | *O65272* | Uniprot |
| *A. thaliana* | KEA3 (A. thaliana) | *Q9M0Z3* | Uniprot |
| *A. thaliana* | KEA4 (A. thaliana) | *Q9ZUN3* | Uniprot |
| *A. thaliana* | KEA5 (A. thaliana) | *Q8VYR9* | Uniprot |
| *A. thaliana* | KEA6 (A. thaliana | *B5X0N6* | Uniprot |
| *E. coli* | KefC (E. coli) | *P03819* | Uniprot |
| *P. patens* | *Pp3c7_22160* | *Pp3c7_22160V3.1* | Phytozome |
| *P. patens* | *Pp3c11_22410* | *Pp3c11_22410V3.1* | Phytozome |
| *P. patens* | *Pp3c11_6640* | *Pp3c11_6640V3.1* | Phytozome |
| *P. patens* | *Pp3c8_16170* | *Pp3c8_16170V3.1* | Phytozome |
| *P. patens* | *Pp3c24_12350* | *Pp3c24_12350V3.1* | Phytozome |
| *C. reinhardtii* | *Cre04.g220200* | *Cre04.g220200* | Phytozome |
| *C. reinhardtii* | *Cre12.g493000* | *Cre12.g493000* | Phytozome |
| *C. reinhardtii* | *Cre16.g687450* | *Cre16.g687450* | Phytozome |
| *P. tricornutum* | *Phatr3_J39274* | *Phatr3_J39274* | Ensembl protists |

| | | | |
|---|---|---|---|
| *P. tricornutum* | *Phatr3_J11843* | *Phatr3_J11843* | Ensembl protists |
| *P. multistriata* | *Psmu _091370* | *Psnmu_V1.4_Aug-ev_pasav3_091370* | Ensembl protists |
| *P. multistriata* | *Psmu _0083060* | *Psnmu_V1.4_Aug-ev_pasav3_0083060* | Ensembl protists |
| *T. pseudonana* | *Thapsdraft_38289* | *Thapsdraft_38289* | Ensembl protists |
| *T. pseudonana* | *Thapsdraft_262069* | *Thapsdraft_262069* | Ensembl protists |
| *T. pseudonana* | *Thapsdraft_4710* | *Thapsdraft_4710* | Ensembl protists |
| *T. pseudonana* | *Thapsdraft_33205* | *Thapsdraft_33205* | Ensembl protists |
| *F. cylindrus* | *Fracydraft_156905* | *Fracydraft_156905* | Ensembl protists |
| *F. cylindrus* | *Fracydraft_260848* | *Fracydraft_260848* | Ensembl protists |
| *F. cylindrus* | *Fracydraft_157103* | *Fracydraft_157103* | Ensembl protists |
| *F. cylindrus* | *Fracydraft_147433* | *Fracydraft_147433* | Ensembl protists |
| *E. siliculosus* | *Esi_0131_0051* | *Esi_0131_0051* | Ensembl protists |
| *E. siliculosus* | *Esi_0035_0123* | *Esi_0035_0123* | Ensembl protists |
| *E. siliculosus* | *Esi_0070_0026* | *Esi_0070_0026* | Ensembl protists |
| *C. crispus* | *Chc_T5414001* | *Chc_T00005414001* | Ensembl plants |
| *C. crispus* | *Chc_T383001* | *Chc_T00000383001* | Ensembl plants |
| *C. crispus* | *Chc_T9033001* | *Chc_T00009033001* | Ensembl plants |
| *C. merolae* | Cms232C | *CMS232CT* | Ensembl plants |
| *C. merolae* | Cmk288C | *CMK288CT* | Ensembl plants |

***TABLE 9.1. LIST OF IDENTIFIERS OF THE PROTEINS OF THE KEA FAMILY USED IN THIS MANUSCRIPT.***

## 9.2 LIST OF MUTANTS CREATED

In Table 9.2 below are listed some of the mutants created and discussed in this study.

| Mutant name | Description | Technique and experimenter |
|---|---|---|
| *kea3-1* | KO-mutant of kea3 generated by CRISPR-Cas9 | Biolistics, G. Allorent |
| *kea3-2* | KO-mutant of kea3 generated by CRISPR-Cas9 | Biolistics, G. Allorent |
| *kea3-1/*KEA3-GFP | Complementation of *kea3-1* with kea3 fused to egfp in C-terminal under the control of the Lhcf1 promotor | Biolistics, G. Allorent |
| *mOrange-5B* | Heterologous expression of mOrange in WT cells under the control of the H4 promotor | Bacterial conjugation, C. Giustini |
| *mOrange-6A* | Heterologous expression of mOrange in WT cells under the control of the H4 promotor | Bacterial conjugation, C. Giustini |
| *kea3-1*/mOrange | Heterologous expression of mOrange in WT cells under the control of the H4 promotor | Bacterial conjugation, C. Seydoux |

| Mutant name | Description | Technique and experimenter |
|---|---|---|
| *ΔEF-1* | Mutant of KEA3 generated by CRISPR-Cas9 bearing the kea3 gene deprived of EF-hand | Biolistics, C. Seydoux |
| *ΔEF-2* | Mutant of KEA3 generated by CRISPR-Cas9 bearing a frameshift aberrant sequence instead of the EF-hand. | Biolistics, C. Seydoux |

***TABLE 9.2. LIST OF SOME OF THE MUTANTS GENERATED IN THIS STUDY***

## 9.3 POTENTIAL REGULATORS OF THE P.M.F. IN *P. TRICORNUTUM*

The ion channels identified as potential regulators of the chloroplast proton motive force in Section 6.3.2 are listed in the two tables below (Table 9.3 are Table 9.4). Table 9.3 lists the genes identified from homology with known chloroplast ion channels and transporters in *A. thaliana.*

| Gene in *A. thaliana* | Homologue in *P. tricornutum* | Predicted localization (Hectar) | Predicted localization (Asafind) |
|---|---|---|---|
| AtClCe | **Phatr3_J43785 (top hit)** | Signal peptide | Plastid, low confidence |
| | Phatr3_J39421 | Other localization | SignalP negative |
| AtVCCN1 and AtVCCN2 | Phatr3_EG02285 (top hit) | Signal peptide | SignalP negative |
| | **Phatr3_J37111** | Signal peptide | Plastid, high confidence |
| | **Phatr3_J26635** | Signal peptide | Plastid, high confidence |
| | **Phatr3_EG02292** | Chloroplast | Plastid, high confidence |
| | **Phatr3_J46336** | Chloroplast | Plastid, high confidence |
| | Phatr3_J46360 | Other localization | SignalP negative |
| AtTPK3 | Phatr3_J43530 (top hit) | Signal anchor | SignalP negative |
| | Phatr3_J43171 | Signal peptide | SignalP negative |
| | Phatr3_J3676 | Other localization | SignalP negative |
| | **Phatr3_J38821** | Signal peptide | Plastid, high confidence |

***TABLE 9.3. BLAST HITS AND PUTATIVE LOCALIZATION OF HOMOLOGUES OF CLCE, VCCN AND TPK3 IN P. TRICORNUTUM.***

*Proteins likely to be plastid-localized are highlighted in bold. The localization of the proteins were predicted using Hectar, Asafind and SignalP.* (Gschloessl, Guermeur and Cock, 2008; Petersen *et al.*, 2011; Gruber *et al.*, 2015)

Table 9.4 lists the genes identified by crossing Hectar prediction results (Gschloessl, Guermeur and Cock, 2008) with the Membrane Transport Database(Elbourne *et al.*, 2017).

| Gene ID | Localization (Hectar) | Transporter family (Membrane Transport Database) | Predicted mode of transport |
|---|---|---|---|
| Phatr3_J23830 | Chloroplast | Phosphate inorganic transporter (PiT) | $HPO_4^{2-}/H^+$ symport |
| Phatr3_J39274 | Chloroplast | Monovalent cation:H+ antiporter (CPA2) | $K^+/H^+$ antiport |
| Phatr3_J43194 | Chloroplast | Anion exchanger (AE) | $Na^+/HCO_3^-$ symport |
| Phatr3_J45656 | Chloroplast | Anion exchanger (AE) | $Na^+/HCO_3^-$ symport |
| Phatr3_J10409 | Signal peptide | Monovalent cation:H+ antiporter (CPA1) | $Na^+/H^+$ antiport |
| Phatr3_J14996 | Signal peptide | YggT family | $K^+$ channel? |
| Phatr3_J43171 | Signal peptide | Voltage activated inward channel (VIC) | $K^+$ channel |
| Phatr3_J43785 | Signal peptide | Chloride carrier/channel (ClC) | $Cl^-$ channel |
| Phatr3_J47666 | Signal peptide | Phosphate:sodium symporter (PNaS) | $HPO_4^{2-}/Na^+$ symport |
| Phatr3_J47784 | Signal peptide | Chloride carrier/channel (ClC) | $Cl^-$ channel |
| Phatr3_J49064 | Signal peptide | Na+:H+ antiporter (NhaC) | $Na^+/H^+$ antiport |
| Phatr3_J50012 | Signal peptide | Small conductance mechanosenstitive ion channel (MscS) | $Na^+/H^+$ antiport |

***TABLE 9.4. LIST OF POTENTIAL CHLOROPLAST LOCALIZED ION TRANSPORTERS IDENTIFIED BY CROSSING HECTAR RESULTS WITH THE MEMBRANE TRANSPORT DATABASE.***

*ATP synthase subunits and metal transporters (Zn, Cu) have been excluded from this table. The gene Phatr3_J39274, which we have identified here as PtKEA3, appears in this table.*

# BIBLIOGRAPHY


Abida, H. *et al.* (2015) 'Membrane glycerolipid remodeling triggered by nitrogen and phosphorus starvation in Phaeodactylum tricornutum', *Plant Physiology*, 167(1), pp. 118–136. doi: 10.1104/pp.114.252395.

Ahmed, S. and Booth, I. R. (1983) 'The use of valinomycin, nigericin and trichlorocarbanilide in control of the protonmotive force in Escherichia coli cells', *Biochemical Journal*, 212(1), pp. 105–112. doi: 10.1042/bj2120105.

Allorent, G. *et al.* (2013) 'Dual strategy to cope with high light in Chlamydomonas reinhardtii', *Plant Cell*, 25(2), pp. 545–557. doi: 10.1105/tpc.112.108274.

Allorent, G. *et al.* (2018) 'Generation of mutants of nuclear-encoded plastid proteins using CRISPR/Cas9 in the diatom Phaeodactylum tricornutum', in *Methods in Molecular Biology*. doi: 10.1007/978-1-4939-8654-5_24.

Annunziata, R. *et al.* (2019) 'BHLH-PAS protein RITMO1 regulates diel biological rhythms in the marine diatom Phaeodactylum tricornutum', *Proceedings of the National Academy of Sciences of the United States of America*, 116(26), pp. 13137–13142. doi: 10.1073/pnas.1819660116.

Aranda-Sicilia, M. N. *et al.* (2012) 'Arabidopsis KEA2, a homolog of bacterial KefC, encodes a K +/H+ antiporter with a chloroplast transit peptide', *Biochimica et Biophysica Acta - Biomembranes*. Elsevier B.V., 1818(9), pp. 2362–2371. doi: 10.1016/j.bbamem.2012.04.011.

Aranda-Sicilia, M. N. *et al.* (2016) 'Envelope K+/H+ antiporters AtKEA1 and AtKEA2 function in plastid development', *Plant Physiology*, 172(1), pp. 441–449. doi: 10.1104/pp.16.00995.

Armbrust, E. V. *et al.* (2004) 'The genome of the diatom Thalassiosira Pseudonana: Ecology, evolution, and metabolism', *Science*, 306(5693), pp. 79–86. doi: 10.1126/science.1101156.

Armbruster, U. *et al.* (2014) 'Ion antiport accelerates photosynthetic acclimation in fluctuating light environments', *Nature Communications*. Nature Publishing Group, 5. doi: 10.1038/ncomms6439.

Armbruster, U. *et al.* (2016) 'Regulation and levels of the thylakoid K+/H+ antiporter KEA3 shape the dynamic response of photosynthesis in fluctuating light', *Plant and Cell*

*Physiology*, 57(7), pp. 1557–1567. doi: 10.1093/pcp/pcw085.

Bailleul, B. *et al.* (2010) 'An atypical member of the light-harvesting complex stress-related protein family modulates diatom responses to light', *Proceedings of the National Academy of Sciences of the United States of America*, 107(42), pp. 18214–18219. doi: 10.1073/pnas.1007703107.

Bailleul, B. *et al.* (2015) 'Energetic coupling between plastids and mitochondria drives CO 2 assimilation in diatoms', *Nature*, 524(7565), pp. 366–369. doi: 10.1038/nature14599.

Ballottari, M. *et al.* (2016) 'Identification of ph-sensing sites in the light harvesting complex stress-related 3 protein essential for triggering non-photochemical quenching in chlamydomonas reinhardtii', *Journal of Biological Chemistry*, 291(14), pp. 7334–7346. doi: 10.1074/jbc.M115.704601.

Bascuñán-Godoy, L. *et al.* (2010) 'Leaf functional and micro-morphological photoprotective attributes in two ecotypes of Colobanthus quitensis from the Andes and Maritime Antarctic', *Polar Biology*, 33(7), pp. 885–896. doi: 10.1007/s00300-010-0765-4.

Bellaflore, S. *et al.* (2005) 'State transitions and light adaptation require chloroplast thylakoid protein kinase STN7', *Nature*, 433(7028), pp. 892–895. doi: 10.1038/nature03286.

Berges, J. A., Franklin, D. J. and Harrison, P. J. (2001) 'Evolution of an artificial seawater medium: Improvements in enriched seawater, artificial water over the last two decades', *Journal of Phycology*. doi: 10.1046/j.1529-8817.2001.01052.x.

Berry, E. A., Guergova-Kuras, M. and Crofts, A. R. (2000) 'Structure and Function of Cytochrome bc Complexes', *Annual Review of Biochemistry*, 69(1), pp. 1005–1075.

Bhattacharya, D., Yoon, H. S. and Hackett, J. D. (2004) 'Photosynthetic eukaryotes unite: Endosymbiosis connects the dots', *BioEssays*. doi: 10.1002/bies.10376.

Blommaert, L. *et al.* (2017) 'Contrasting NPQ dynamics and xanthophyll cycling in a motile and a non-motile intertidal benthic diatom', *Limnology and Oceanography*, 62(4), pp. 1466–1479. doi: 10.1002/lno.10511.

Bölter, B. *et al.* (2019) 'The topology of plastid inner envelope potassium cation efflux antiporter KEA1 provides new insights into its regulatory features', *Photosynthesis Research*. Springer Netherlands, (0123456789). doi: 10.1007/s11120-019-00700-2.

Bowler, C. *et al.* (2008) 'The Phaeodactylum genome reveals the evolutionary history of diatom genomes', *Nature*, 456(7219), pp. 239–244. doi: 10.1038/nature07410.

Bowler, C., Vardi, A. and Allen, A. E. (2010) 'Oceanographic and Biogeochemical Insights from Diatom Genomes', *Annual Review of Marine Science*, 2(1), pp. 333–365. doi: 10.1146/annurev-marine-120308-081051.

Boyer, P. D. (1999) 'Molecular motors: What makes ATP synthase spin?', *Nature*, 402(6759), pp. 247–249. doi: 10.1038/46193.

Brand, J. J. and Becker, D. W. (1984) 'Evidence for direct roles of calcium in photosynthesis', *Journal of Bioenergetics and Biomembranes*, 16(4), pp. 239–249. doi: 10.1007/BF00744278.

Bratt, C. E. *et al.* (1995) 'Regulation of violaxanthin de-epoxidase activity by pH and ascorbate concentration', *Photosynthesis Research*, 45(2), pp. 169–175. doi: 10.1007/BF00032588.

Brembu, T. *et al.* (2014) 'The chloroplast genome of the diatom Seminavis robusta: New features introduced through multiple mechanisms of horizontal gene transfer', *Marine Genomics*. The Authors, 16(1), pp. 17–27. doi: 10.1016/j.margen.2013.12.002.

Buck, J. M. *et al.* (2019) 'Lhcx proteins provide photoprotection via thermal dissipation of absorbed light in the diatom Phaeodactylum tricornutum', *Nature Communications*. Springer US, 10(1). doi: 10.1038/s41467-019-12043-6.

Butler, W. L. (1978) 'Energy distribution in the photochemical apparatus of photosynthesis', *Annual Review of Plant Phyisiology*, 29(1), pp. 345–378.

Campanella, M. *et al.* (2009) 'IF1: setting the pace of the F1Fo-ATP synthase', *Trends in Biochemical Sciences*. doi: 10.1016/j.tibs.2009.03.006.

Cardol, P., Forti, G. and Finazzi, G. (2011) 'Regulation of electron transport in microalgae', *Biochimica et Biophysica Acta - Bioenergetics*. Elsevier B.V., 1807(8), pp. 912–918. doi: 10.1016/j.bbabio.2010.12.004.

Carradec, Q. *et al.* (2018) 'A global ocean atlas of eukaryotic genes', *Nature Communications*, 9(1). doi: 10.1038/s41467-017-02342-1.

Carraretto, L. *et al.* (2013) 'A thylakoid-located two-pore K+ channel controls photosynthetic light utilization in plants', *Science*. doi: 10.1126/science.1242113.

Chakraborty, A. *et al.* (2014) 'Trapping effect analysis of AlGaN/InGaN/GaN Heterostructure by conductance frequency measurement', in *MRS Proceedings*, pp. 81–87. doi: 10.1007/s13398-014-0173-7.2.

Chanroj, S. *et al.* (2012) 'Conserved and diversified gene families of monovalent cation/H+

antiporters from algae to flowering plants', *Frontiers in Plant Science*, 3(FEB), pp. 1–18. doi: 10.3389/fpls.2012.00025.

Chauton, M. S. *et al.* (2013) 'Gene Regulation of Carbon Fixation, Storage, and Utilization in the Diatom Phaeodactylum tricornutum Acclimated to Light/Dark Cycles 1[C][W][OA]', *Plant Physiology Ò*, 161, pp. 1034–1048. doi: 10.1104/pp.112.206177.

Chow, W. S. (2003) 'Photosynthesis: From Natural Towards Artificial', *Journal of Biological Physics*, 29(4), pp. 447–459. doi: 10.1023/A:1027371022781.

Cock, J. M. and Coelho, S. M. (2011) 'Algal models in plant biology', *Journal of Experimental Botany*, 62(8), pp. 2425–2430. doi: 10.1093/jxb/err117.

Colin, S. *et al.* (2017) 'Quantitative 3D-imaging for cell biology and ecology of environmental microbial eukaryotes'. doi: 10.7554/eLife.26066.001.

Correa-Galvis, V. *et al.* (2020) 'H+ transport by K+ EXCHANGE ANTIPORTER3 promotes photosynthesis and growth in chloroplast ATP synthase mutants', *Plant Physiology*, 182(April), p. pp.01561.2019. doi: 10.1104/pp.19.01561.

Crofts, A. R. (1967) 'Amine Uncoupling of Energy Transfer in Chloroplasts', *The Journal of Biological Chemistry*, 242(14), pp. 3352–3359.

Cruz, S. *et al.* (2011) 'Impact of chlororespiration on non-photochemical quenching of chlorophyll fluorescence and on the regulation of the diadinoxanthin cycle in the diatom Thalassiosira pseudonana', *Journal of Experimental Botany*, 62(2), pp. 509–519. doi: 10.1093/jxb/erq284.

Darrouzet, E. *et al.* (2000) 'Uncovering the [2Fe2S] domain movement in cytochrome bc1 and its implications for energy conversion', *Proceedings of the National Academy of Sciences of the United States of America*, 97(9), pp. 4567–4572. doi: 10.1073/pnas.97.9.4567.

Demmig-Adams, B. and Adams, W. W. (1996) 'The role of xanthophyll cycle carotenoids in the protection of photosynthesis', *Trends in Plant Science*, 1(1), pp. 21–26. doi: 10.1016/S1360-1385(96)80019-7.

Demmig, B. and Winter, K. (1986) 'Sodium, potassium, chloride and proline concentrations of chloroplasts isolated from a halophyte, Mesembryanthemum crystallinum L.', *Planta*, 168(3), pp. 421–426. doi: 10.1007/BF00392371.

Dereeper, A. *et al.* (2008) 'Phylogeny.fr: robust phylogenetic analysis for the non-specialist', *Nucleic acids research*, 36(Suppl_2), pp. W465–W469. doi: 10.1093/nar/gkn180.

Dereeper, A. *et al.* (2010) 'BLAST-EXPLORER helps you building datasets for phylogenetic

analysis', *BMC Evolutionary Biology*, 10(1), pp. 1–6. doi: 10.1186/1471-2148-10-8.

Dinc, E. *et al.* (2016) 'LHCSR1 induces a fast and reversible pH-dependent fluorescence quenching in LHCII in Chlamydomonas reinhardtii cells', *Proceedings of the National Academy of Sciences of the United States of America*, 113(27), pp. 7673–7678. doi: 10.1073/pnas.1605380113.

Diner, R. E. *et al.* (2016) 'Refinement of the diatom episome maintenance sequence and improvement of conjugation-based DNA delivery methods', *Frontiers in Bioengineering and Biotechnology*, 4(AUG). doi: 10.3389/fbioe.2016.00065.

Duan, Z. *et al.* (2016) 'A bestrophin-like protein modulates the proton motive force across the thylakoid membrane in Arabidopsis', *Journal of Integrative Plant Biology*, 58(10), pp. 848–858. doi: 10.1111/jipb.12475.

Dukic, E. *et al.* (2019) 'K+ and Cl− channels/transporters independently fine-tune photosynthesis in plants', *Scientific Reports*, 9(1), pp. 1–12. doi: 10.1038/s41598-019-44972-z.

Eberhard, S., Finazzi, G. and Wollman, F.-A. (2008) 'The Dynamics of Photosynthesis', *Annual Review of Genetics*, 42(1), pp. 463–515. doi: 10.1146/annurev.genet.42.110807.091452.

Eilers, U. *et al.* (2016) 'Identification of genes coding for functional zeaxanthin epoxidases in the diatom Phaeodactylum tricornutum', *Journal of Plant Physiology*. Elsevier GmbH., 192, pp. 64–70. doi: 10.1016/j.jplph.2016.01.006.

Eisenhut, M. *et al.* (2018) 'The Plastid Envelope CHLOROPLAST MANGANESE TRANSPORTER1 Is Essential for Manganese Homeostasis in Arabidopsis', *Molecular Plant*. Elsevier Ltd, 11(7), pp. 955–969. doi: 10.1016/j.molp.2018.04.008.

Elbourne, L. D. H. *et al.* (2017) 'TransportDB 2.0: A database for exploring membrane transporters in sequenced genomes from all domains of life', *Nucleic Acids Research*. doi: 10.1093/nar/gkw1068.

Falciatore, A. *et al.* (2000) 'Perception of environmental signals by a marine diatom', *Science*, 288(5475), pp. 2363–2366. doi: 10.1126/science.288.5475.2363.

Falciatore, A. *et al.* (2020) 'Diatom Molecular Research Comes of Age: Model Species for Studying Phytoplankton Biology and Diversity', *The Plant cell*, 32(3), pp. 547–572. doi: 10.1105/tpc.19.00158.

Falconet, D. (2011) 'Origin, Evolution and Division of Plastids', in, pp. 35–61. doi:

10.1007/978-94-007-1579-0_2.

Falkowski, P. (2012) 'Ocean science: The power of plankton', *Nature*, 483(7387), pp. S17–S20. doi: 10.1038/483S17a.

Falkowski, P. G. *et al.* (1981) 'Effects of Growth Irradiance Levels on the Ratio of Reaction Centers in Two Species of Marine Phytoplankton', *Plant Physiology*, 68(4), pp. 969–973. doi: 10.1104/pp.68.4.969.

Finazzi, G. (2002) 'Redox-coupled proton pumping activity in cytochrome b6f, as evidenced by the pH dependence of electron transfer in whole cells of Chlamydomonas reinhardtii', *Biochemistry*, 41(23), pp. 7475–7482. doi: 10.1021/bi025714w.

Finazzi, G. and Rappaport, F. (1998) 'In Vivo Characterization of the Electrochemical Proton Gradient Generated in Darkness in Green Algae and Its Kinetic Effects on Cytochrome b 6 f Turnover †', 2960(98), pp. 9999–10005. doi: 10.1021/bi980320j.

Fischer, S. and Gräber, P. (1999) 'Comparison of ΔpH- and Δφ-driven ATP synthesis catalyzed by the H+-ATPases from Escherichia coli or chloroplasts reconstituted into liposomes', *FEBS Letters*, 457(3), pp. 327–332. doi: 10.1016/S0014-5793(99)01060-1.

Flori, S. *et al.* (2016) 'Ultrastructure of the Periplastidial Compartment of the Diatom Phaeodactylum tricornutum.', *Protist*, 167(3), pp. 254–67. doi: 10.1016/j.protis.2016.04.001.

Flori, S. *et al.* (2017) 'Plastid thylakoid architecture optimizes photosynthesis in diatoms', *Nature Communications*. Nature Publishing Group, 8. doi: 10.1038/ncomms15885.

Foyer, C. H. and Shigeoka, S. (2011) 'Understanding oxidative stress and antioxidant functions to enhance photosynthesis', *Plant Physiology*, 155(1), pp. 93–100. doi: 10.1104/pp.110.166181.

Fujisawa, M., Ito, M. and Krulwich, T. A. (2007) 'Three two-component transporters with channel-like properties have monovalent cation/proton antiport activity', *Proceedings of the National Academy of Sciences of the United States of America*, 104(33), pp. 13289–13294. doi: 10.1073/pnas.0703709104.

Giovagnetti, V. and Ruban, A. V. (2018) 'The evolution of the photoprotective antenna proteins in oxygenic photosynthetic eukaryotes', *Biochemical Society Transactions*, 46(5), pp. 1263–1277. doi: 10.1042/BST20170304.

Goss, R. *et al.* (2006) 'The importance of a highly active and ΔpH-regulated diatoxanthin epoxidase for the regulation of the PS II antenna function in diadinoxanthin cycle containing

algae', *Journal of Plant Physiology*, 163(10), pp. 1008–1021. doi: 10.1016/j.jplph.2005.09.008.

Goss, R. and Jakob, T. (2010) 'Regulation and function of xanthophyll cycle-dependent photoprotection in algae', *Photosynthesis Research*, 106(1–2), pp. 103–122. doi: 10.1007/s11120-010-9536-x.

Goss, R. and Lepetit, B. (2015) 'Biodiversity of NPQ', *Journal of Plant Physiology*, 172, pp. 13–32. doi: 10.1016/j.jplph.2014.03.004.

Graindorge, M. *et al.* (2010) 'Identification of a plant gene encoding glutamate/aspartate-prephenate aminotransferase: The last homeless enzyme of aromatic amino acids biosynthesis', *FEBS Letters*, 584(20), pp. 4357–4360. doi: 10.1016/j.febslet.2010.09.037.

Graven, S. N., Estrada-O, S. and Lardy, H. A. (1966) 'Alkali metal cation release and respiratory inhibition induced by nigericin in rat liver mitochondria.', *Proceedings of the National Academy of Sciences of the United States of America*, 56(2), p. 654. doi: 10.1073/pnas.56.2.654.

Grouneva, I. *et al.* (2006) 'Influence of ascorbate and pH on the activity of the diatom xanthophyll cycle-enzyme diadinoxanthin de-epoxidase', *Physiologia Plantarum*, 126(2), pp. 205–211. doi: 10.1111/j.1399-3054.2006.00613.x.

Grouneva, I. *et al.* (2013) 'Phylogenetic viewpoints on regulation of light harvesting and electron transport in eukaryotic photosynthetic organisms', *Planta*. doi: 10.1007/s00425-012-1744-5.

Gruber, A. *et al.* (2015) 'Plastid proteome prediction for diatoms and other algae with secondary plastids of the red lineage', *Plant Journal*, 81(3), pp. 519–528. doi: 10.1111/tpj.12734.

Gschloessl, B., Guermeur, Y. and Cock, J. M. (2008) 'HECTAR: A method to predict subcellular targeting in heterokonts', *BMC Bioinformatics*, 9, pp. 1–13. doi: 10.1186/1471-2105-9-393.

Guglielmi, G. *et al.* (2005) 'The light-harvesting antenna of the diatom Phaeodactylum tricornutum: Evidence for a diadinoxanthin-binding subcomplex', *FEBS Journal*, 272(17), pp. 4339–4348. doi: 10.1111/j.1742-4658.2005.04846.x.

Hahn, A. *et al.* (2018) 'Structure, mechanism, and regulation of the chloroplast ATP synthase', *Science*, 360(6389). doi: 10.1126/science.aat4318.

Hao, T. Bin *et al.* (2018) 'Light-harvesting protein Lhcx3 is essential for high light acclimation of Phaeodactylum tricornutum', *AMB Express*. Springer Berlin Heidelberg, 8(1).

doi: 10.1186/s13568-018-0703-3.

Herdean, A., Teardo, E., *et al.* (2016) 'A voltage-dependent chloride channel fine-tunes photosynthesis in plants', *Nature Communications*, 7(May), pp. 1–11. doi: 10.1038/ncomms11654.

Herdean, A., Nziengui, H., *et al.* (2016) 'The Arabidopsis thylakoid chloride channel AtCLCe functions in chloride homeostasis and regulation of photosynthetic electron transport', *Frontiers in Plant Science*, 7(FEB2016), pp. 1–15. doi: 10.3389/fpls.2016.00115.

Hieber, A. D., Bugos, R. C. and Yamamoto, H. Y. (2000) 'Plant lipocalins: Violaxanthin de-epoxidase and zeaxanthin epoxidase', *Biochimica et Biophysica Acta - Protein Structure and Molecular Enzymology*, 1482(1–2), pp. 84–91. doi: 10.1016/S0167-4838(00)00141-2.

Hisabori, T. *et al.* (2002) 'Molecular devices of chloroplast F1-ATP synthase for the regulation', *Biochimica et Biophysica Acta - Bioenergetics*. doi: 10.1016/S0005-2728(02)00269-4.

Howe, C. J. *et al.* (2006) 'The novel cytochrome c6 of chloroplasts: A case of evolutionary bricolage?', *Journal of Experimental Botany*, 57(1), pp. 13–22. doi: 10.1093/jxb/erj023.

Ishitani, M. *et al.* (2000) 'SOS3 function in plant salt tolerance requires N-myristoylation and calcium binding', *Plant Cell*. doi: 10.1105/tpc.12.9.1667.

Jakob, T., Goss, R. and Wilhelm, C. (1999) 'Activation of diadinoxanthin de-epoxidase due to a chlororespiratory proton gradient in the dark in the diatom Phaeodactylum tricornutum', *Plant Biology*, 1(1), pp. 76–82. doi: 10.1111/j.1438-8677.1999.tb00711.x.

Jakob, T., Goss, R. and Wilhelm, C. (2001) 'Unusual pH-dependence of diadinoxanthin de-epoxidase activation causes chlororespiratory induced accumulation of diatoxanthin in the diatom Phaeodactylum tricornutum', *Journal of Plant Physiology*. Elsevier GmbH, 158(3), pp. 383–390. doi: 10.1078/0176-1617-00288.

Jiang, Y. *et al.* (2002) 'Crystal structure and mechanism of a calcium-gated potassium channel', *Nature*. doi: 10.1038/417515a.

Johnson, M. P. *et al.* (2008) 'The xanthophyll cycle pool size controls the kinetics of non-photochemical quenching in Arabidopsis thaliana', *FEBS Letters*, 582(2), pp. 262–266. doi: 10.1016/j.febslet.2007.12.016.

Johnson, M. P. and Ruban, A. V. (2014) 'Rethinking the existence of a steady-state $\Delta\psi$ component of the proton motive force across plant thylakoid membranes', *Photosynthesis Research*, 119(1–2), pp. 233–242. doi: 10.1007/s11120-013-9817-2.

Joliot, P. and Joliot, A. (2008) 'Quantification of the electrochemical proton gradient and activation of ATP synthase in leaves', *Biochimica et Biophysica Acta - Bioenergetics*, 1777(7–8), pp. 676–683. doi: 10.1016/j.bbabio.2008.04.010.

Karas, B. J. *et al.* (2015) 'Designer diatom episomes delivered by bacterial conjugation', *Nature Communications*. Nature Publishing Group, 6. doi: 10.1038/ncomms7925.

Kirchhoff, H. *et al.* (2008) 'Protein diffusion and macromolecular crowding in thylakoid membranes', *Plant Physiology*, 146(4), pp. 1571–1578. doi: 10.1104/pp.107.115170.

Kleine, T., Maier, U. G. and Leister, D. (2009) 'DNA Transfer from Organelles to the Nucleus: The Idiosyncratic Genetics of Endosymbiosis', *Annual Review of Plant Biology*, 60(1), pp. 115–138. doi: 10.1146/annurev.arplant.043008.092119.

Kohzuma, K. *et al.* (2013) 'Light- and metabolism-related regulation of the chloroplast ATP synthase has distinct mechanisms and functions', *Journal of Biological Chemistry*, 288(18), pp. 13156–13163. doi: 10.1074/jbc.M113.453225.

Kramer, D. M., Cruz, J. A. and Kanazawa, A. (2003) 'Balancing the central roles of the thylakoid proton gradient', *Trends in Plant Science*, 8(1), pp. 27–32. doi: 10.1016/S1360-1385(02)00010-9.

Krause, G. H. (1991) 'Chlorophyll fluorescence and photosynthesis: the basics', *Annual Review of Plant Phyisiology*, 42, pp. 313–349. doi: 10.1002/9780470122563.ch3.

Krieger-Liszkay, A. (2005) 'Singlet oxygen production in photosynthesis', *Journal of Experimental Botany*, 56(411), pp. 337–346. doi: 10.1093/jxb/erh237.

Krieger-Liszkay, A., Fufezan, C. and Trebst, A. (2008) 'Singlet oxygen production in photosystem II and related protection mechanism', *Photosynthesis Research*, 98(1–3), pp. 551–564. doi: 10.1007/s11120-008-9349-3.

Krogh, A. *et al.* (2001) 'Predicting transmembrane protein topology with a hidden Markov model: Application to complete genomes', *Journal of Molecular Biology*, 305(3), pp. 567–580. doi: 10.1006/jmbi.2000.4315.

Kroth, P. G. *et al.* (2018) 'Genome editing in diatoms: achievements and goals', *Plant Cell Reports*. Springer Berlin Heidelberg, 37(10), pp. 1401–1408. doi: 10.1007/s00299-018-2334-1.

Kunz, H.-H. *et al.* (2014) 'Plastidial transporters KEA1, -2, and -3 are essential for chloroplast osmoregulation, integrity, and pH regulation in Arabidopsis', *Proceedings of the National Academy of Sciences of the United States of America*, 111(20), pp. 7480–7485. doi:

10.1073/pnas.1323899111.

Laemmli, U. K. (1970) 'Cleavage of Structural Proteins during the Assembly of the Head of Bacteriophage T4', *Nature*, 227, pp. 680–685.

Lavaud, J. *et al.* (2002) 'Influence of the diadinoxanthin pool size on photoprotection in the marine planktonic diatom Phaeodactylum tricornutum', *Plant Physiology*, 129(3), pp. 1398–1406. doi: 10.1104/pp.002014.

Lavaud, J. and Kroth, P. G. (2006) 'In diatoms, the transthylakoid proton gradient regulates the photoprotective non-photochemical fluorescence quenching beyond its control on the xanthophyll cycle', *Plant and Cell Physiology*, 47(7), pp. 1010–1016. doi: 10.1093/pcp/pcj058.

Lavaud, J., Rousseau, B. and Etienne, A.-L. (2004) 'General features of photoprotection by energy dissipation in planktonic diatoms (Bacillariophyceae)', *Journal of Phycology*, 40(1), pp. 130–137. doi: 10.1046/j.1529-8817.2004.03026.x.

Legendre, L. *et al.* (2015) 'The microbial carbon pump concept: Potential biogeochemical significance in the globally changing ocean', *Progress in Oceanography*. Elsevier Ltd, 134, pp. 432–450. doi: 10.1016/j.pocean.2015.01.008.

Lewit-Bentley, A. and Réty, S. (2000) 'EF-hand calcium-binding proteins', *Current Opinion in Structural Biology*, 10, pp. 637–643.

Li, D. *et al.* (2016) 'Expression and preliminary characterization of human MICU2', *Biology Open*, 5(7), pp. 962–969. doi: 10.1242/bio.018572.

Li, X.-P. *et al.* (2000) 'A pigment-binding protein is essential for regulation of photosynthetic light harvesting', *Nature*, 403(January), pp. 391–395.

Li, X.-P. *et al.* (2004) 'Regulation of photosynthetic light harvesting involves intrathylakoid lumen pH sensing by the PsbS protein', *Journal of Biological Chemistry*, 279(22), pp. 22866–22874. doi: 10.1074/jbc.M402461200.

Liu, X. *et al.* (2016) 'Addressing various compartments of the diatom model organism Phaeodactylum tricornutum via sub-cellular marker proteins', *Algal Research*, 20, pp. 249–257. doi: 10.1016/j.algal.2016.10.018.

Lohr, M. and Wilhelm, C. (1999) 'Algae displaying the diadinoxanthin cycle also possess the violaxanthin cycle', *Proceedings of the National Academy of Sciences of the United States of America*. Proceedings of the National Academy of Sciences, 96(15), pp. 8784–8789. doi: 10.1073/pnas.96.15.8784.

Lyngberg, L. *et al.* (2011) 'KefF, the regulatory subunit of the potassium efflux system KefC, shows quinone oxidoreductase activity', *Journal of Bacteriology*, 193(18), pp. 4925–4932. doi: 10.1128/JB.05272-11.

Marchand, J. *et al.* (2018) 'Ion and metabolite transport in the chloroplast of algae: lessons from land plants', *Cellular and Molecular Life Sciences*. Springer International Publishing, 75(12), pp. 2153–2176. doi: 10.1007/s00018-018-2793-0.

Matuszyńska, A. *et al.* (2016) 'A mathematical model of non-photochemical quenching to study short-term light memory in plants', *Biochimica et Biophysica Acta - Bioenergetics*, 1857(12), pp. 1860–1869. doi: 10.1016/j.bbabio.2016.09.003.

Maxwell, K. and Johnson, G. N. (2000) 'Chlorophyll fluorescence - a pratical guide', *Journal of Experimental Botany*, 51(345), pp. 659–668. doi: 10.1016/j.rsci.2018.02.001.

Mewes, H. and Richter, M. (2002) 'Supplementary ultraviolet-B radiation induces a rapid reversal of the diadinoxanthin cycle in the strong light-exposed diatom Phaeodactylum tricornutum', *Plant Physiology*, 130(3), pp. 1527–1535. doi: 10.1104/pp.006775.

Meyer, M. T., Whittaker, C. and Griffiths, H. (2017) 'The algal pyrenoid: key unanswered questions', *Journal of experimental botany*, 68(14), pp. 3739–3749. doi: 10.1093/jxb/erx178.

Miller, S. *et al.* (2000) 'Identification of an ancillary protein, YabF, required for activity of the KefC glutathione-gated potassium efflux system in Escherichia coli', *Journal of Bacteriology*, 182(22), pp. 6536–6540. doi: 10.1128/JB.182.22.6536-6540.2000.

Mitchell, A. L. *et al.* (2019) 'InterPro in 2019 : improving coverage , classification and access to protein sequence annotations', 47(November 2018), pp. 351–360. doi: 10.1093/nar/gky1100.

Mitchell, P. (1975) 'The protonmotive Q cycle: a general formulation', *FEBS Letters*, 59(2), pp. 137–139.

Moog, D. *et al.* (2015) 'Localization and evolution of putative triose phosphate translocators in the diatom phaeodactylum tricornutum', *Genome Biology and Evolution*, 7(11), pp. 2955–2969. doi: 10.1093/gbe/evv190.

Morán, X. A. G. *et al.* (2010) 'Increasing importance of small phytoplankton in a warmer ocean', *Global Change Biology*, 16(3), pp. 1137–1144. doi: 10.1111/j.1365-2486.2009.01960.x.

Mulders, K. J. M. (2014) *Phototrophic pigment production with microalgae*. doi:

10.1111/jpy.12173 T4 - Biological constraints and opportunities PM - 26988181 M4 - Citavi.

Murakami, S. *et al.* (2018) 'Structure of the γ–ε complex of cyanobacterial F 1 -ATPase reveals a suppression mechanism of the γ subunit on ATP hydrolysis in phototrophs', *Biochemical Journal*, 475(18), pp. 2925–2939. doi: 10.1042/BCJ20180481.

Niyogi, K. K. and Truong, T. B. (2013) 'Evolution of flexible non-photochemical quenching mechanisms that regulate light harvesting in oxygenic photosynthesis', *Current Opinion in Plant Biology*. Elsevier Ltd, 16(3), pp. 307–314. doi: 10.1016/j.pbi.2013.03.011.

Nymark, M. *et al.* (2013) 'Molecular and Photosynthetic Responses to Prolonged Darkness and Subsequent Acclimation to Re-Illumination in the Diatom Phaeodactylum tricornutum', *PLoS ONE*, 8(3). doi: 10.1371/journal.pone.0058722.

Oja, V., Laisk, A. and Heber, U. (1986) 'Light-induced alkalization of the chloroplast stroma in vivo as estimated from the CO2 capacity of intact sunflower leaves', *BBA - Bioenergetics*, 849(3), pp. 355–365. doi: 10.1016/0005-2728(86)90147-7.

Ovide, C. *et al.* (2018) 'Comparative in depth RNA sequencing of P. tricornutum's morphotypes reveals specific features of the oval morphotype', *Scientific Reports*, 8(1), pp. 1–19. doi: 10.1038/s41598-018-32519-7.

Owens, T. G. (1986) 'Light-Harvesting Function in the Diatom Phaeodactylum tricornutum', *Plant Physiology*, 80(3), pp. 739–746. doi: 10.1104/pp.80.3.739.

Peers, G. *et al.* (2009) 'An ancient light-harvesting protein is critical for the regulation of algal photosynthesis', *Nature*. Nature Publishing Group, 462(7272), pp. 518–521. doi: 10.1038/nature08587.

Petersen, T. N. *et al.* (2011) 'SignalP 4.0: Discriminating signal peptides from transmembrane regions', *Nature Methods*. doi: 10.1038/nmeth.1701.

Pfeil, B. E., Schoefs, B. and Spetea, C. (2014) 'Function and evolution of channels and transporters in photosynthetic membranes', *Cellular and Molecular Life Sciences*, 71(6), pp. 979–998. doi: 10.1007/s00018-013-1412-3.

Pierella Karlusich, J. J., Ibarbalz, F. M. and Bowler, C. (2020) 'Phytoplankton in the Tara Ocean', *Annual Review of Marine Science*, 12(1), pp. 233–265. doi: 10.1146/annurev-marine-010419-010706.

Pu, R. Y., Wang, Y. and Chen, C. H. (1995) 'Enthalpy changes in the formation of the proton electrochemical potential and its components', *Biophysical Chemistry*, 53(3), pp. 283–290.

doi: 10.1016/0301-4622(94)00120-9.

Robinson, S. P. and Downton, W. J. S. (1984) 'Potassium, sodium, and chloride content of isolated intact chloroplasts in relation to ionic compartmentation in leaves', *Archives of Biochemistry and Biophysics*, 228(1), pp. 197–206. doi: 10.1016/0003-9861(84)90061-4.

Roosild, T. P. *et al.* (2002) 'A mechanism of regulating transmembrane potassium flux through a ligand-mediated conformational switch', *Cell*. doi: 10.1016/S0092-8674(02)00768-7.

Roosild, T. P. *et al.* (2009) 'KTN (RCK) Domains Regulate K+ Channels and Transporters by Controlling the Dimer-Hinge Conformation', *Structure*. Elsevier Ltd, 17(6), pp. 893–903. doi: 10.1016/j.str.2009.03.018.

Rost, B., Fariselli, P. and Casadio, R. (1996) 'Topology prediction for helical transmembrane proteins at 86% accuracy', *Protein Science*, 5(8), pp. 1704–1718. doi: 10.1002/pro.5560050824.

Ruban, A. V. *et al.* (2004) 'The super-excess energy dissipation in diatom algae: Comparative analysis with higher plants', *Photosynthesis Research*, 82(2), pp. 165–175. doi: 10.1007/s11120-004-1456-1.

Ruban, A. V. (2016) 'Nonphotochemical chlorophyll fluorescence quenching: Mechanism and effectiveness in protecting plants from photodamage', *Plant Physiology*, 170(4), pp. 1903–1916. doi: 10.1104/pp.15.01935.

Ryther, J. H. and Guillard, R. R. L. (1962) ' STUDIES OF MARINE PLANKTONIC DIATOMS:II. USE OF CYCLOTELLA NANA HUSTEDT FOR ASSAYS OF VITAMIN B 12 IN SEA WATER ', *Canadian Journal of Microbiology*. doi: 10.1139/m62-057.

Schneider, A. *et al.* (2016) 'The evolutionarily conserved protein PHOTOSYNTHESIS AFFECTED MUTANT71 is required for efficient manganese uptake at the thylakoid membrane in Arabidopsis', *Plant Cell*, 28(4), pp. 892–910. doi: 10.1105/tpc.15.00812.

Schober, A. F. *et al.* (2018) 'Isolation of Plastid Fractions from the Diatoms Thalassiosira pseudonana and Phaeodactylum tricornutum', in *Plastids*, pp. 189–203.

Schubert, M. *et al.* (2002) 'Proteome map of the chloroplast lumen of Arabidopsis thaliana', *Journal of Biological Chemistry*, 277(10), pp. 8354–8365. doi: 10.1074/jbc.M108575200.

Serif, M. *et al.* (2018) 'One-step generation of multiple gene knock-outs in the diatom Phaeodactylum tricornutum by DNA-free genome editing', *Nature Communications*, 9(1). doi: 10.1038/s41467-018-06378-9.

Serôdio, J. and Lavaud, J. (2011) 'A model for describing the light response of the nonphotochemical quenching of chlorophyll fluorescence', *Photosynthesis Research*, 108(1), pp. 61–76. doi: 10.1007/s11120-011-9654-0.

Spetea, C., Hideg, É. and Vass, I. (1997) 'Low pH accelerates light-induced damage of photosystem II by enhancing the probability of the donor-side mechanism of photoinhibition', *Biochimica et Biophysica Acta - Bioenergetics*, 1318(1–2), pp. 275–283. doi: 10.1016/S0005-2728(96)00145-4.

Stephan, A. B. *et al.* (2016) 'Rapid hyperosmotic-induced Ca2+ responses in Arabidopsis thaliana exhibit sensory potentiation and involvement of plastidial KEA transporters', *Proceedings of the National Academy of Sciences of the United States of America*, 113(35), pp. E5242–E5249. doi: 10.1073/pnas.1519555113.

Strenkert, D. *et al.* (2019) 'Multiomics resolution of molecular events during a day in the life of Chlamydomonas', *Proceedings of the National Academy of Sciences of the United States of America*, 116(6), pp. 2374–2383. doi: 10.1073/pnas.1815238116.

Sunagawa, S. *et al.* (2020) 'Tara Oceans: towards global ocean ecosystems biology', *Nature Reviews Microbiology*. doi: 10.1038/s41579-020-0364-5.

Szabò, I. and Spetea, C. (2017) 'Impact of the ion transportome of chloroplasts on the optimization of photosynthesis', *Journal of Experimental Botany*, 68(12), pp. 3115–3128. doi: 10.1093/jxb/erx063.

Taddei, L. *et al.* (2016) 'Multisignal control of expression of the LHCX protein family in the marine diatom Phaeodactylum tricornutum', *Journal of Experimental Botany*, 67(13), pp. 3939–3951. doi: 10.1093/jxb/erw198.

Taddei, L. *et al.* (2018) 'Dynamic changes between two LHCX-related energy quenching sites control diatom photoacclimation', *Plant Physiology*. American Society of Plant Biologists (ASPB), 177(3), pp. 953–965. doi: 10.1104/pp.18.00448.

Tesson, B., Gaillard, C. and Martin-Jézéquel, V. (2009) 'Insights into the polymorphism of the diatom Phaeodactylum tricornutum Bohlin', *Botanica Marina*, pp. 104–116. doi: 10.1515/BOT.2009.012.

Thomas, M. K. *et al.* (2012) 'A global pattern of thermal adaptation in marine phytoplankton', *Science*, 338(6110), pp. 1085–1088. doi: 10.1126/science.1224836.

Tian, L. *et al.* (2019) 'PH dependence, kinetics and light-harvesting regulation of nonphotochemical quenching in Chlamydomonas', *Proceedings of the National Academy of Sciences of the United States of America*, 116(17), pp. 8320–8325. doi:

10.1073/pnas.1817796116.

Tikhonov, A. N. (2014) 'The cytochrome b6f complex at the crossroad of photosynthetic electron transport pathways', *Plant Physiology and Biochemistry*. Elsevier Masson SAS, 81, pp. 163–183. doi: 10.1016/j.plaphy.2013.12.011.

Tréguer, P. *et al.* (2018) 'Influence of diatom diversity on the ocean biological carbon pump', *Nature Geoscience*. Springer US, 11(1), pp. 27–37. doi: 10.1038/s41561-017-0028-x.

Tsujii, M. *et al.* (2019) 'Evidence for potassium transport activity of Arabidopsis KEA1-KEA6', *Scientific Reports*, 9(1), pp. 1–13. doi: 10.1038/s41598-019-46463-7.

Uwizeye, C. *et al.* (2020) 'In-cell quantitative structural imaging of phytoplankton using 3D electron microscopy', *bioRxiv*, (May), p. 2020.05.19.104166. doi: 10.1101/2020.05.19.104166.

De Vitry, C. *et al.* (2004) 'The chloroplast rieske iron-sulfur protein. At the crossroad of electron transport and signal transduction', *Journal of Biological Chemistry*, 279(43), pp. 44621–44627. doi: 10.1074/jbc.M406955200.

Wang, C. *et al.* (2016) 'A Putative Chloroplast-Localized Ca 2+ /H + Antiporter CCHA1 Is Involved in Calcium and pH Homeostasis and Required for PSII Function in Arabidopsis'. doi: 10.1016/j.molp.2016.05.015.

Wang, C. *et al.* (2017) 'Fine-tuned regulation of the K+/H+ antiporter KEA3 is required to optimize photosynthesis during induction', *Plant Journal*, 89(3), pp. 540–553. doi: 10.1111/tpj.13405.

Wang, C. and Shikanai, T. (2019) 'Modification of activity of the thylakoid H+/K+ antiporter Kea3 disturbs ΔpH-dependent regulation of photosynthesis', *Plant Physiology*, 181(2), pp. 762–773. doi: 10.1104/pp.19.00766.

Wang, L. G. *et al.* (2020) 'Treeio: An R Package for Phylogenetic Tree Input and Output with Richly Annotated and Associated Data', *Molecular Biology and Evolution*. doi: 10.1093/molbev/msz240.

Wang, Y. *et al.* (2019) 'Golgi-localized cation/proton exchangers regulate ionic homeostasis and skotomorphogenesis in Arabidopsis', *Plant Cell and Environment*, 42(2), pp. 673–687. doi: 10.1111/pce.13452.

Werdan, K., Heldt, H. W. and Milovancev, M. (1975) 'The role of pH in the regulation of carbon fixation in the chloroplast stroma. Studies on CO2 fixation in the light and dark', *BBA - Bioenergetics*, 396(2), pp. 276–292. doi: 10.1016/0005-2728(75)90041-9.

Witt, H. T. (1979) 'Energy conversion in the functional membrane of photosynthesis. Analysis by light pulse and electric pulse methods. The central role of the electric field', *BBA Reviews On Bioenergetics*, 505(3–4), pp. 355–427. doi: 10.1016/0304-4173(79)90008-9.

Yamamoto, H. Y., Nakayama, T. O. M. and Chichester, C. O. (1962) 'Studies on the Light and Dark Interconversion of Leaf Xanthophylls', *Archives of Biochemistry and Biophysics*, 97, pp. 168–173.

Yap, K. L. *et al.* (1999) 'Diversity of conformational states and changes within the EF-hand protein superfamily', *Proteins: Structure, Function and Genetics*, 37(3), pp. 499–507. doi: 10.1002/(SICI)1097-0134(19991115)37:3<499::AID-PROT17>3.0.CO;2-Y.

Zhang, C. and Hu, H. (2014) 'High-efficiency nuclear transformation of the diatom Phaeodactylum tricornutum by electroporation', *Marine Genomics*, 16, pp. 63–66. doi: 10.1016/j.margen.2013.10.003.

Zhou, Y., Frey, T. K. and Yang, J. J. (2009) 'Viral calciomics: Interplays between Ca2+ and virus', *Cell Calcium*, 46(1), pp. 1–17. doi: 10.1016/j.ceca.2009.05.005.

Zhu, X. *et al.* (2018) 'K + efflux antiporters 4, 5, and 6 mediate pH and K + homeostasis in endomembrane compartments', *Plant Physiology*, 178(4), pp. 1657–1678. doi: 10.1104/pp.18.01053.

# LIST OF ABBREVIATIONS

AOX – Alternative oxidase

ATP – Adenosine tri-phosphate

CDS – Coding sequence

CRISPR – Clustered regularly interspaced short palindromic repeats

cTP – Chloroplast transit peptide

Dd – Diadinoxanthin

DDE – Diadinoxanthin de-epoxidase

DEP – Diatoxanthin epoxidase

Dt - Diatoxanthin

DES – De-epoxidation state

ECS – Electrochromic shift

ETR – Electron transfer rate

FNR – Ferredoxin NADPH-reductase

FPKM – metric Fragment Per Kilobase of transcript per Million mapped reads

GFP – Green fluorescent protein

HL – High light

HPLC – High pressure liquid chromatography

ISP – Iron-sulfur protein

KEA – $K^+$ exchange antiporter

$k_{epox}$ – Rate constant of DEP

$k_{de\text{-}epox}$ – Rate constant of DDE

KO – Knock-out

KTN – $K^+$ transport nucleotide

LHC – Light harvesting complex

LHCSR – Light harvesting complex, stress related

LL – Low light

ML – Moderate light

NADH – Nicotinamide adenine dinucleotide

NADPH – Nicotinamide adenine dinucleotide phosphate

NPQ – Non-photochemical quenching

$NPQ_{max}$ – Maximum capacity for non-photochemical quenching

OEC – Oxygen evolving complex

PAM – Pulse amplification modulator

PCR – Polymerase chain reaction

PSI – Photosystem I

PSII – Photosystem II

PQ – Plastoquinone

$PQH_2$ – Plastoquinol

p.m.f. – Proton motive force

qE – Energy quenching

qI – Photoinhibition

qT – State transition dependent quenching

RCK – Regulator of $K^+$ conductance

rETR – Relative electron transfer rate

ROS – Reactive oxygen species

VDE – Violaxanthin de-epoxidase

WT – Wild-type

XP – Xanthophyll pool

ZEP – Zeaxanthin epoxidase

# TABLE OF FIGURES

# TABLE OF TABLES

La lumière du soleil est la source d'énergie primaire sur dont dépendent directement ou indirectement tous les organismes pour leurs besoins métaboliques. Malgré les nombreux avantages de l'utilisation d'une source d'énergie abondante et inépuisable, la lumière est néanmoins intrinsèquement variable et intermittente. Afin de survivre, les organismes photosynthétiques doivent constamment adapter leur machinerie moléculaire de capture de la lumière, en particulier par l'induction de mécanismes de quenching non-photochimiques (NPQ). Le contrôle de l'équilibre entre photosynthèse et photoprotection s'effectue chez les plantes supérieures et les algues vertes par une régulation fine des composantes électrique et osmotique de la force proton motrice à travers la membrane des thylacoïdes. L'homéostasie ionique joue donc un rôle majeur dans la régulation de la photosynthèse. La modulation de la composition de la force proton motrice par des échangeurs ioniques est un moyen pour les organismes photosynthétiques de réguler efficacement l'induction du NPQ, c.à.d. en minimisant les pertes d'énergie tout en préservant la synthèse d'ATP.

Les diatomées ont un rôle écologique primordial dans les océans, notamment par leur contribution à la mitigation du réchauffement climatique par leur rôle dans la pompe biogéochimique du carbone ou par leur rôle de source de nourriture pour l'ensemble de la vie marine. Nous avons montré chez la diatomée modèle *Phaeodactylum tricornutum* que le pH des thylacoïdes régule directement l'induction et la relaxation du NPQ. Nous avons ainsi affiné le modèle de la dynamique du NPQ chez *P. tricornutum*, où le contrôle cinétique du cycle des xanthophylles par le pH joue un rôle prépondérant.

Nous avons identifié l'antiport proton/potassium KEA3 et déterminé qu'il est un régulateur important de la force proton motrice chez les diatomées. Par l'étude de mutants CRISPR-Cas9, nous avons observé que ce transporteur module le pH du lumen et ainsi permet d'adapter la réponse NPQ selon les conditions environnementales. KEA3 convertit la composante ΔpH de la force proton motrice en ΔΨ, et de ce fait n'induit aucune perte d'énergie et maintient donc la synthèse d'ATP.

Sunlight is the inextinguishable primary energy source on which all living beings eventually rely on for their metabolic needs. In spite of the many advantages of light utilization, it conveys heavy, inherent burdens: intermittency and variability. In order to survive, photosynthetic organisms must constantly reshape their light harvesting machinery, in particular by inducing non-photochemical quenching (NPQ) mechanisms. Controlling the balance between photosynthesis and photoprotection is achieved in higher plants and green algae by a fine interplay between the electrical and the osmotic components of the thylakoid proton motive force. Ion homeostasis has therefore a key role in photosynthesis. Fine-tuning the composition of the proton motive force by specific ion exchange is a means for photosynthetic organisms to regulate NPQ induction efficiently, i.e. minimizing energy leaks and preserving ATP synthesis.

Diatoms have a foremost ecological role in the global oceans, both as key contributors of the biogeochemical carbon pump and as feedstock for marine life. In diatoms, the molecular of NPQ are just starting to be identified. We have demonstrated, using the model organism *Phaeodactylum tricornutum*, that NPQ is univocally controlled by the pH component of the proton motive force. We were thus able to refine the current model for NPQ dynamics in *P. tricornutum*, with a preponderant role of the kinetic control of the xanthophyll cycle by pH.

We have identified the K+/H+ antiporter KEA3 as a major regulator of the proton motive force in diatoms. Using a set of CRISPR-Cas9 constructed mutants, we have determined that this transporter is able to modulate the lumen pH and hence to adapt the NPQ response according to environmental conditions. KEA3 converts the ΔpH component of the proton motive force into ΔΨ, thereby not leading to any energy loss, i.e. maintaining the ATP output.